Stony Brook University

Alternate pore isoforms of a mechanosensory ion channel in Drosophila

A Dissertation Presented

By

Shao-Kuei Huang

to

The Graduate School

in Partial Fulfillment of the

Requirements

for the Degree of

Doctor of Philosophy

in

Neuroscience

Stony Brook University

December 2014

Stony Brook University
The Graduate School

Shao-Kuei Huang

We, the dissertation committee for the above candidate
for the Doctor of Philosophy degree, hereby recommend
acceptance of this dissertation.

Maurice Kernan – Dissertation Advisor
Associate Professor, Department of Neurobiology and Behavior

Glenn Turner – Chairperson of Defense
Associate Professor, Cold Spring Harbor Laboratory

Gary G. Matthews
Professor, Department of Neurobiology and Behavior

Daniel F. Eberl
Professor, Department of Biology
Director, Graduate Program in Genetics
The University of Iowa

This dissertation is accepted by the Graduate School

Charles Taber
Dean of the Graduate School

Abstract of the Dissertation
Alternate pore isoforms of a mechanosensory ion channel in *Drosophila*
by
Shao-Kuei Huang
Doctor of Philosophy
in
Neuroscience
Stony Brook University
2014

This thesis examines the expression and function of alternately spliced isoforms of No Mechanoreceptor Potential C (NOMPC), a TRPN ion channel protein expressed in several types of mechanosensory neuron in *Drosophila*. *nompC* mutant flies are severely uncoordinated; electrophysiological recordings show that they lack receptor currents in mechanosensory bristles and have reduced sound-evoked potentials in the antennal nerve.

Exons 14 and 15 of the *nompC* gene both encode a highly conserved part of the protein, including the channel pore. To find how these exons are used, I first identified six different cDNA isoforms. Among these were two major isoforms with mutually exclusive splice patterns including either exons 13 and 14, or exon 15. Conservation of the alternate exons in several holometabolan insect orders suggests that both are functional. This was confirmed by rescuing *nompC* mutants by expressing single isoforms from cDNA transgenes. Both β and γ isoforms rescue the *nompC* mutant phenotypes, but they show different mechanoreceptor current properties: the γ isoform has a larger adapting current amplitude, and a smaller adaptation time constant.

Quantitative RT-PCR showed that the γ isoform is the more abundant form in all tissues and developmental stages, and that the β isoform is most enriched in the haltere. To detect isoform expression patterns with cellular resolution, I designed two splice-reporter genes *UAS-FSR-β* and *UAS-FSR-γ*; each produces a visible product only when the corresponding pore exon is included in the mRNA. Mechanosensilla on the wing blade showed a perfect correlation between isoform production and previously described physiology: FSR-β is produced in slowly adapting (tonic) neurons and FSR-γ in fast adapting neurons. In haltere and wing hinge sensilla, the reporters revealed overlapping but differentiated expression patterns. Bristles on the notum or legs produced only FSR-γ. In the antennal chordotonal organ, FSR-γ was produced in all neurons, but FSR-β was detected only in a subset of neurons thought to respond to low-frequency stimuli. Other chordotonal organs also showed differential isoform expression.

I conclude that through alternate splicing, different *nompC* isoforms are produced in different sensory neurons and that they are specialized for sensing diverse mechanical stimuli.

Table of Contents

List of Figures/Tables/Illustrations

Acknowledgments

I thank Maurice for his patient and encouraging me keep working on difficult projects. He always can rationalize my immature ideas and complicate observations by asking critical questions. I learned how to do solid research and to connect evidences to draw more comprehensive conclusions. He also help me a lot in my most underdeveloped skill, writing.

I thank members of Gergen lab, Erezyilmaz lab, and Frohman lab for helping me with experiments.

I thank Dr Yun Doo Chung for providing NOMPC antiserum and the discussion about my project. I am appreciating the GAL4 lines gifted by Drs. Ryan Kavlie and Joerg T. Albert to help me determine the isoform expression patterns.

I thank for the input of my committee member, Drs. Glenn Turner, Gary Matthews, and Daniel Eberl. They help me to see the bigger picture and realize the value of my work.

I would like to thank for the financial support of my Program in Neuroscience. Without it, I cannot pursue the science I enjoying the most. I thank the NIH funding support the project.

Finally, I thank God for letting me have several technical breakthroughs throughout years to push my project forward and finally form a comprehensive story.

Chapter 1
Background

My thesis project is to illustrate the function, expression, and evolution of isoforms with alternate pore regions in a mechanosensory ion channel, NOMPC in *Drosophila*. In this chapter, I will review the structure and function of mechanosensory organs in fly, everything we know about NOMPC from origin, expression, function, to protein structure, and rare examples of alternative splicing in channel pore region. NOMPC is expressed in neurons of mechanosensory organs. Based on previous knowledge about the function and location of mechanosensory organs, we can assay the properties of different isoform pores and know where to look.

Mechanosensation is the most basic sense to detect the physical world around an organism, but its mechanism is still elusive. It involves a channel that senses a change in the force between the membrane it floats in, and an anchor. This anchor can be at the cytoskeleton like microfilament or microtubule, or the membrane itself. Here I use *Drosophila* as model system to study the isoforms of NOMPC ion channel with alternate channel pore in neuronal mechanosensation, which needs faster response than detecting osmotic pressure on the membrane and is more complicated.

A. Mechanosensory organs in *Drosophila*

Mechanosensory organs in the fly can be classified into three categories: external sensory organ (ESO), chordotonal organ (CHO), and multiple dendritic (MD) neurons. NOMPC is expressed in all three types of sensory neurons (Cheng et al., 2010; Lee et al., 2010; Walker et al., 2000), but may not perform the same function in each organ. ESOs include bristles for tactile sense, hair plate for proprioception, and campaniform sensilla for sensing local cuticle tension

(Keil, 1997; Murphey et al., 1989). CHOs are near the joint for proprioception and in Johnston's organ, a chordotonal organ in the second segment of the antenna which detects sound, air flow and gravity. MD neurons, unlike CHO or ESO, are not ciliated. Different classes of MD neuron detect chemical, heat, nociception, or act as proprioceptors. The ESO and CHO are the main focus of my work; no MD neuron is involved in this project.

i. External sensory organs (ESO): bristles and campaniform sensilla

The bristles that cover most of the fly's body are examples of external sensory organs (ESO) and are responsive to touch. Each ESO is constructed by five cells: shaft, socket, sheath, glia and neuron. The apical surface of the neuron is totally wrapped by the sheath cell, including a thin layer of dendritic sheath covering the cilium. The socket cell supports the shaft, forms tight junctions with surrounding cells to form a separated apical receptor lymph space, and electrogenic ion transports on these cells secrete high potassium receptor lymph fluid which is important for maintaining trans-epithelial potential (TEP). The shaft serves as a lever to pass a stimulus to the neuronal cilium inserted at its base (Fig. 1-1 A, B)(Keil, 1997). The displacement scale is reduced from micrometer to nanometer level. Deflection of the bristle compresses the dendritic sheath and cilium and leads to the influx of cations, specifically potassium and calcium, into the cilium. An EM image of fly bristle ESO in longitudinal section give us a hint that bristle deflection may activate the NOMPC ion channel either by generating a pulling force applied on outer segment through dendritic sheath, or by pressure on those layers around outer segment, as in Pacinian corpuscles (Fig. 1-1B).

Campaniform sensilla (CS) are specialized ESO, similar to small bristles but with a dome-shaped cap instead of a bristle shaft (Fig. 1-1C). They are activated by compression or tension in the surrounding cuticle when the surface is bent. Eight sensilla distributed over wing vein in fixed pattern (Fig 1-1E) (Dickinson and Palka, 1987), dozens on wing base (Cole and Palka, 1982), and single or small patches of them around the joints (Merritt and Murphey, 1992). Halteres, which only exist in the order Diptera, are a specialized derivative of the hind wing. During flight, they beat synchronously with the forewing and serve as gyroscopes. There are about 300 sensilla with raised semicircular collars that form three matrices at the base of haltere (Fig 1-1D) (Keil, 1997) These sensilla detect Coriolis forces of body angle rotation in three

different planes, and provide feedback to the wing steering muscles as equilibrium reflexes (Chan et al., 1998).

ii. Chordotonal organs (CHO)

Chordotonal organs (CHO) do not have structure outside the cuticle but use attachment cell to attach to cuticular apodemes or to the hypodermis. The scolopidium, the unit of CHO, contains the signature scolopale cell, glia, attachment (cap) cell, and one or more neurons (Fig. 1-2A, B) (Chung et al., 2001; Keil, 1997). The scolopale cell generates a barrel-shaped sleeve called a scolopale, which surrounds the cilia of the innervating neuron(s). The distal ends of cilia are inserted into a dendritic cap produced by the attachment (cap) cell. When a CHO is activated by stretching, cations flow from receptor lymph in the scolopale space into the cilia. CHOs sensing proprioception are located near the joints such as the distal end of femur (Fig.1-2C) or the first segment of abdomen. Tympanal organs (TO) and Johnston's Organ (JO) are two types of insect auditory organ composed of scolopidia. A TO is an air-filled multi-layered structure on the tibia and is evolved in crickets, cicadas, katydids, moths, and locusts (Hoy and Robert, 1996; Yack, 2004). Johnston's organ, in the second segment of *Drosophila* antenna, serves as a sound, wind, and gravity receiver (Kamikouchi et al., 2009; Yorozu et al., 2009).

Among the *Drosophila* chordotonal organs, JO has the largest number of scolopidia, about 225 units per JO. Scolopidia attach to the hinge of third antenna segment (Fig. 1-2D). When the arista is deflected or vibrated, it twists the hinge and stretches CHOs, and the NOMPC and other ion channels are activated. The JO scolopidia can be divided into five groups, based on their axonal projections to the antennal mechanosensory and motor center (AMMC) of the brain (Kamikouchi et al., 2006). Scolopidia projecting to zones A and B are responsive to sound, and scolopidia projecting to zones C and E respond to stationary stimuli like wind and gravity (Kamikouchi et al., 2009; Yorozu et al., 2009).

iii. Multiple dendritic (MD) neurons

Non-ciliated MD neurons are well defined in larvae state (Grueber et al., 2003). There are dendritic arborization (da) neurons, the bipolar dendrite (bd) neurons, and the tracheal dendrite (td) neurons. Based on their dendritic fields, da neurons were identified as class one, the simplest dendrite relay, to class 4 which has a big dendritic field and a complex dendritic tree. It

senses stimulus by the nerve ends. NOMPC-L is detected at proximal part of dendrites (Cheng et al., 2010).

B. NOMPC, a member of transient receptor potential (TRP) channel superfamily

The *no mechanoreceptor potential C* (*nompC*) locus was identified in a genetic screen in for proprioceptive mutants with defects in mechanosensory transduction (Kernan et al., 1994). In *nompC* null mutants, there is no mechanoreceptor potential in external sensory organs (ESO), and the antennal sound-evoked potentials are reduced (Eberl et al., 2000); or by some measures, near absent (Effertz et al., 2011). It was identified by positional cloning (Walker et al., 2000) as encoding a new branch of the transient receptor potential (TRP) superfamily of channel proteins, and has homologs in nematode (TRP-4, (Li et al., 2006)), zebrafish TRPN1 (Sidi et al., 2003), frog (Shin et al., 2005), turtle (*Chrysemys picta bellii*), and alligator (*Alligator mississippiensis*), but not in mammals (Pedersen et al., 2005) or birds.

i. TRP superfamily channel respond to a variety of modalities.

The TRP channel superfamily contains many branches including TRPA, TRPC, TRPM, TRPML, NOMPC/TRPN, TRPP, and TRPV (Gees et al., 2012; Montell, 2005; Pedersen et al., 2005) (Fig. 1-3A). TRP channels respond to variety of modalities. For example TRPAs respond to different temperature ranges, TRPM responds to heat, TRPVs respond to pain, capsaicin and heat, and TRP/TRPL are involved in light sensing when triggered by secondary messengers. Among them, TRPA1 (Corey et al., 2004), and NOMPC (Walker et al., 2000) have been considered the candidates for mechanosensory transducer channels based on their expression patterns and loss-of-function phenotypes. TRPA1 as was ruled out as the mechanosensory transducer in mammalian hair cells when TRPA1 KO mice was made (Kwan et al., 2006).

ii. General structure of NOMPC

Based on amino acid sequence similarity and secondary structure predictions, most TRP channels share the same core structure with 6 trans-membrane domains and a pore region between TM5 and TM6 (Fig. 1-3B). Each functional channel is a homo- or a hetero-tetramer

(Fig.1-3C). NOMPC has 29 Ankyrin repeats (AR) at N-terminal side, the most in the TRP family. It followed by a conserved link region and the channel domain. ARs are highly conserved between NOMPC homologs. AR has many functions in different contexts. For example, AR bind to ATP, PIP2 and calmodulin in TRPV1 (Lishko et al., 2007), multiple AR may form spring like structure to contribute to mechanosensitivity (Lee et al., 2006). TRPC, TRPM, TRPV and NOMPC channels contain the TRP-box after TM6, the most conserved part. In TRP channel superfamily, only the protein structure of TRPV1 is solved (Cao et al., 2013; Liao et al., 2013). These structural data confirm that the general TRP structure is similar to voltage-gated channels which have voltage sensitive TM1-TM4 outer ring and TM5-TM6 inner ring with pore loop between S5 and S6. TRP domain interacts with S4-S5 link and ARs-S1 link to fortify the scaffold. TRPV1 has wide extracellular opening and short selective filter. Beside upper selective filter, there is also another lower gate which capsaicin mainly targeted. Based on the similarity of secondary structure (Pedersen et al., 2005) and the alignment of TM5 to TRP box region (Fig. 1-3D), the TRPV1 structure can give us an idea of the general structure of NOMPC (Fig. 1-3E). In this thesis, I identified NOMPC isoforms that use different exons for their pore region, and show that they have different receptor current properties and expression patterns.

iii. Function and localization of NOMPC and its homologs

TRPN is selectively expressed in mechanosensory neurons in fly, in *C. elegans*, epithelial and inner hair cell cilia in *Xenopus* and the hair cells of zebra fish ear (Li et al., 2006; Shin et al., 2005; Sidi et al., 2003; Walker et al., 2000). *nompC* null mutants have no physical response in bristle recording (Walker et al., 2000) and no nonlinear amplification in auditory response (Gopfert et al., 2006). In *Drosophila*, NOMPC is expressed in cilia tip of CHO (Fig. 1-3A), ESO (Fig. 1-3C, D) (Lee et al., 2010) and in proximal part of dendrite of multiple dendritic (MD) neurons (Cheng et al., 2010; Yan et al., 2013)(Fig. 1-3F). *nompC* null mutant flies are viable but highly uncoordinated, and they usually have an eclosion defect. Sound-evoked receptor potential is reduced to half in *nompC* null mutants (Eberl et al., 2000) (Fig. 1-3B). The receptor potential of touching bristle is diminished in null mutants, and in hypomorph mutant $nompC^{4}$, the receptor potential become hyper-adaptive (Fig. 1-3E). Yan's group found a functional isoform *nompC-L* in MD neurons where it facilitates muscle contraction in larva crawling and adult walking (Fig. 1-3G, H) and responds to gentle touch (Cheng et al., 2010; Yan et al., 2013). NOMPC-L without

first 12 ankyrin repeats do not attach to microtubule. TRP-4, NOMPC homologue in C. elegans, is expressed at cilia and cell body of dopaminergic sensory neurons CEP and ADE, and at axon and cell body of two interneurons, DVA and DVC (Kang et al., 2010; Li et al., 2006; Walker et al., 2000). TRP-4 mutant worms have defective locomotion and mechanoreceptor currents. NOMPC homologue is enriched in microtubule-based cilia in epithelial cells, including kinocilial bulb of Xenopus inner ear (Shin et al., 2005). After EGTA treatment to break links between cilia, NOMPC moves to the base of kinocilia.

iv. Is NOMPC is the hearing transducer? -Evidence for and against it

In the long history of the search for the transducer of hearing, NOMPC was always been a popular candidate. Here I summarize the evidence for and against this idea.

From the expression pattern, NOMPC was expressed at the tip of cilia of CHO and ESO (Lee et al., 2010). This would be the best site for the task compare to Nanchung and Inactive, two TRPV channels, which are expressed in the middle of cilia. NOMPC also was detected in inner hair cell of zebra fish (Sidi et al., 2003), but in Xenopus, NOMPC is only expressed in kinocilia where no transduction happens. Another indirect evidence is the point mutation on TRP-4 pore and $NOMPC^{4}$ change receptor current, and so did *NOMPCβ* and *NOMPCγ*, which I will describe later. The auditory response potential is reduced by half in the null mutants, and the remaining signal probably is due to the fact that antenna also sense wind and gravity (Effertz et al., 2011).

In vertebrate and insect auditory system, the stiffness of inner hair cilia or insect arista reduces while transducing. Arista stiffness reduction is proportional to NOMPC protein level. K_{lin}(steady force stiffness) don't change in *nompC* mutant (Effertz et al., 2011). Nonlinear Amplification of antennal vibrations is also diminished in *nompC* mutant. Lehnert and his colleagues did patch clamp on giant fiber neuron and recorded sound-evoked generator current (Lehnert et al., 2013). They found the current is abolished in *nanchung* and *inactive* mutants but only reduced in $nompC^{1/3}$ null mutant line. The only suspicion I have about this evidence is the *nompC* alleles maybe contaminated because few labs request the same stock from stock center communicated with us about contamination, and I did find second lethal mutation in my $nompC^{1}$ stock.

The vertebrates that have retained NOMPC live in water environment in whole or part of their life stages. If we consider NOMPC is the alpha subunit of auditory transducer in insect and possible in other classes, animal ancestors moving from water to land may adapt new ion channel for hearing. The auditory range of sea turtles are 100~1000Hz (Ketten and Bartol, 2005), and insect like *Drosophila* responds to courtship songs around 200~400 Hz (Yorozu et al., 2009). In mammals, human hears 20~20,000 Hz, and bat can hear ultrasound up to 212 KHz (Fenton and Bell, 1981). Although there is no *nompC* homolog in mammal, study the property of NOMPC shed light on the general mechanism of mechanosensory ion channel.

C. Alternative splicing in channel pore region (most in TRP channels)

Because a rigid structure is important for ion channel selectivity, the regulation of channel function is usually not through modifying pore region but other parts of alpha subunit or beta subunit. Alternative splicing is an efficient way to increase diversity of channels but alternative splicing in pore region like NOMPC is uncommon. Several channels with similar splicing pattern have been reported and most of them are TRP channels. Here I summarize their splicing pattern and their functions to shed a light on NOMPC isoform's biophysical properties.

i. TRP channels

- Rat TRPM1 was reported with amino acid 1066-1071 deleted where is the putative pore region (Lis et al., 2005). Human TRPM1/AF071787 also has this variant. These forms arise by alternative splicing from donor site in intron 22 to generate extended exon 22. Physiological significance is unknown.
- In TRPM3 alternative splicing isoforms, TRPM3α1 is 12 amino acids longer than TRPM3α2 in pore region and the proline immediate after is substituted by alanine (Oberwinkler et al., 2005). It makes TRPM3α2 highly permeable to divalent cations.
- Polycystin 2 L2 (PKD2L2) is one of 5 polycystin gene in mammal (Sutton et al., 2006). It has an alternate beta isoform with part of TM4, pre-pore loop, TM5, and TM6 are truncated. It was predicted to form a 4TM channel but no conductance was detected.

ii. Non-TRP channels

- Human Cav1.2 has mutually exclusive alternative splicing between exon 8 and exon 8a which encode transmembrane segment in domain 1. Two isoforms are expressed in different tissue specific patterns and have different dihydropyridine sensitivity. Untreated N2a neuron cell line makes 82% of exon 8. When polypyrimidine tract-binding protein presents, the splicing shifts to 7%~10% exon 8 (Tang et al., 2011; Welling et al., 1997). Similar gene structure was found in Cav1.3, too.
- hSK3 channel was reported an isoform, hSK3_ex4, transcribe exon4 which extended the pre-pore loop by 15 aa and co-expressed in embryo neuron and other tissue (Wittekindt et al., 2004). hSK3_ex4 is less voltage dependent than hSK3, and is only small conductance calcium activated potassium (SK) channel insensitive to SK blockers (Ex: apamin, scyllatoxin, and d-tubocurarine)
- I_h in *Drosophila* has three alternative splicing exons. Variant b lies between TM3-TM4 and variant c is between TM4 and TM5 (Gisselmann et al., 2005). Physiological significance is unknown.
- Shaker in lobster has several alternative N-termini and two variants from TM5 to pore region (pore I and pore II) (French et al., 2005). Isoforms with pore II have higher inactivating current and lower non-inactivating current and slightly stronger voltage dependent.

Figure 1-1 Structure of external sensory organ (ESO)

A) Schematic diagram of tactile bristle ESO (Chung et al., 2001). When the shaft is deflected toward the body surface, the shaft base may either compress the side of the cilium or stretch the top of it. These movements open NOMPC channels on the cilium and generate the receptor current.

B) Transmission EM of a scutellar bristle in longitudinal section (Avidor-Reiss et al., 2004). Abbreviations: ep, epithelium cell; OS, outer dendritic segment; IS, inner dendritic segment; TB, tubular body; DS, dendritic sheath; CC, connecting cilium; BB, basal body.

C) Schematic of a campaniform sensillum (Keil, 1997). It senses one dimension of compression from surrounding body walls.

D) Campaniform sensilla on haltere (Cole and Palka, 1982). Abbreviations: Met.Pap., he metathoracic papillae; d.Scab., sensilla of the dorsal scabellum; d.Ped., sensilla of the dorsal pedicellus; v.Scab., sensilla of the ventral scabellum; v.Ped., sensilla of the ventral pedicellus.

E) Campaniform sensilla on the wing vein. Adapted from (Dickinson and Palka, 1987).

Figure 1-2 Structure of chordotonal organs

A) Schematic of a scolopidium (Chung et al., 2001). The attachment cell connects to hypodermis or apodeme. When stretched, cations flow from receptor lymph in scolopale space into cilium. There may be more than one ciliated neuron in each scolopale.

B) Transmission EM of a scolopidium of *Helicoverpa armigera* (Keil, 1997). Cp, cap.

C) Femoral chordotonal organs labeled by splicing reporter genes are at the proximal end of the tibia.

D) Schematic of Johnston Organ mechanics. When an antenna rotates clockwise (red circle arrow), it stretches the scolopidia, which are attached to the stalk. The scolopodia are arranged three dimensionally.

Figure 1-1 Structure of external sensory organs (ESO)

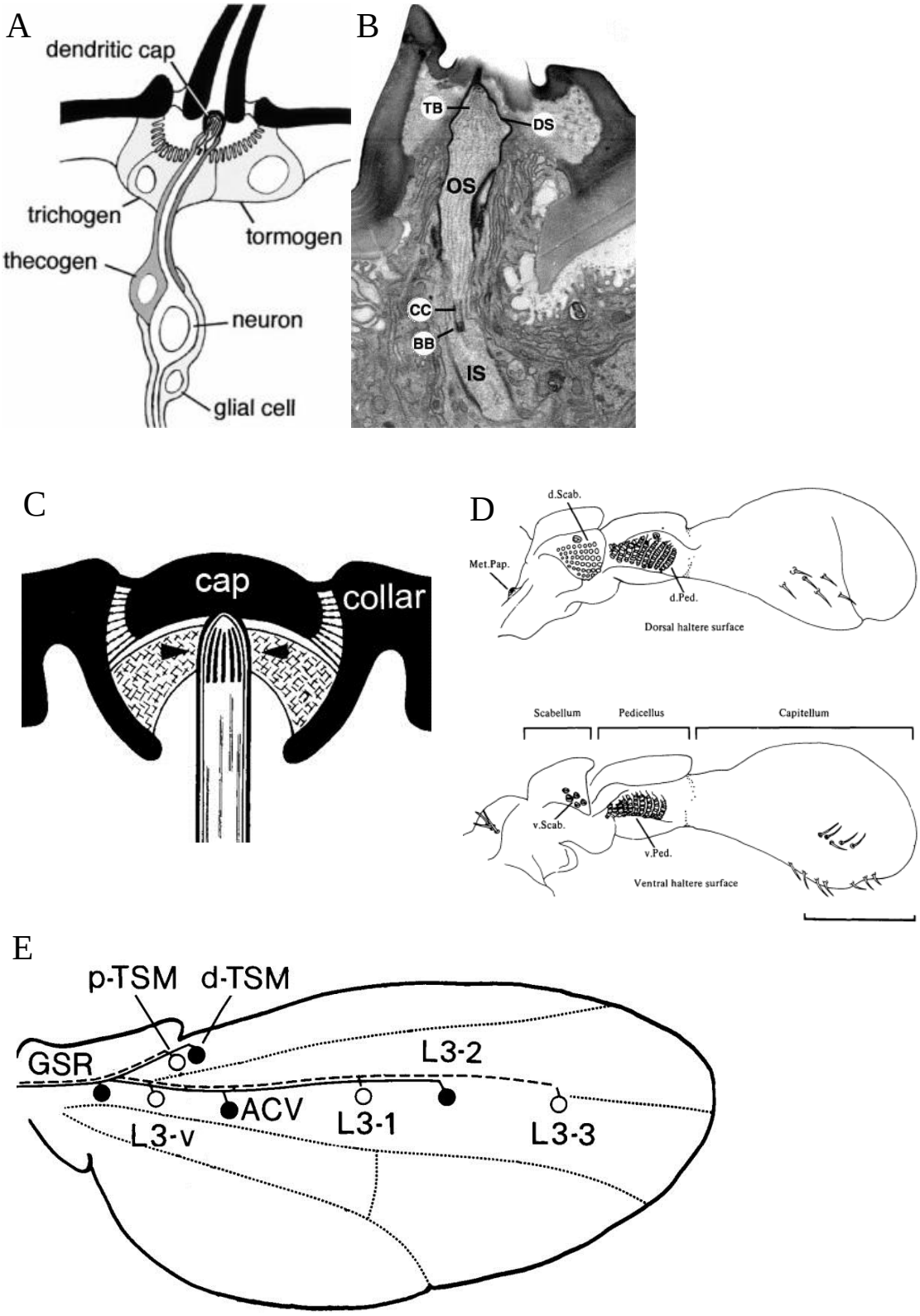

Figure 1-2 Structure of chordotonal organs (CHO)

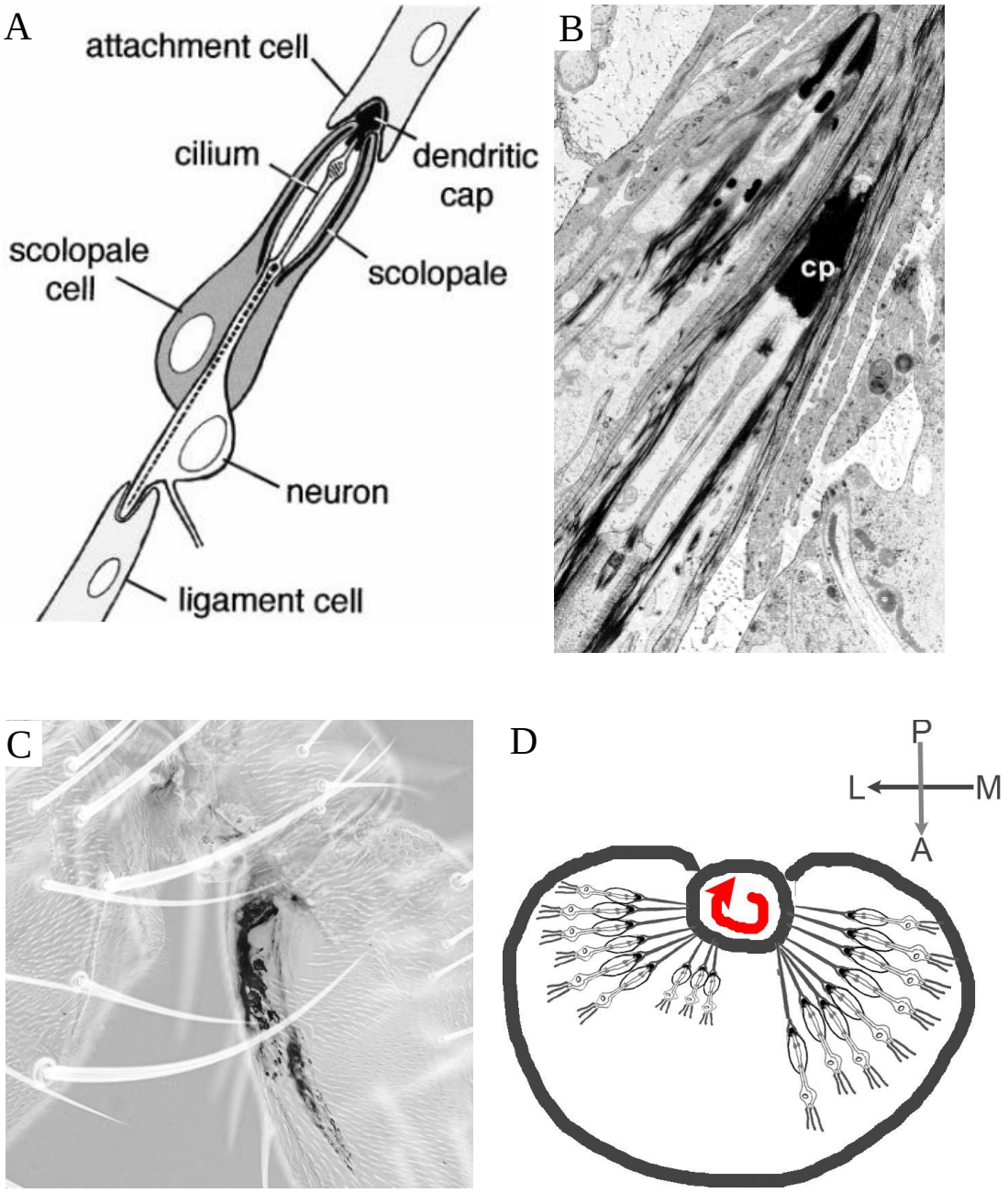

Figure 1-3 NOMPC, TRP channel superfamily N subfamily.

A) NOMPC belongs to TRP channel superfamily N subfamily (Pedersen et al., 2005). It has homologs in zebrafish and worm (nematode), but not in humans. NOMPC has 29 ankyrin repeats (AR), the longest within the superfamily. Other members with AR are the TRPA with 14 AR, and TRPV with 5 AR.

B) Predicted secondary structure of NOMPC. It has N-terminal 29 ankyrin repeats, a link region, a 6TM channel domain with pore region between TM5 and TM6, and TRP box.
C) NOMPC is predicted to form homo- or heterotetramer.
D) Alignment of two NOMPC isoforms and rat TRPV1. The similarity of TM5, TM6, and TRP domain are high. The pore helix region is labeled in green with the selective filter "GMGD" in TRPV1.
E) TRPV1 protein structure from cryo-EM (Cao et al., 2013; Liao et al., 2013). Only TM5 and after is shown. Base on similarity between NOMPC and TRPV1 in this region, correspondent domains, TM5, pore, TM6, and TRP domains, are labeled in the same color as D).

Figure 1-3 NOMPC, TRP channel superfamily N subfamily

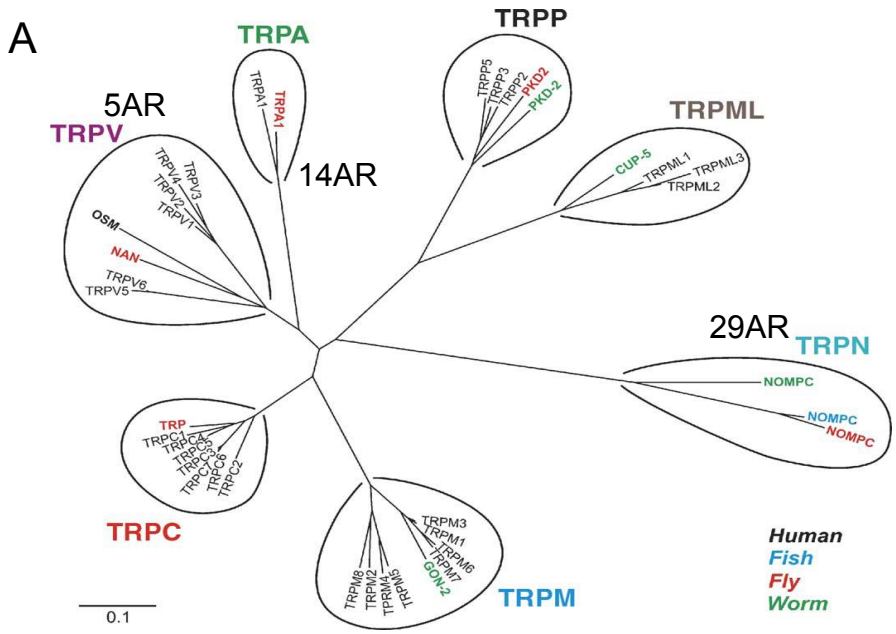

Pedersen et al. cell calcium 2005

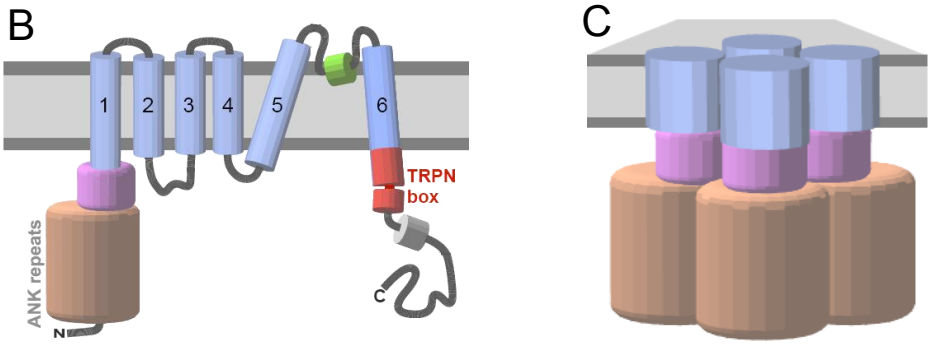

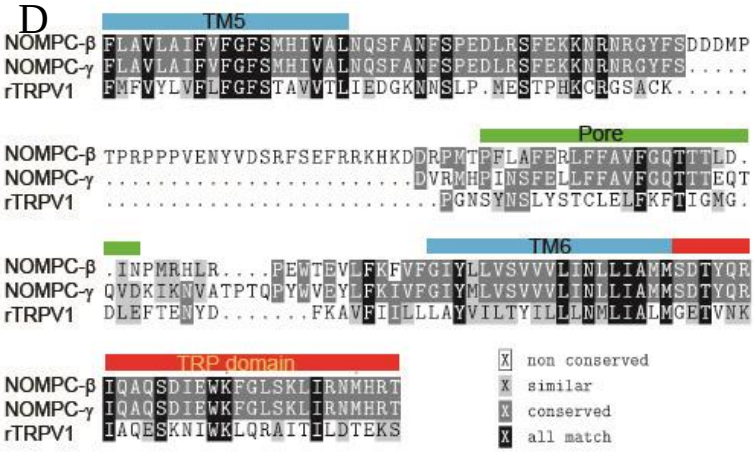

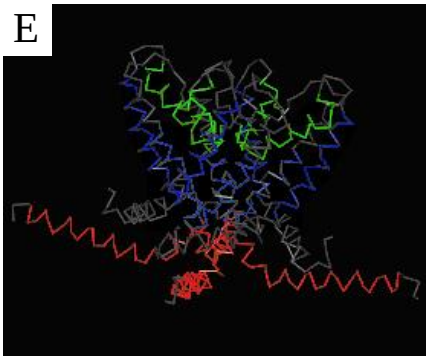

Figure 1-4 Localization of NOMPC

A) NOMPC is expressed at the tip of CHO cilia. The scheme on the right is combined by three antibody stainings on the left. NOMPA marks dendritic sheath. REMPA marks cilium dilation. IAV labels inner segment of cilium (Lee et al., 2010).

B) Sound-evoked potential is reduced in half in *nompC* null mutant (Eberl et al., 2000).

C) NOMPC is labeled at the tip of cilia by the antiserum. Dendritic sheath is labeled by NOMPA, and EYS marks the proximal end of the sensory cilia.

D) Scheme of ESO.

E) Receptor potential (RP) is diminished in $nompC^{1/2}$ null mutant and hyperadaptive in $nompC^{4}$ hypomorphic allele.

F) NOMPC-L is labeled at proximal dendrite by GFP tag.

NOMPC-L overexpressed by *nompC*-GAL4 rescues *nompC* null mutant larvae crawling speed (G), and adult walking speed (H).

Figure 1-4 Localization of NOMPC

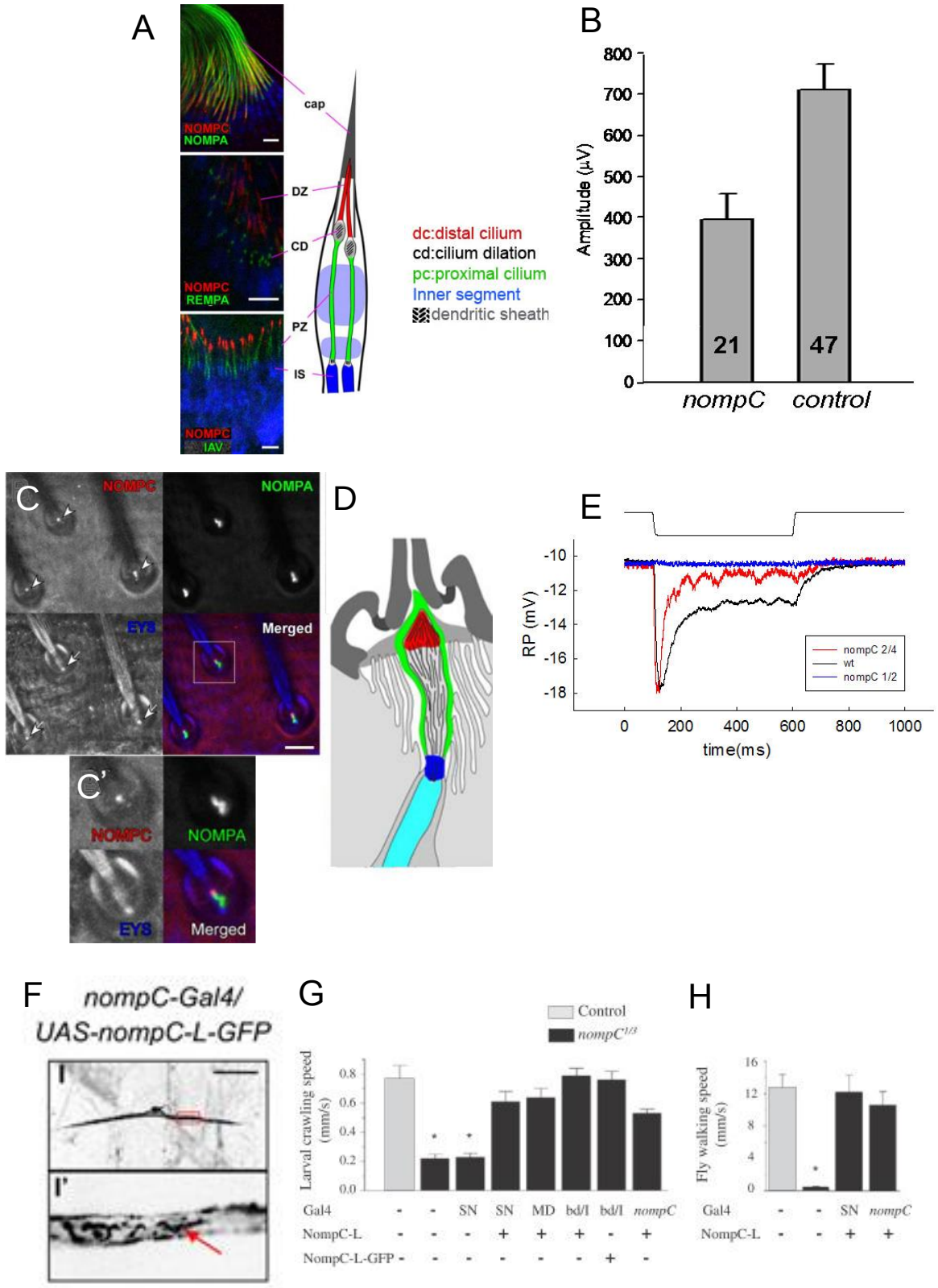

Chapter 2: Identification of *nompC* isoforms

Summary

In order to find the functional NOMPC products, we isolated transcript isoforms of *nompC,* and used evolutionary evidence to predict which isoforms are functional. There are seven transcripts of *nompC* predicted on Flybase with support of cDNAs or partial EST sequences. These include *nompC-RA*, which was cloned by Walker (Walker et al., 2000) (Fig. 2-1). Another transcript, *nompC-L*,was cloned after this part of my project (Cheng et al., 2010). I made my own prediction by using the Fgenesh-M program (Salamov and Solovyev, 2000). It predicted three different transcripts from exon 1 to exons 15, 19, or 21 (N15, N19, and N21, Fig 2-1B) of the *nompC* genomic region. Among these predictions, there are no alternate isoforms in the N-terminal, ankyrin repeat region. All the isoforms are generated by alternative splicing in the channel pore-forming domain, near the C-terminus.

Based on the predictions, I amplified and cloned cDNAs corresponding to six different isoforms, which I named α, β, γ, δ, ε, and ζ. The α isoform with an extended exon 15 matches *nompC-RA* (Fig. 2-1C). The other isoforms fall into two groups, differentiated by mutually exclusive splicing: isoforms β and ε include exon 13 and 14, and isoforms γ and δ include exon 15. In isoform β, exon 13 encodes a longer pre-pore loop and exon 14 encodes the pore region, TM6 and part of the TRP domain (fig. 2-1D). Isoform γ uses exon 15s for similar pore region, TM6 and TRP-box. We used VISTA DNA sequence alignments to compare *nompC* sequences from different *Drosophila* species, and found that exons 13, 14 and 15 are conserved (Fig. 2-2). Amino-acid alignment of exon 14 to 15 between Diptera (*Drosophila melanogaster* and *Anopheles gambiae*) and Lepidoptera (*Bombyx mori*, and *Danaus plexippus*) reveals that both exons are conserved (Fig. 2-3). These data indicate that duplication generated exon 14 and 15 in

common ancestor of these insect orders, and that both exons are functional with their own variations. Those conserved, charged amino acids may affect the ion selectivity of the NOMPC channel. Therefore we believe NOMPC-β and NOMPC-γ play significantly different roles in mechanosensation.

An independent triplication of the entire C-terminal region in the more distant order Hymenoptera, suggests that there has been evolutionary selective pressure for generating and maintaining *nompC* isoforms in Holometabolan insect orders.

Identification of *nompC* isoforms

The *Drosophila nompC* gene was isolated and cloned by Walker (Walker et al., 2000). It encodes a TRP channel and is the major candidate for a transducing channel for the auditory and tactile senses in *Drosophila* (Goodman et al., 2004; Kernan, 2007). NOMPC is expressed in chordotonal organs (CHO), external sensory organs (ESO) and multiple dendritic (MD) neurons (Cheng et al., 2010; Lee et al., 2010). When comparing the first published amino acid sequence with homologs in other species, we found that the *Drosophila* NOMPC-PA does not have a conserved TRP box. When using the extended exon 15 fragment after TM6 as a query to search the PBLASTN insect database, we found no significantly similar matches. Walker et al. used a genomic BAC clone, not this *nompC* cDNA sequence, to rescue the *nompC* null mutant. For these reasons, we suspected that NOMPC-PA was non-functional, and decided to study in more detail property of NOMPC, starting with the isolation of other transcripts.

Materials and Methods

i. **Prediction and isolation of *nompC* isoforms.** The region of interest I chose is 25,001 base pairs of *nompC* genomic region (Genbank AE014134.6), extending from 1858 base upstream of translation start site (ATG) which includes 143 base of a natural transposon (Doc) insertion. The Fgenesh-M program (Salamov and Solovyev, 2000) predicted three transcripts from exon 1 to exon 15, 19, or 21 (Fig 2-1B). Then I looked for consensus poly-adenylation sites in the

region of *nompC* exons 12~21 to determine the end of transcripts. Fifteen poly-A signal sequences ("AATAAA" with a following GT-rich region (Levitt et al., 1989)) were found. Three sets of primers, 3.4A, 3.4B, and 3.4F (Table 2-1), are designed to detect the most likely 3' ends. 3.4A is designed for *nompC-RA*. 3.4B is designed for RNA isoforms similar to those predicted in Flybase. 3.4F is for detecting the longest gene prediction. Exon 1~12 was detected in two fragments, exon 1~9 and exon 9~12.

ii. **Reverse transcription-PCR.** Total mRNA was isolated from 50 antennae of Oregon-R adult flies following standard TRIzol protocol (http://www.mrcgene.com/tri.htm). Total cDNA was reverse-transcribed by Transcriptor reverse transcriptase (Roche) with 3' primer nC-2-3' r for fragment 1 and fragment 2 (Fig.3-1A), nC3-3' polydT_XbaI for fragment 3a, 3b, and 3f (Fig. 2-1B, Table 2-1).

iii. **Multiple sequence alignment of NOMPC homologs.** All NOMPC homolog sequences are from NCBI database. The amino acid sequence of the transmembrane domain of NOMPCβ (encoded by exons 12, 13, 14, and 16) or NOMPCγ (encoded by exons 12, 15, and 16) was used as a query to run TBLASTN alignment (http://blast.st-va.ncbi.nlm.nih.gov/Blast.cgi?PROGRAM=tblastx&PAGE_TYPE=BlastSearch&LINK_LOC=blasthome) against translated (predicted) mRNA. All the hits are considered *nompC* homologs after confirmed by amino acid alignment in full length. The *nompC* homolog in *Danaus plexippus* was located by BLAST tool in the EnsemblMetazoa database (http://metazoa.ensembl.org/Danaus_plexippus/blastview). DNA sequences used in Fig. 2-3 are *Drosophila nompC*, *Anopheles gambiae* (AGAP008559-PA, 1275416), *Bombyx mori* (LOC101741868), and *Danaus plexippus* (KGM_11323). The four-species alignment was done with BOXSHADE tool of Biology WorkBench (http://seqtool.sdsc.edu/CGI/BW.cgi#!). More homologs used in alignment within Arthropoda (Fig. 2-4) are from *Tribolium castaneum* (LOC662890), *Nasonia vitripennis* (LOC100122337), *Apis mellifera* (NompC, 408777), *Acyrthosiphon pisum* (LOC100169435), *Pediculus humanus corporis* (ankyrin repeat domain-containing protein, 8236462), *Daphnia pulex* (NCBI_GNO_8800027) and *Ixodes scapularis* (ion channel NOMPC, putative, 8044102).

Results

i. Prediction and isolation of *nompC* cDNAs

The *nompC* gene was cloned by Walker *et al.* (Walker et al., 2000). We suspected that the published protein sequence is not functional because it did not include the highly conserved TRP domain, and they did not make cDNA rescue construct. To understand the function of NOMPC, finding the functional cDNA was a necessary first step.

There are 6 transcripts of *nompC* on Flybase: *nompC-RD, nompC-RE, nompC-RF, nompC-RG, nompC-RH, and nompC-RA* (Fig. 2-1). *nompC-RA* corresponds to the cDNAs cloned by Walker, and the rest are predictions based on partial cDNA sequences. *nompC-L* described by the Jan group in 2010 (Cheng et al., 2010) is another transcript which produces a functional protein.

I made my own prediction by using the Fgenesh-M program (Salamov and Solovyev, 2000). This program was developed to detect gene structure with organism-specific parameters with 90% accuracy in coding sequence identification, and with 14% chance of false positives. It predicted three isoforms and total 21 exons in the *nompC* region (Fig 2-1c).

I then looked for matches to the consensus poly-adenylation site, "AATAAA" with GT-rich region nearby, (Levitt et al., 1989) for the end of *nompC* transcripts. A total of 15 potential poly-A signals were found. If I set *nompC* translation start site as position 1, the potential signals start at positions 13739, 14448, 14949, 16761, 18925, 19132, 19427, 19578, 20048, 20353, 20729, 21318, 22463, 22580, and 22620 (Fig. 2-2).

Three sets of primers were designed to detect the most likely 3' transcript ends. 3.4A was designed for *nompC-RA*. 3.4B was designed for RNA isoforms similar to the Flybase predictions. 3.4F was for detected longest gene prediction (Fig. 2-1B). I chose antenna as the cDNA source because of the large number of chordotonal neurons in Johnston's organ which is located in the second segment of antenna.

With the 3.4A primer set, we successfully amplified *nompC-RA*, confirming the previous result (Walker et al., 2000). The 3.4B primer set generated five new isoforms, named β, γ, δ, ε, ζ (Fig. 2-1C). The 3.4F primer set did not detect any product. No other isoform is detected in

other fragment. Isoform β is alternatively spliced to include exons 13 and 14. Exon 13 encodes a longer pre-pore loop and exon 14 encodes the pore region, TM6 and part of the TRP domain (fig. 2-1D). Isoform γ includes exon 15s for pore region, TM6 and part of TRP domain. Compared to the NOMPC-L isoform (Cheng et al., 2010), NOMPCγ is identical through the alternatively spliced region, but 14 amino acids shorter at the C-terminus. Lacking exon 17, isoform δ, ε, and ζ are frame-shifted, and the shifted amino acid sequence has no similarity to any other protein. They were considered probably nonfunctional.

nompC-β and *nompC-γ* isoforms represent two different groups we found, and the difference between them lies in exon 13 to 15 which encodes pre-pore loop, pore region, TM6, and part of TRP domain. To answer the question 'Which isoform produces a functional product?', I generated single isoform rescue lines (chapter 3) and compared *nompC* orthologs of model species.

ii. *nompC* exons 13 and 14 are conserved within the *Drosophila* genus

VISTA (http://genome.lbl.gov/vista/index.shtml) is a web-based comparative genomics tool (Dubchak et al., 2000; Frazer et al., 2004). It compares genome of several *Drosophila* species. We zoom in the alignment of *nompC* region between *D. melanogaster* and *D. simulans, D. ananassae,* or *D. pseudoobscura* (Fig. 2-2A). Here, exons 13 to 19 all have a greater than 80% similarity between species, and the similarity is decreased between less related species. According to the well-defined *Drosophila* phylogenetic tree (Clark et al., 2007), *melanogaster* diverged from *simulans, ananassae,* and *pseudoobscura* 5, 43, and 54 million years ago, respectively (Fig. 2-2B). The similarity drops dramatically in intron regions, and *pseudoobscura* seems not to have an exon 19. These data suggest that the gene structure of *nompC* is conserved between closely related *Drosophila* species, and that two versions of the pore region, encoded by exon 14 and 15, respectively, really exist. No similarity in the region of exons 20 or 21 was detected in VISTA alignment.

iii. Pore regions translated from exon 14 and 15 are conserved within Diptera and Lepidoptera

We used CLUSTALW (Thompson et al., 2002) to align and compare the amino acid sequences of pore region encoded by exons 14 and15 between order Diptera (*Drosophila melanogaster* and *Anopheles gambiae*) and Lepidoptera (*Bombyx mori*, and *Danaus plexippus*), both β and γ isoform are conserved (Fig. 2-3). In exon 14, a positively charged arginine is conserved across all four species, but contrasts with a hydrophobic residue, leucine, which is conserved at the same position in exon 15 and its homologs. Another positively charged residue, histidine/asparagine before the pore helix in exon 15 also conserved. Exon 14 and 15 also conserve a different motif (DIN in exon 14 and QTQ in exon15), at the possible position of a selective filter, following the pore helix. This selective filter position is aligned with TRPV1 selective filter "GMGD" (Fig. 1-3D, E (Cao et al., 2013; Liao et al., 2013)). There is a negative charge E/D in front of QTQ in exon 15. The extended pre-pore loop in β isoform encoded by exon 13 is conserved in length but not in sequence, within Diptera only. These data indicate that a duplication generated exon 14 and 15 in the common ancestor of Lepidoptera and Diptera at least 280 million years ago, and that both exons are functional with their own variations. Those conserved charge amino acids may affect the ion selectivity of NOMPC channel.

iv. Phylogenetic tree of *nompC* in Arthropoda

No alternate pore exons were found in the *nompC* orthologs in nematode (*Caenorhabditis elegans*,) or the vertebrates *Xenopus*, or zebrafish. To trace the origin of the duplication event, and gain insight into the function of alternate pore region, we searched for multiple NOMPC pore domain exons in sequenced genomes across the Arthropoda. Sequences of orthologs were acquired by running TBLASTN with a protein sequence query of TM5~TM6 of NOMPCβ and NOMPCγ.

We found that multiplication of *nompC* isoforms happened about 340 million years ago, only within the Endopterygota (Holometabola) (Fig. 2-4). In Diptera, exons 13, 14 and 15 are highly conserved. All the exon boundaries are kept tidily. Exon 13, which encodes the extended pre-pore loop in the β isoform, is conserved only in length but not in sequence. Beyond Diptera,

exons corresponding to exons 14, 15, and 16 in *Drosophila* are found in Lepidoptera and Coleoptera, but the similarity of exon 13 is less clear.

In Hymenopterans such as wasp (*Nasonia*) and bee (*Apis*), we also find multiple similar exons in this region, but with a different structure: three repeats of the entire C-terminal part of the protein.

Ion channel proteins rarely change their pore region because the channel core needs to be tightly regulated to ensure its proper function. Most ion channels regulate their properties by modifying domains outside the pore region, or by changing an associated beta subunit. Two exon multiplications happened in Holometabola suggests that through generating redundancy, NOMPC gained a chance to evolve for different functions. The fact that β and γ isoform expression are completely separated in wing vein sensilla (chapter 4, Fig. 4-3) indicates the selective force here was expanding the frequency sensing range. In Dipterans, gene structure of exon 13~16 are almost identical, which suggests that the alternate splicing mechanism may existed and kept the introns.

Consistent with our current understanding of phylogeny of insects (Misof et al., 2014), there were at least two independent multiplications within Holometabola based on the repeated gene structures (Fig. 2-5). The duplication of the pore exon happened in a common ancestor of the Diptera, Coleoptera and Lepidoptera,, 290-330 million years ago. An independent set of events happened in the ancestral lineage of Hymenopterans, between 240-340 million years ago. The key feature of Holometabola is that the insect has completely different morphologies in the larval and the adult states. It is possible the tactile sense in larvae is not fit for adult and need some adjustment. Another possible explanation is that to achieve better flight control, sensors became specialized for different types of mechanical stimulus.

Table 2-1 Primers for isolating *nompC* cDNA and reverse-transcription PCR

Primers	Sense	Anti-sense
nompC-ex1~9	accat ggtacc gctagctcatccccccctgcc	gatggatgctgctgcaggaag
nompC-ex9~12	gccaaactcttcctgcagcagc	cgtcactgaagtagcctctatttc
3.4A	cgcagcttcgagaagaagaacc	tggttagcgaggtgcgcgatgttgg
3.4B	cgcagcttcgagaagaagaacc	tcaagtacagttaacaattttatgcgctc
3.4F	cgcagcttcgagaagaagaacc	tggcatcatcgccgctggcattcgtc
nC-2-3'r		cgtcactgaagtagcctctatttc
nC3-3'poly-dT_XbaI		ttttt tctaga ttttttttttttttttttt

Figure 2-1 *nompC* gene structure

A) *nompC* gene structures. RA is the sequence published by Walker et al. (Walker et al., 2000). RD - RH are predicted transcripts in Flybase (FB2014_06). N15, N19, and N21 are the transcripts predicted by the Fgenesh-M program (Salamov and Solovyev, 2000). *nompC-L* is the isoform cloned by Cheng (Cheng et al., 2010). It is identical to RF except for the different start of exon 18.

B) Thirteen poly-A signals are indicated by green lines. Two more poly-A signals, lying downstream of exon 21, are not shown. The primer set 3.4A (black and orange arrowheads) was used to amplify transcript isoform RA or other transcripts including an extended exon 15. The primer set 3.4B (black and blue arrowhead) was used to amplify isoforms ending in exon 19. The primer set 3.4F (black and brown arrowhead) was used to amplify transcripts ending in exon 21.

C) Six *nompC* isoforms were isolated, including the RA (α) isoform, and I isolated three β isoform clones and nineteen γ isoform clones. Only exon 10 and after are shown. β and ε isoforms are have exon 13 and use exon 14 for pore region. γ and δ isoforms do not include exon 13 and use exon 15(short) for pore region and S6. ε, δ, and ζ isoforms have frame shift at exon 17 so they may not be functional.

D) Schematic of the NOMPC protein. Exons encoding the corresponding channel domain are labeled in the same color. Exon 12 encodes the transmembrane domain, with transmembrane helices S1~S5. Exon 13 encodes an extended pre-pore loop. Exons 14 and 15 encode similar but not identical pore region, S6, and part of the TRP domain. Exon 16 encodes the rest of the TRP domain.

Figure 2-1 *nompC* gene structure

A

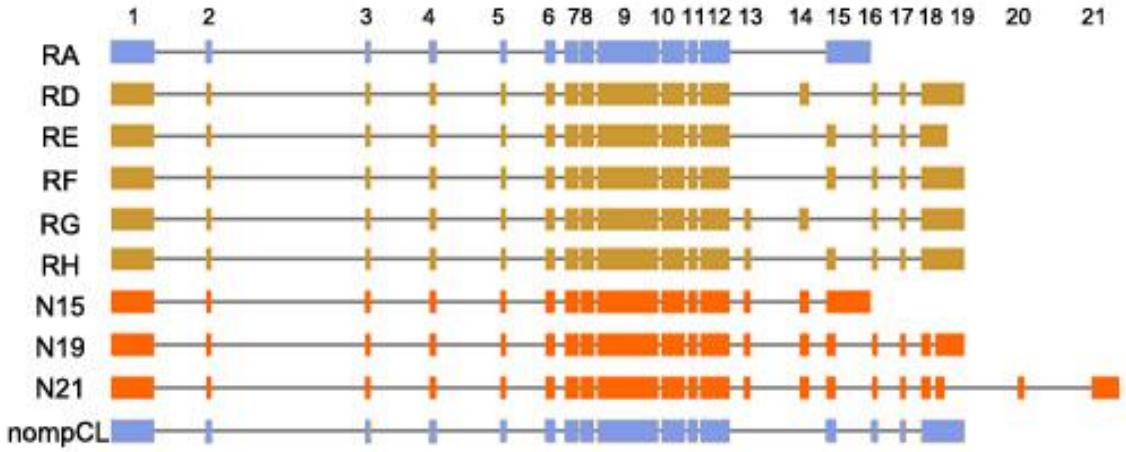

B

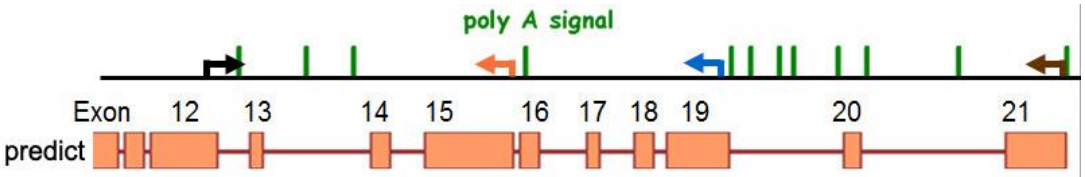

C

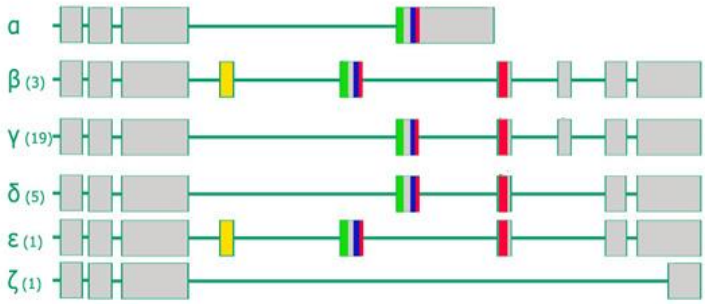

D

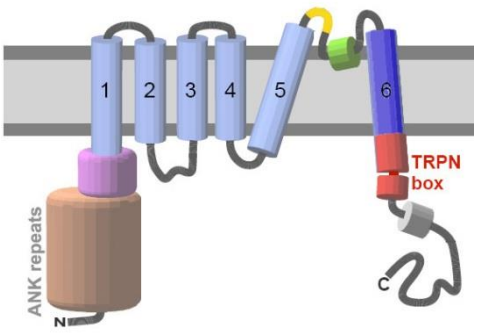

Figure 2-2 Alignment of *nompC* between *Drosophila* species

A) This is the VISTA genomic alignment of *nompC* exon 12 and after (position 5,360,000~5,368,000 in the *melanogaster* 2L sequence) between *D. melanogaster* and three other *Drosophila* species, *D. simulans*, *D. ananassae*, and *D. pseudoobscura*. Transcript RA is published by Walker (Walker et al., 2000), and RD is Flybase prediction. β, γ and δ isoforms are shown. For three rows of VISTA alignment, the Y-axis shows percentage identity from 50%~100%. Although the similarity of introns is reduced between the less closely related species, exons 12 to 19 have higher than 80% similarity. This indicates that exon 13 and 14 are functional in these *Drosophila* species. The extended exon 15 in RA is not conserved between these *Drosophila* species.

B) According to the well-defined *Drosophila* phylogenetic tree (Clark et al., 2007), *D. melanogaster* diverged from *D. simulans*,*D. ananassae*, and *D. pseudoobscura* 5, 43, and 54 million years ago, respectively.

Figure 2-2 Alignment of *nompC* between *Drosophila* species

A

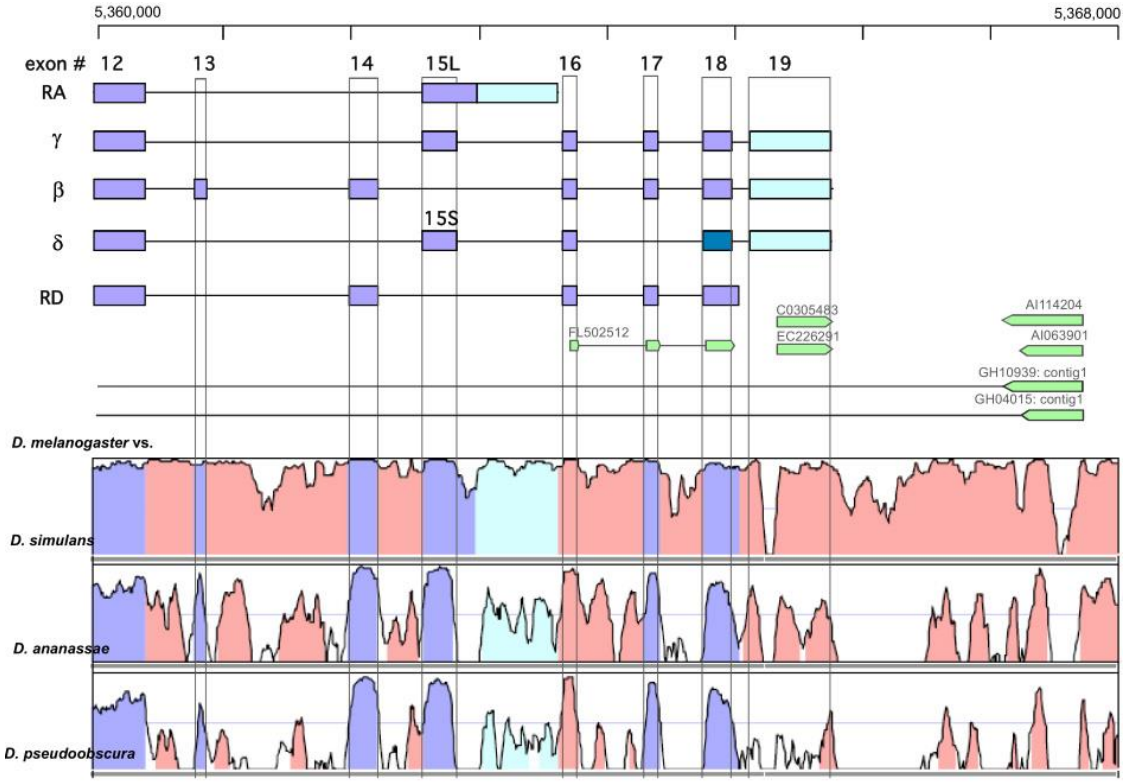

B

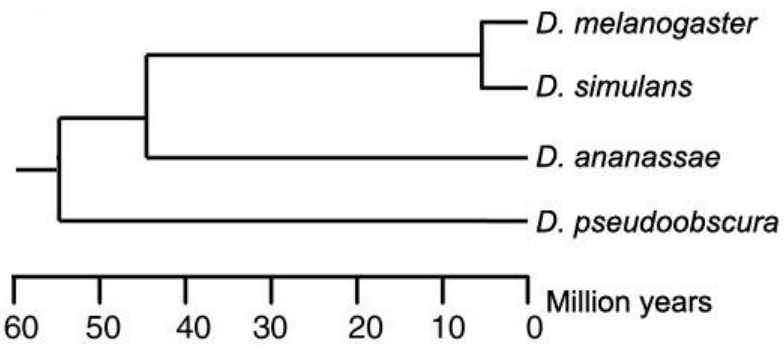

Figure 2-3 Amino acid alignment of exons 14 and 15 from *Drosophila*, mosquito, moth, and butterfly.

A) Schematic of a NOMPC single unit. The pre-pore loop encoded by exon 13 is labeled yellow. The pore helix is labeled in green. Transmembrane domains are labeled in blue.

B) Transcripts of *nompC* homologs, exon 12~18, in *Drosophila melanogaster*, *Anopheles gambiae* and *Bombyx mori*. All of them have two sets of pore helix, TM6, and TRP box encoded by exon 14 and 15.

C) Amino acid sequence alignment of exons 14 and 15 from two Dipterans, *Drosophila melanogaster* and *Anopheles gambiae*, and two Lepidopterans, *Bombyx mori* and *Danaus plexippus*. H1492 in exon 15 is a conserved positively charged histidine/asparagine before pore helix (green bar). R1582 in exon 14 is another conserved positively charged arginine/lysine. L1499 in exon 15 represents the same position as R1582 in exon 14 without charge, and it is conserved across species. The possible selective filter regions DIN1541-3 in exon 14 and QTQ1512-4 in exon 15 are also conserved across species. Other charged amino acids such as E1511, R1549, and Q1523 are also conserved.

Figure 2-3 Amino acid alignment of exons 14 and 15 between *Drosophila*, mosquito (*Anopheles*), silkmoth (*Bombyx*), and monarch butterfly (*Danaus*)

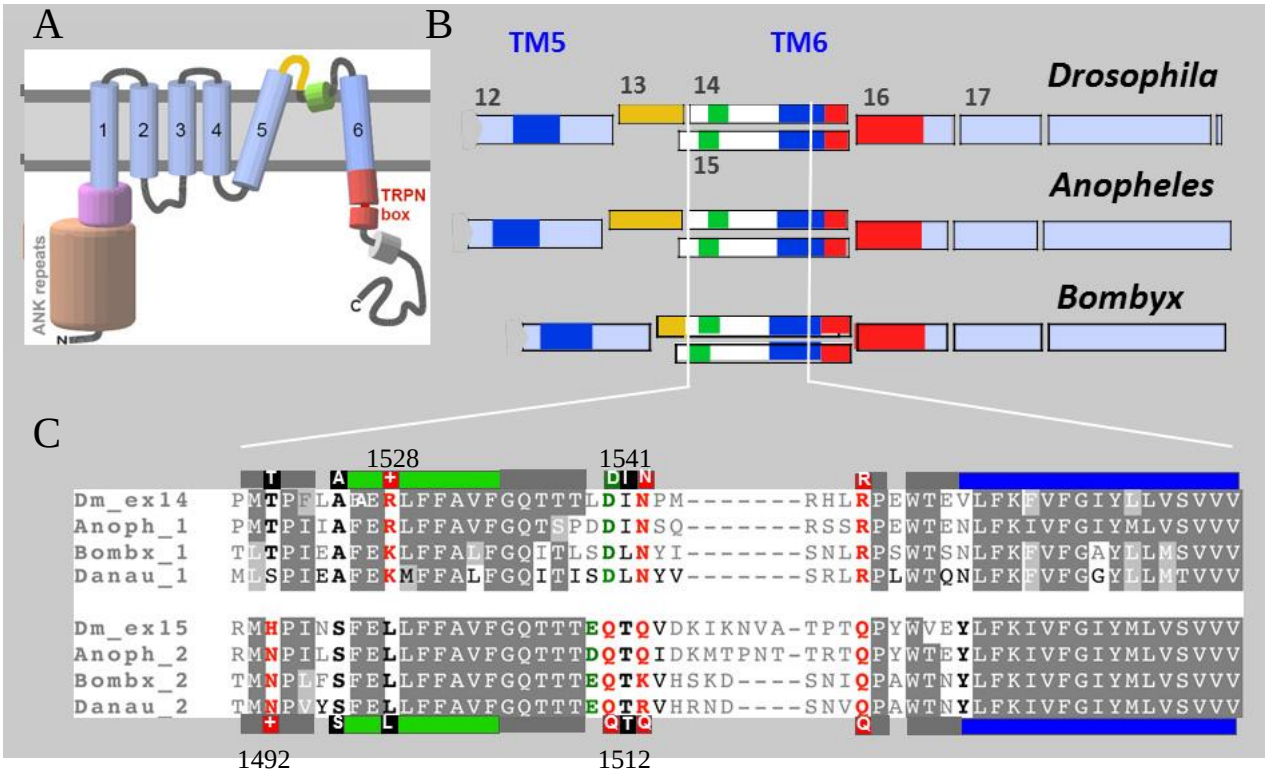

Figure 2-4 Alignment of NOMPC in Insecta

Schematic figure of the exons encoding the TM5 - C-terminal region of NOMPC across the Arthropoda. Exons are shown to scale; introns, not to scale, are indicated by gaps between exons. Common exons are shaded in light blue, with predicted protein motifs (TMs, pre-pore helix, TRP domain) colored. Presumptive alternate exons are in white, and are shown stacked; their order within each genome reads first (in Hymenopterans) left to right, then top to bottom. The status of the exons encoding the extracellular loop following TM5 in beetles and Hymenopterans is uncertain; it could be either constitutively spliced, or alternately spliced as in *Drosophila*.

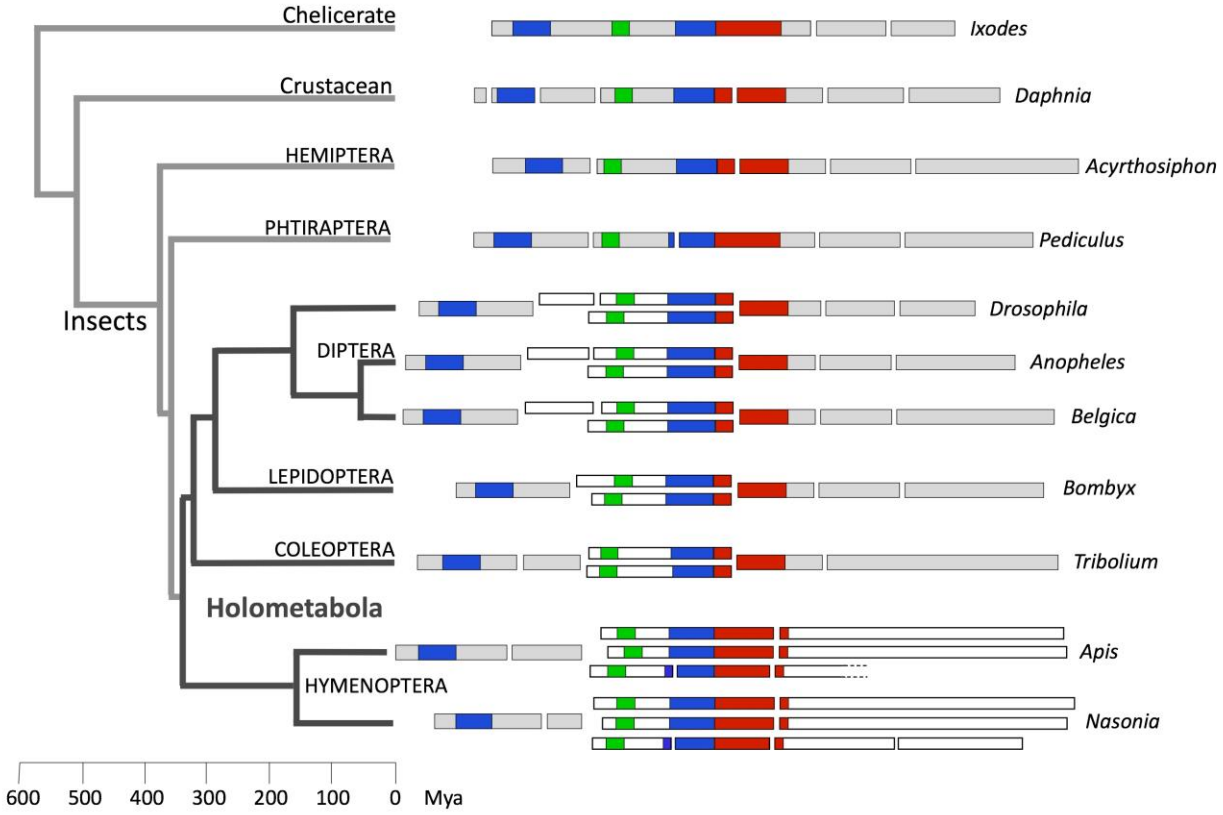

Figure 2-5 Phylogenetic tree of Holometabola

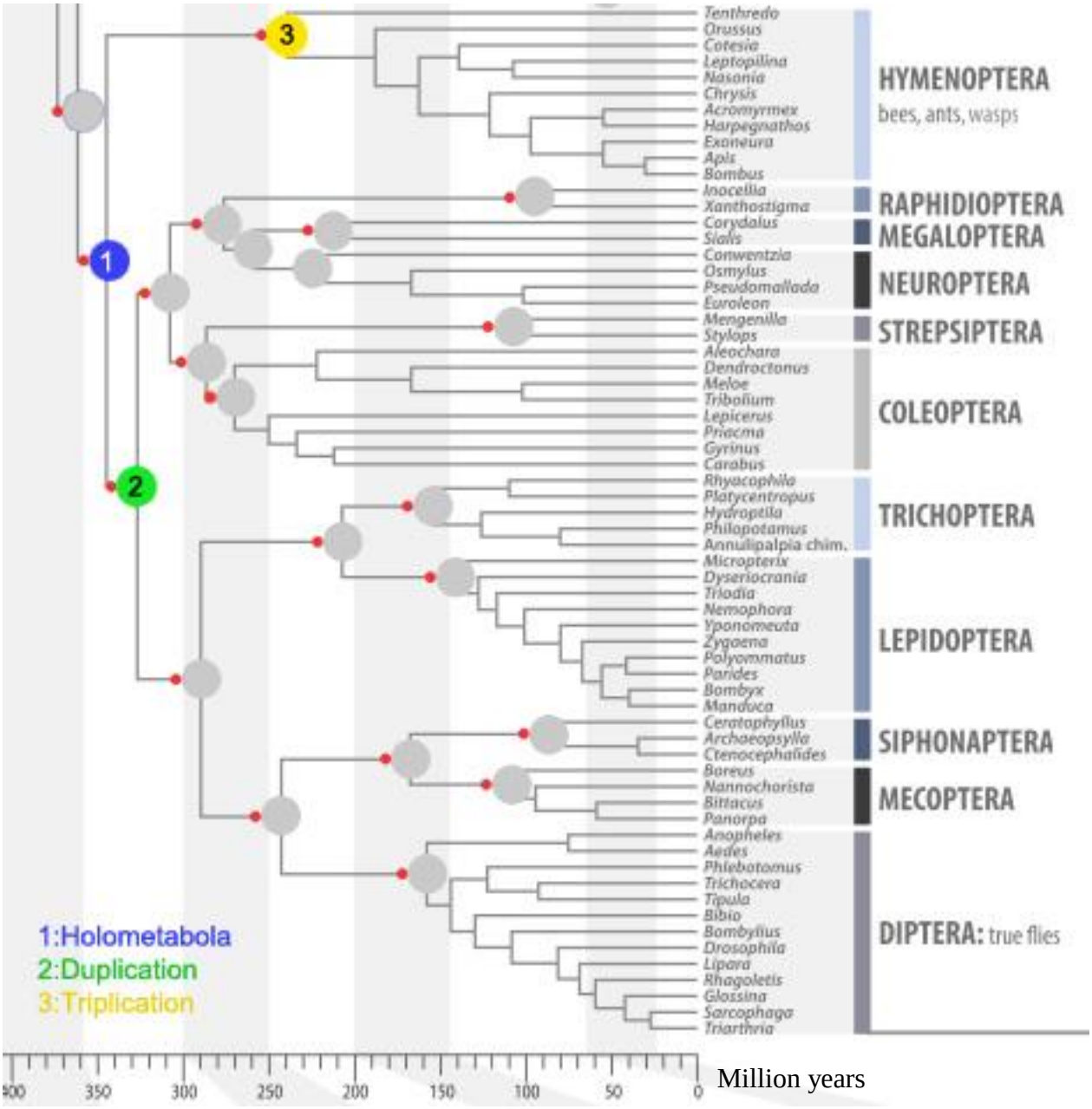

Using well-defined phylogeny of insect (Misof et al., 2014), all pore region multiplications happened in Holometabolan (node 1). The duplication in *Drosophila* happened when Aparaglossata started to diverge at least 327 million years ago (node 2), and the triplication in Hymenoptera happened at least 240 million years ago (node 3).

Chapter 3: Functional analysis of transgenic flies expressing defined NOMPC isoforms

Summary

The previous chapter described *nompC* transcripts including either of two exons that each encode predicted pore regions of the channel protein, and showed that these alternate exons are conserved in several Holometabolan insect orders. The conserved differentiation of specific residues in the probable channel pore region suggests that the isoforms have adaptive, differentiated functions, perhaps differing in channel permeability or selectivity.

To test if each subunit isoform was functional when expressed by itself, and to search for functional evidence of biologically significant differences between the isoforms, I compared their ability to restore normal locomotor behavior and sensory electrophysiology to *nompC* mutants. I constructed full-length *nompC* genes in which the pore region was derived from spliced cDNA sequences corresponding to the three major isoforms. These constructs were placed, by transgene insertion, and genetic recombination, into a null mutant background, so that the transgenic flies could express only one isoform, or a known combination of isoforms. Transgenic flies were compared to wild type and mutant controls in simple assays for walking and climbing ability. I also recorded NOMPC–dependent receptor currents from single mechanosensory bristles in transgenic and control flies.

The α isoform transgene was non-functional in all assays, behavioral and electrophysiological, probably because it does not have enough TRP domain to hold channel structure together. The β and γ isoforms could rescue locomotor activity when expressed in

isolation, and their combination gave performance that was the closest to control group while climbing. Bristles in flies expressing β or γ isoforms both showed adapting bristle mechanoreceptor currents, but differed in their current properties, with bristles expressing the γ isoform having a greater peak amplitude, faster adaptation and a proportionally smaller non-adapting current than bristles expressing the β isoform. Bristles expressing both isoforms showed currents with intermediate properties.

Materials and Methods

i. **Fly stocks**. *nompC* null alleles *nompC*^{1}, *nompC*^{2}, and the hypomorphic allele *nompC*^{4} were described (Walker et al., 2000). The integration site stocks *attP_51D* and *attP_58A* (Bloomington stock center # 24484 and #24488) are used for *nompC* rescue construct insertion by ΦC31 integrase mediated site specific integration (Bischof et al., 2007). Both lines were recombined with *nompC*^{2} before microinjections. A stock with the transgene *nompC*^{28}*-GAL4* (Sun et al., 2009) was a gift from Dr. Daniel F. Eberl. The transgene includes 2kb of the region upstream of the *nompC* translation start site.

ii. **Reverse transcription-PCR**. Total mRNA was isolated from 50 antennae of Oregon-R adult fly following a standard TRIzol protocol (http://www.mrcgene.com/tri.htm). cDNA was reverse transcribed by Transcriptor reverse transcriptase (Roche) with 3' primer nC-2-3' r for fragment 1 and fragment 2, nC3-3'polydT_XbaI for fragment 3a, 3b, and 3f.

iii. **Molecular cloning**. The *nompCβ* and *nompCγ* rescue constructs were generated by joining four fragments (Figure 3-1), two of which were amplified from wild type (Oregon R) cDNA templates and two from cloned genomic DNA. Fragment 0 starts 1.7 kb upstream from the *nompC* ATG, right after a natural transposon (Doc) insertion, and includes exon 1, intron 1 and part of exon 2. Fragment 1 includes exon 2 to the middle of exon 9. Fragment 2 includes the rest of exon 9 through exon 12. The different versions of fragment 3 each include a different set of exons after exon 12. Fragment 0 was PCR amplified from a *nompC*-containing BAC clone (BACR05M06) with nC0.1KpnI_S (5'-caaggaacgtagagagtaacatgg) and nC-0.1r_AS (5'-ctcaatcatgcgatccattatggc). Fragment 1 was PCR amplified from the cDNA with primers nC-1.1r_S (5'-ctgggcgccgatgtgggag) and nC-1.1-enPst_AS (5'-tgcaggaagagtttggccacttc). We first attempted to amplify fragment 2 from cDNA but multiple

point mutations in the amplified product were produced and could not be eliminated. Instead because all three introns in this fragment are less than 75 bp, fragment 2 was amplified from the *nompC* BAC clone with primer nC-2.1_enPst_S (5'-gcagcatccatccctggtgaatg) and nC-2.2_AS (5'-cagatcctccggtgagaaattggc). The alternate cDNA segments for fragment 3 were PCR-amplified from total antennal cDNA using the 5' primer nC-3.1-5' (gccaatttctcaccggaggatctg), and 3' primers nC-3.4a1 _AS (tggttagcgaggtgcgcgatgttgg), nC-3.4bc1 _AS (tcaagtacagttaacaattttatgcgctc), or nC-3.4f1_ AS (tggcatcatcgccgctggcattcgtc) for the three predicted 3' ends. All fragments from RTPCR were cloned into the pCR2.1-TOPO vector with a TOPO TA cloning kit (Invitrogen). Fragment 0 and fragment 1, which were designed partially overlaped, were linearized and joined by PCR extension with primers nC-0.1KpnI_S (5'-caaggaacgtagagagtaacatgg) and nC-1.2-enPst_AS (5'-ggaagagtttggccacttcagag). Fragment 2 was joined to each of the fragment 3 isoforms, also by PCR extension, with primers nC-2.1 enPst_S and M13R (5'-caggaaacagctatgac) to include BamHI site on the vector. Each fragment (2+3x) was cut with PstI and BamHI and ligated into the plasmid containing fragment (0+1) to complete the transgenes. Then the complete gene was transferred into a pTattB vector for microinjection. The pTattB vector was modified from pPTGAL (Sharma et al., 2002) by deleting the PstI GAL4 fragment and inserting a BamH1-PstI fragment containing *attP*, the ΦC31 integrase-mediated integration site,. I also introduced a SpeI site and killed the PstI site (Appendix, Fig. A-1).

UAS-nompCβ and *UAS-nompCγ* constructs (referred to in Chapter 4 but described here for convenience) were generated by fusing 1xUAS-HSP70, *nompC* exons 1~3, and *nompC* exons 4~18. *nompC* exon 1~3 was amplified from total antennal cDNA by primers UnC1-5.2BglII (5'-atccc agatct ccggattgtggagcagtaactag) and UnC1-3.2XbaI (5'-agttt tctaga gcgagccaccggtggagaag) and subcloned into pUAST vector at 3' of 5xUAS-HSP70. 1xUAS-HSP70-exon1~3 fragment was amplified by primers UAS-KpnI (5'-catgc ggtacc gtcggagtactgtcctccgagc) and UnC1-3.2_XbaI (agttt tctaga gcgagccaccggtggagaag), digested by KpnI and BamHI, and ligated to partial digested *nompC* exon 4~18 in pTattb vector (Appendix, Fig. A-2 and 3).

iv. **Single isoform rescue**. Two *nompC*α lines, six *nompC*β lines, and three *nompC*γ lines were acquired at the *attP_51D* landing site but none at the 58A landing site. I recombined

attP_51D flies with the *nompC*^{2} mutant allele before integrating transgenes into them to ensure the genetic background similarity. Crossing these rescue lines with CRE lines removed the loxP-flanked RFP and GFP markers at the *attP_51D* insertion.

v. **Immunohistochemistry**. It was performed with a standard protocol (Rajan et al., 2009). 48~72 hours after pupa formation (APF), pupal antennae were dissected and fixed in 4% formaldehyde in PBT for 15~20 min and washed in PBT for 10 min three times. The primary antisera used are: rabbit anti-NOMPC (1:50 dilution) (Lee et al., 2010), which is directed against N-terminal cytoplasmic protein segment (amino acids 14-117), expected to be common to all isoforms expressed; and mouse monoclonal Ab 22C10 (1:100), which detects microtubule-associated protein Futsch in neuron (Zipursky et al., 1984). The secondary antibodies used are: Alexa Fluor 488 and 546 (Molecular Probes, both 1:1000).

vi. **Flat chamber walking assay.** Each fly was anesthetized on ice briefly and placed alone in a closed circular arena (diameter 35mm; high 3.5mm). The chamber has 3.5 mm space between floor and ceiling to constrain the fly to walk only. The tests were performed at room temperature. After 5 minutes recovery, free walking behavior was recorded in 60 frames per second format for 10 minutes (Fig.3-3A). 4 frames per second walking tracks were digitized by C-trax (http://ctrax.sourceforge.net/), (Branson et al., 2009). The total walking distance was calculated by Behavioral Microarray Matlab Toolbox.

vii. **Slope climbing assay.** The climbing assay was done in an enclosed rectangular plastic chamber (12cm X 8.5 cm X 3.5mm) set at 75 degrees from horizontal to induce negative gravitaxis. A fly anesthetized on ice is placed at one end of the chamber and allowed to move freely in the chamber. After recovery for 5 minutes, test box was shocked to drop the fly to the center of bottom line before recording. Each trial was videorecorded from when the fly starts to walk until it reaches the top or side of the chamber, or stops for more than 3 seconds. Walking tracks were digitized by C-trax (http://ctrax.sourceforge.net/),(Branson et al., 2009). Walking velocity and acceleration are analyzed by Behavioral Microarray Matlab Toolbox.

viii. **Mechanoreceptor current recording**. To record mechanoreceptor currents (mechanically evoked transepithelial currents) we followed the protocol published by Walker (Walker et al., 2000). A 2- to 7 day-old fly is anesthetized on ice for 5 min then its head and wings are removed. The fly body is impaled from neck opening through the thorax by a chlorided silver pin, which serves as the electrical ground and the holder. The anterior notopleural (ANP)

bristle on each side is cut to half its length with a microscissors (FST, model 15000-08), and the fly and pin (mounted in a holder) are fixed to a rotatable and translatable stage. A micropipette pulled from thin-walled glass blanks (World Precision Instruments, TW100F-3) is filled with a high-potassium saline, with ion concentrations as measured in the receptor lymph of *Calliphora* (Grunert and Gnatzy, 1987), then the tip is broken to an opening larger than the bristle diameter. The micropipette is mounted on a piezoelectric microstage, controlled by a voltage step driver (Burleigh, Inc.) and placed over the cut ANP bristle end so that a step displacement stimulus deflects the bristle towards the body wall (Figure 3-5A). To measure transepithelial currents, the transepithelial potential (TEP) is controlled by a voltage-clamp amplifier (List Medical, Patch Clamp L/M-EPC7). The TEP is clamped at a holding potential in the range from +70mv to -200mV before applying a mechanical stimulus. At each holding potential, the baseline current is measured before the stimulus, to calculate the transepithelial resistance (TER). The recordable TER range is from 70~400 MΩ. For quality control, only TER recordings with standard deviation smaller than 1.5 fold of mean (SD<1.5X mean) are used for further analysis. We used SuperScope II (GW Instruments, Inc.) for data acquisition and analysis. All the recordings were filtered with low-pass Hamming window (sample rate 3.3%, frequency cutoff 168.3Hz) This filter will not distort the kinetics of rapid adaptating phase because the adaptation duration generally is between 30ms~110ms. One exception is the fastest adaptation in *nompC*^{4} allele (9.76 ms, holding TEP 60mV), which may be underestimated by the noise reduction filter.

Results

i. Assembling full-length, functional *nompC* genes

To confirm the function of *nompC* isoforms, generating rescue constructs is the crucial step. From the RTPCR result shown in chapter 2, we predicted that the most abundant β and γ isoforms are more likely to be functional so we generated a genomic-cDNA fusion construct of each of them with endogenous promoter (fig 3-1A). An α isoform rescue construct was also made to confirm our hypothesis of its lack of function.

Full-length *nompC* genes were amplified in four fragments from cloned genomic DNA and

antennal cDNA, because antennae have a high concentration of sensory neurons and sense many types of stimuli. The first fragment, which was designed to include the endogenous promoter, extended from 1.6kb upstream of the translation start site into exon 2, including the first intron. The second fragment extended from exon 2 to an endogenous *PstI* site in exon 9. The third fragment extended from this *PstI* site to the end of exon 12, and the fourth fragment, which included alternate exons and so varied between isoforms, is the rest (Fig 3-1A). Fragments were linked by PCR elongation when a restriction site was not available. Due to point mutations in fragment 2, we amplified this as a genomic region from a BAC clone instead of cDNA. All the transgenes are inserted into a specific attP locus in the second chromosome (51D) with $nompC^{2}$ mutant background by ΦC31 integrase-mediated integration (Fig 3-1B). The transgene flies were tested for single isoform properties, and the 51D flies were used as positive control in all experiments.

In these transgenic lines, anti-NOMPC antiserum detects NOMPCβ and NOMPCγ, but not NOMPC-α, at the tips of cilia, the location of the endogenous protein, in chordotonal organs (Fig 3-2). More detailed rescue results below from walking assays and receptor current recordings suggest that *nompCβ* and *nompCγ* encode functional products, while *nompC-α* does not.

ii. *nompCβ* and *nompCγ*, but not *nompC*-α, rescue the *nompC* mutant walking phenotype.

$nompC^{2}$ null mutant flies show eclosion and locomotor defects: an adult coming out of pupa with help moves its legs uncoordinately and almost cannot walk (Fig. 3-3B). *nompC* null mutant flies carrying a *nompCβ* or *nompCγ* rescue construct can eclose from pupal cases and have normal activity in vials. *nompC*-α, on the other hand, mostly cannot eclose by themselves and walk uncoordinately like *nompC* null mutant.

Walking involves both tactile and proprioceptive feedback, which are interrupted in *nompC* mutants. To understand the behavioral consequences of the isoforms in more detail, we analysed fly locomotor activity in both flat and sloped chambers.

For the flat chamber walking assay, each fly was anesthetized on ice briefly and placed in a 35mm diameter arena. After 5 minutes recovery, its activity was recorded for 10 minutes and total moving distance was traced by Ctrax (Fig. 3-3A).

Compared to *nompC*^{2} mutant flies (8.0±4.5mm), placing either *nompCβ* (312.6±244.2mm) or *nompCγ* (447.3±437mm) transgenes in a *nompC*^{2} mutant background restored locomotor activity back to control level (Fig. 3-3B). This indicates that either *nompCβ* or *nompCγ* isoform can rescue the walking behavior *nompC* null mutant . In contrast, flies with *nompC-α* in *nompC*^{2} background (48.8±18.4mm) also had improvement in locomotor activity, but they were uncoordinated, fell a lot, and moved significantly less than flies with either *nompCβ* or *nompCγ*.

Most recorded movements were due to the flies beating their wings and tumbling around. The α isoform transgene was non-functional probably because it does not have enough TRP domain to hold channel structure together.

The slope climbing assay is designed to promote fly negative gravitaxis: walking speed and acceleration are measured in a situation where the fly can move freely but generally moves upward. In this assay, fly lines carrying *nompCβ*, *nompCγ*, or one copy of each rescue construct in a *nompC*^{2} mutant background were measured for speed and acceleration. Each fly was allowed to walk freely in a container on a 75 degree slope and video recorded until they reached the boundary or stopped (Fig 3-4A).

nompC mutant flies expressing either the β or the γ isoform rescued walking ability on slope to different levels. *nompC* mutant flies heterozygous for both *nompCβ* and γ transgenes (5.17±1.27 mm/s) moved as fast as wild type control 51D lines (5.15±1.22 mm/s, p=0.96). The mutant flies expressing NOMPCγ (4.27±1.29 mm/s) were slower than control, and flies with NOMPCβ (3.95±1.42 mm/s) were the slowest (Fig 3-4c). *nompC*^{2} mutants were not tested in the climbing assay, because of their severe locomotor defect. These results are consistent with those from the flat chamber walking assay. Both *nompCβ* and *nompCγ* isoforms rescue *nompC* null mutant uncoordinated walking phenotype, but there is a difference between the isoforms. This data suggests when we promote movement by negative gravitaxis, it reveals a speed difference between flies expressing the different isoforms. More experiments need to be done to determine whether this difference is due to the sense of gravity being affected by NOMPC isoforms.

When observing the speed of single fly walking (Fig 3-4B), I found that some flies showed an overall slowing trend; they walked more and more slowly during the assay. To test if this

trend differed between single-isoform expressing lines, I calculated the change in average speeds, over sequential one-second intervals, of each genotype. All the groups are significantly different from each other. Considering decelerating from fast to slow: 51D control flies showed a greater reduction in speed, followed by flies carrying *nompCβ* /γ, *nompCβ*, and *nompCγ* (Fig. 3-4D). There is a trend that the faster their initial speed is, the sooner they get tired. One exception is *nompCγ* lines due to their variable climbing patterns. This slowing trend may reflect flies with different isoforms sensing the gravity differently or fatigue during rushing toward the top.

iii. Mechanoreceptor current kinetics differ between bristles expressing different isoforms.

To investigate the electrophysical properties of mechanosensory neurons expressing defined NOMPC isoforms, I recorded the trans-epithelial current (TEC) from a macrochaete bristle, the anterior notopleural bristle, before and during mechanical stimulation. Currents were recorded through a moveable glass microelectrode connected to a cut bristle, relative to a ground electrode placed inside the thorax (Figure 3-5A). This setting is analogous to an extracellular recording from a single neuron, because there are tight junctions surrounding the apical lymph space of each bristle. The preparation is described in detail under "Mechanoreceptor current recording".

When a bristle is moved, and transducer channels in the sensory are opened, the TEC is increased by cations moving from the apical lymph space into the cilium and sensory process. Because a direct patch clamp on the neuron is unachievable, I held the trans-epithelial potential (TEP), at levels ranging from –200mV to +70mV, to partially control the apical membrane potential. For example, holding the TEP at +25mV is equivalent to +95mV apical transmembrane potential for the neuron, assuming a -70mV resting potential across the basolateral neuronal membrane. The resting TEP in a wild type fly, which is maintained by electrogenic ion transport by sensory support cells, is usually +20 to +30mV. The current flow during stimulus is considered the mechanoreceptor current (MRC).

We consider two components of the receptor current. One is an adapting component which rises quickly to a peak (I_{MAX}) within 10msec after the stimulus onset and decays exponentially.

The non-adapting component $I_{plateau}$, is maintained throughout the stimulus (Fig. 3-5B). To calculate an actual $I_{plateau,}$ I chose the median value of the TEC in two time windows, 400~700ms (Fig 3-5D) or 800~1100ms (Fig 3-5E) because in few recordings the baseline drifted at the end of stimulus and made the $I_{plateau}$ hard to measure. The data from holding TEP values below -70mV were unpredictable because -70mV in TEP is about equal to 0mV at neuron membrane, and any lower holding TEP is considered not physiological resting membrane potential.

Compared to wild type, bristle currents in NOMPCβ expressing flies have a smaller peak current and a larger non-adapting component. Conversely, bristles in NOMPCγ expressing flies showed a larger peak current and smaller plateau (Fig. 3-5C). When the ratio of I_{MAX}-$I_{plateau}$ to I_{MAX} is plotted against holding TEP (Fig 3-5D-E), this property is more clear. Bristles of *nompCγ* heterozygous flies show current properties similar to wild type. Bristles of *nompCβ*/ *nompCγ* heterozygous flies show intermediate current properties. In chapter four, I found that the notum bristle ES neurons only produce γ isoform splice reporter, FSR-γ. These data support that notum bristles only express NOMPCγ. One interesting finding is that the adaptation is slightly voltage dependent in all groups: the degree of adaptation rises with holding TEP.

The first thing I noticed was that the TEC traces in flies expressing only NOMPCγ were stacked together in Fig. 3-5C because these flies have a higher trans-epithelial resistance (TER). The TERs of bristle of transgenic flies were summarized in Fig. 3-S1. The TER of ANP bristle in a wild type fly is about 200 MΩ. Bristles in NOMPCγ expressing flies have the highest TER, and bristles in NOMPCβ expressing flies have the lowest. TER of the bristles in NOMPCβ/γ expressing flies is similar to TER in 51D fly bristles. The actual TER of bristles in NOMPCβ flies may be still lower, and the TER of bristles in NOMPCγ flies may be higher, because only bristles with TER around 40~500mΩ can be recorded reliably in this method. These results suggest that NOMPC- β may form an easily opened channel, and NOMPCγ may form a channel with smaller open probability. Another genetic background difference between 51D and transgene flies is the recombination region between *nompC* (cytogenetic map: 25D6-7) and 51D (cytogenetic map: 51D_r5).

I calculated the time constant, the time for adaptive signal to drop to 1/e of the peak value, of the exponential decay of adapting current only (Fig. 3-5B) because our equipment is not fast enough to resolve the fast rising phase part. Bristles in NOMPCγ expressing flies (51.1±20.2ms, at 0mv) has similar time constant to wild type NOMPC (52.2±23.3ms, at 0mv), and time constant of bristles of NOMPCβ expressing flies is much larger (396.3±229.6ms, at 0mv, Fig 3-5F). Adaptation is faster, and time constants are smaller, at higher values of the holding TEP.

With flies expressing single isoforms, I demonstrated that both NOMPCβ and NOMPCγ can restore null mutant functions in locomotor and receptor currents, and two isoforms have different properties.

Figure 3-1 Assembly of *nompC* single-isoform rescue constructs

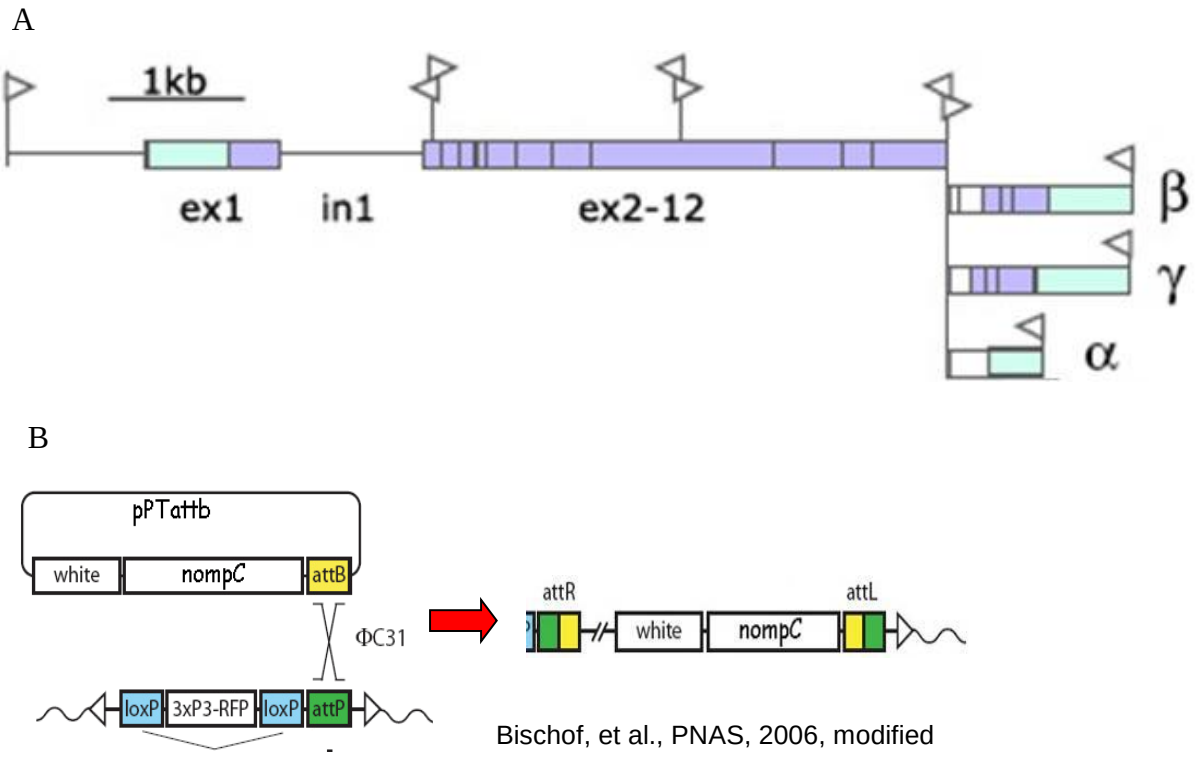

Figure 3-1 Assembly of *nompC* single-isoform rescue constructs.

A) Schematic of the transgenes. Primers used to amplify the four fragments are labeled with arrowheads. Exons are labeled in purple, and 3'UTR is labeled in light blue. 1.6kb sequence before ATG and intron 1 were included as potential regulatory regions. Three isoforms have the same exon 1 to 12. After exon 12, α isoform has a long form of exon 15; β isoform has exon 13~14 and exon 16~19; γ isoform has short form of exon 15 and exon 16~19.

B) Transgenes in pTattB vector were integrated into attP site at 51D locus by ΦC31 integrase. *nompC*^{2} was crossed onto secondary chromosome of 51D_attP carrying fly before integrating. The attP insertion includes an RFP tag which was removed after attB integration by Cre expression.

Figure 3-2 Expression of NOMPCβ and NOMPCγ in antennal chordotonal cilia.

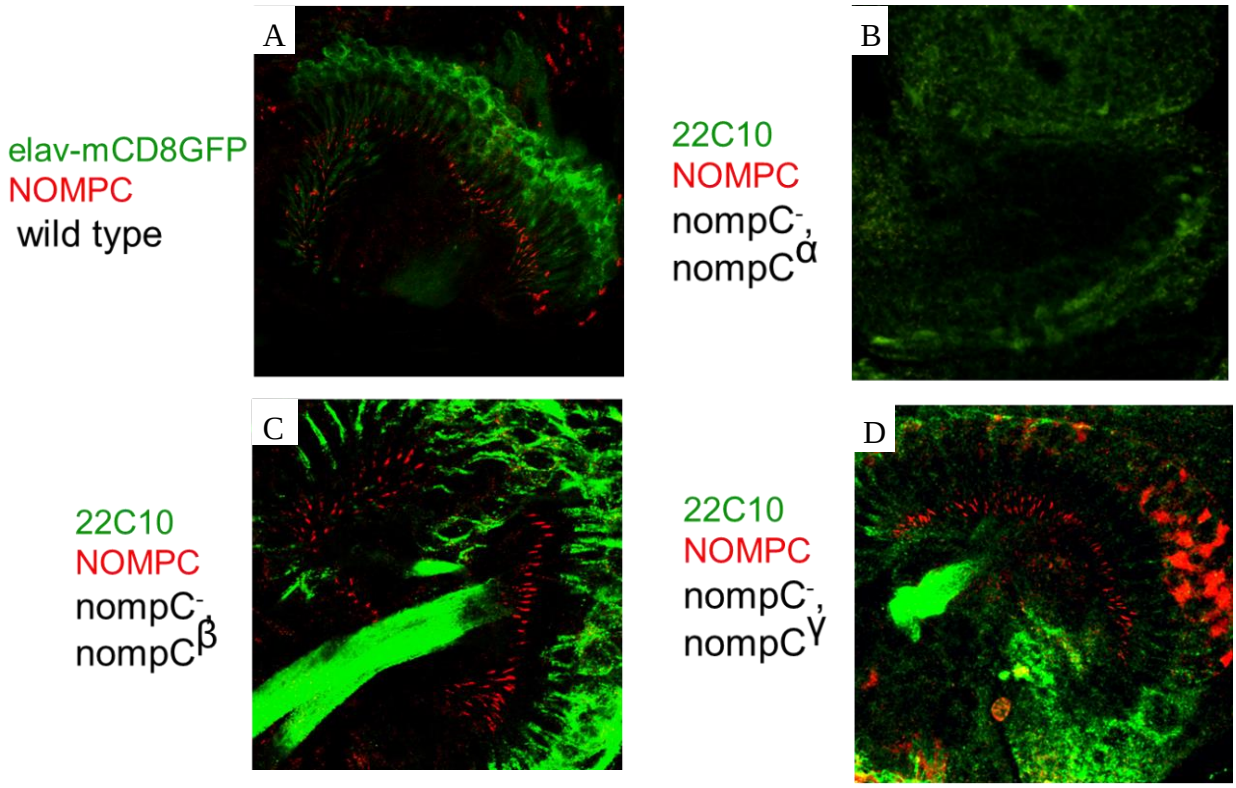

Figure 3-2

NOMPCβ and NOMPCγ driven by the endogenous promoter are expressed at distal part of cilia of chordotonal neurons in Johnston's organ (JO).

A) Anti-NOMPC antiserum detected NOMPC at distal part of cilia of CH neurons labeled by elav-mCD8GFP.

B-D) Chordotonal neuron cell bodies were labeled by 22C10 antibody, which labels a microtubule-associated protein. NOMPC was detected at the distal part of cilia of chordotonal neurons in JO of flies expressing only NOMPCβ (C) or NOMPCγ (D). No NOMPC was detected in JO of flies expressing NOMPC-α in null mutant background (B).

Figure 3-3 Horizontal locomotor activity is restored by either NOMPCβ or NOMPCγ.

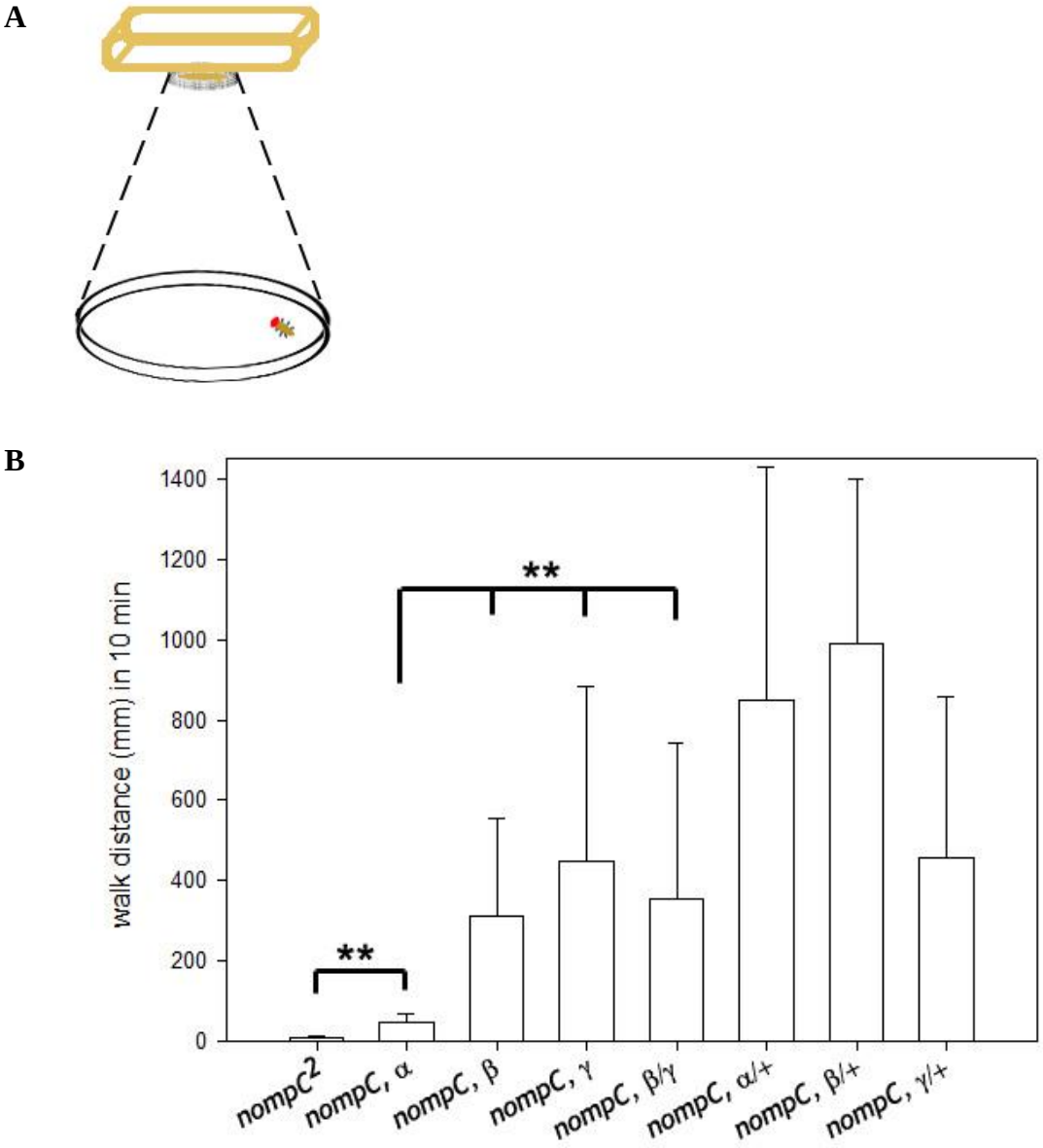

A) Schematic of locomotor activity assay.

B) Locomotor activity was restored in flies expressing NOMPCβ (312.6±244.2mm), NOMPCγ (447.3±437mm), or both NOMPCβ/γ (355.2±387.3mm) in *nompC*^{2} mutant background. *nompC*2 mutant flies almost cannot move (8.0±4.5mm). α isoform-bearing flies moved in an uncoordinated manner and much less (48.8±18.4mm) than the flies carrying the other two isoforms. Flies expressing NOMPCβ, NOMPCγ, or both walk normally like heterozygous control flies (α/+, 848.7±579mm; β/+, 988.9±410.9mm; γ/+, 457.2±403mm).

Figure 3-4 Climbing ability is restored by *nompCβ* and *nompCγ*

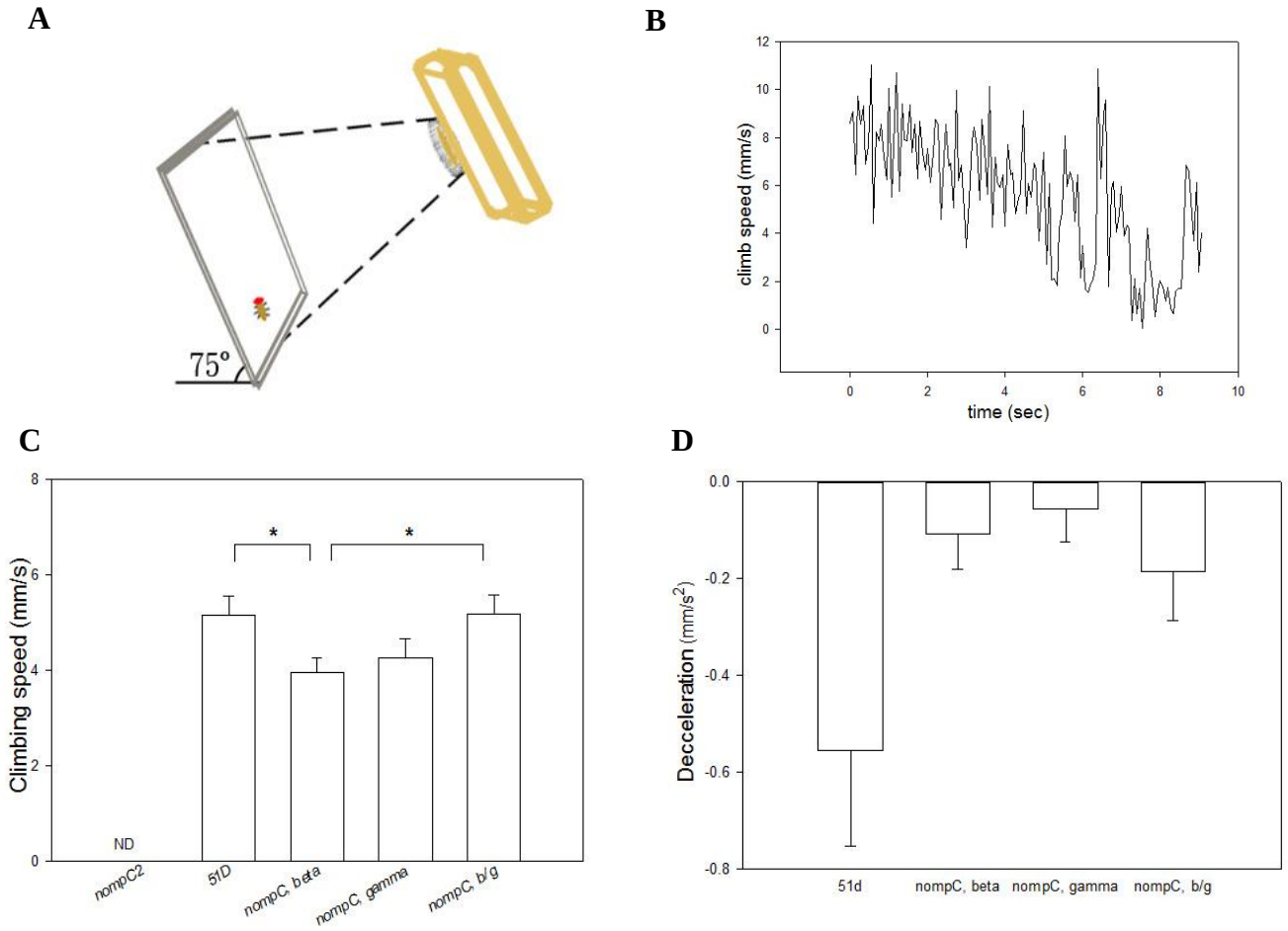

Figure 3-4 Climbing ability is restored in flies expressing either *nompCβ* or *nompCγ* in a *nompC*^{2} null mutant background.

A) Schematic of climbing assay.

B) Climbing speed of a 51D control fly recorded at 15 frames per second. The speed declined with time.

C) Flies with either *nompCβ* or *nompCγ* isoforms rescued climbing speed back to near that of 51D control flies. *nompCβ* only flies climb slower than 51D flies, and flies heterozygous for *nompCβ* and *nompCγ* isoforms climb as fast as 51D flies. The climbing speed difference between flies with only γ isoform and β/γ isoforms is not significant. *nompC*^{2} flies were not tested because they are completely unable to climb.

D) Flies with heterozygous for *nompCβ* and *nompCγ* isoforms (-0.18±0.10mm/s^2) decelerate more than flies with either *nompCβ* (-0.11±0.07mm/s^2) or *nompCγ* isoforms (-0.06 ±0.07mm/s^2).

Figure 3-5 Adaptation kinetics of mechanoreceptor current is different in NOMPCβ and NOMPCγ expressing bristles

A) Schematic of mechanoreceptor current recording. The fly is mounted on a chlorided silver pin inserted into the thorax, which also serves as a ground electrode. A glass microelectrode placed over the end of a cut bristle records the trans-epithelial current (TEC). To stimulate, the electrode is moved towards the fly body to deflect the bristle. The movement triggers cation flow from the receptor lymph space into the cilium, increasing the TEC.

B) TEC recorded at holding TEP 0mV from single wild type fly. The mechanical stimulus used in all trials is shown at the top. I_{MAX} is the peak value of TEC, $I_{plateau}$ is the median of given time windows, 400~700ms or 800~1100ms for Imax-Iplateau/Imax ratio in D and E, respectively. The time constant is defined as the time needed for Imax-Iplateau(1300~1600ms) to fall to 1/e of the peak value.

C) Part of TEC traces recorded at a set of holding TEPs from wild type fly, and *nompC*^{2} mutant flies carrying *nompCγ* or *nompCβ* rescue constructs. TEC of mutant fly with γ isoform has larger Imax and smaller Iplateau compared to a control (51D) fly. Conversely, TEC of mutant fly with β isoform has smaller Imax. The vertical trace distance between different holding TEP reflects the fact that bristles in mutant fly with γ isoform have a larger trans-epithelial resistance (TER), and bristles of mutant fly with β isoform have a smaller TER, compared to bristles of 51D flies.

D) Plot of the ratio of Imax-Iplateau (400-700ms)/Imax against holding TEP. The ratios in mutant flies with *nompC- γ* are almost identical to 51D control group when the holding TEP is above -20mV. The ratio of the *nompCβ* only group is significantly smaller than other groups when holding TEP is above -10mV except at 0mV. The ratio of flies with *nompC- β*/*nompC- γ* is between *nompCβ* and *nompCγ* only group.

E) Plot of Imax-Iplateau (800-1100ms)/Imax ratio against holding TEP. The ratios in mutant flies with *nompCβ/γ* are significantly smaller than wild type or *nompCγ* only group when holding TEP is above -20mV. Ratio of *nompCβ* only group is significantly smaller than other groups when holding TEP is above 0mV.

F) Time constant of *nompCβ* only group (396.3±229.6ms, at 0mv) is much larger than other groups (*nompC*^{2} *nompCγ*, 51.1±20.2ms; wild type, 52.2±23.3ms, at 0mv).

Figure 3-5 Adaptation kinetics of mechanoreceptor current is different in NOMPCβ and NOMPCγ expressing bristles

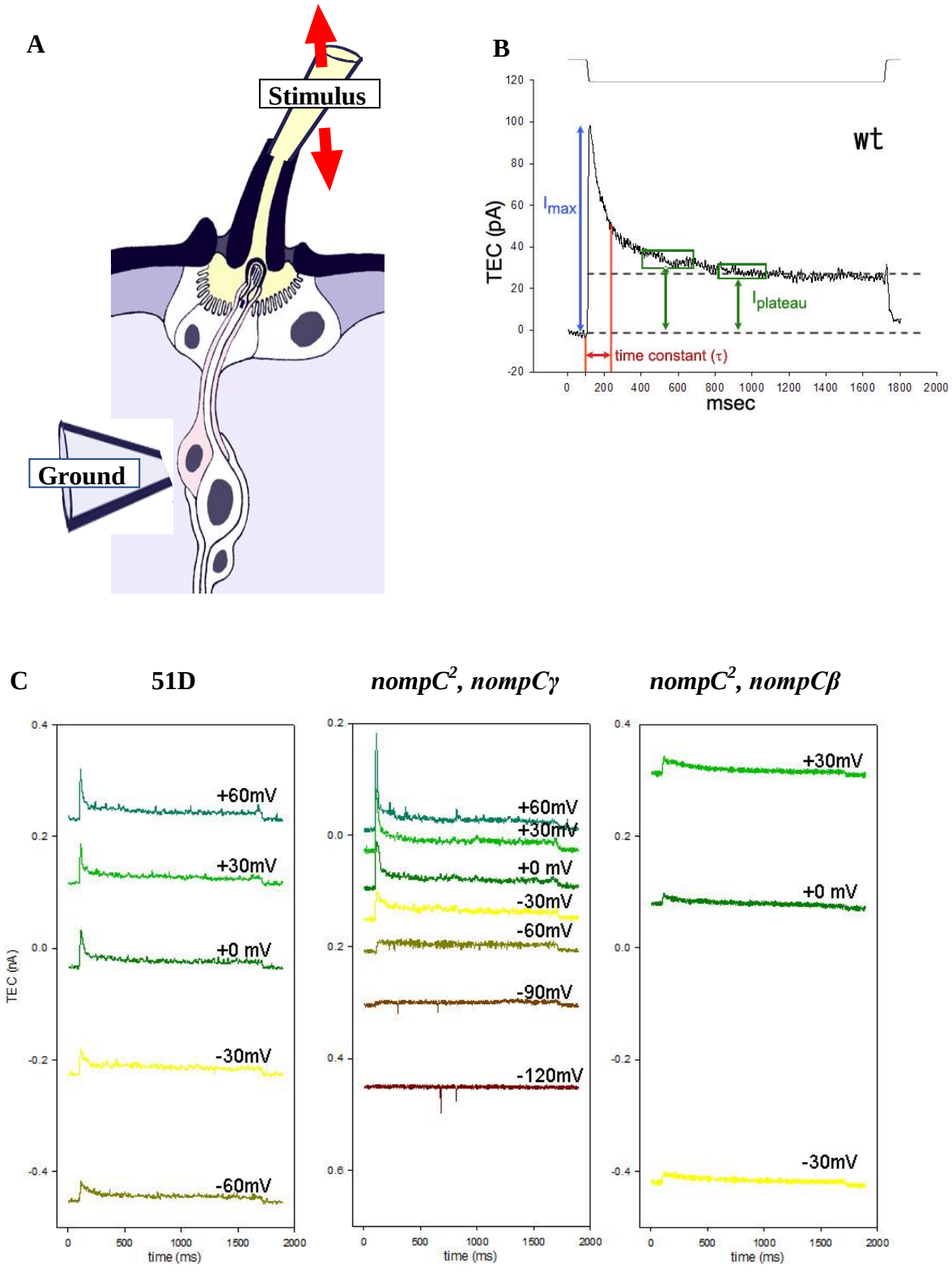

Figure 3-5 continued

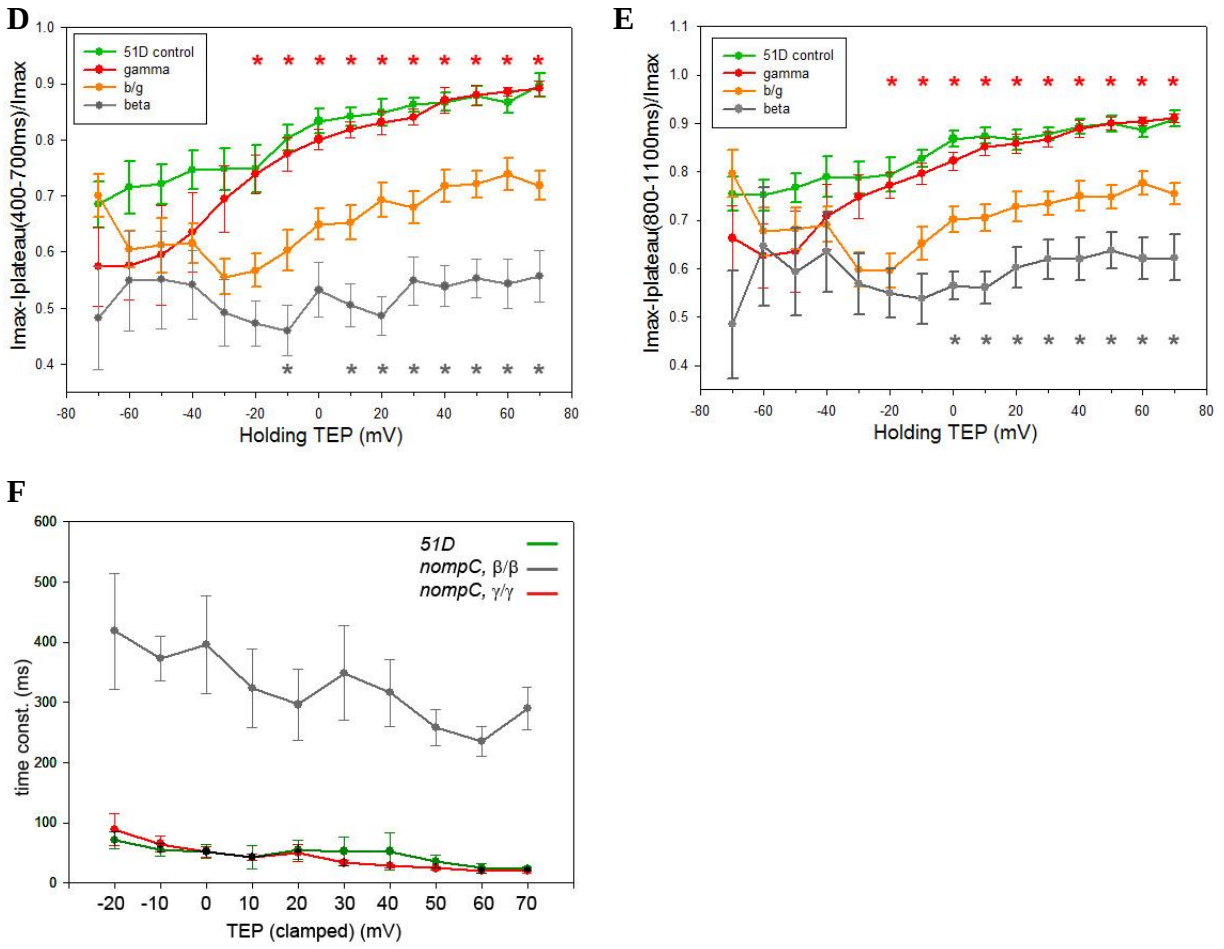

Figure 3-S1 Trans-epithelial resistance (TER) of bristles varies in different genetic backgrounds.

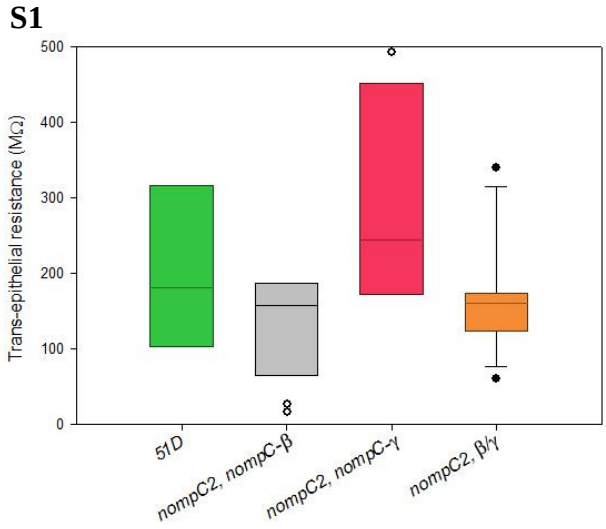

The TER of bristle in wild type 51D flies is 200.5±97.6MΩ. Bristle TER in *nompC*^{2} mutant flies carrying *nompCγ* is higher (315.9±182.8 MΩ), and the TER in mutant flies carrying *nompCβ* is lower (139.2±63.4 MΩ). Many recordings were discarded because the TER is too low or too high (small circles). The TER in mutant flies carrying *nompCβ/γ* is 163±68.9.

Chapter 4
Expression of *nompC β* and *nompC γ* isoforms

Summary

Other than functional differences, the two functional *nompC* isoforms that exist in the fly may differ in their expression patterns. I used QRT-PCR to detect *nompC* mRNA level in antenna, leg, haltere, whole adult body, and larvae. In antenna, leg, and whole body, isoform β and γ maintain an expression ratio about 1:4 to 1:6. In haltere, the ratio increases to about 1:2. This result indicates that *nompC γ* is the predominant form and that *nompC β* is enriched in haltere and may play a role there.

Because isoform β and γ cannot be detected separately by any available antibody, fluorescently-tagged splice reporter (FSR) genes were generated to reveal their expression patterns at the cellular level. *UAS- FSR-β* contains UAS, exon 1~11, genomic fragment of exon 12 to 18 with frame-shifted exon 15 to prevent γ isoform group being translated, and an eGFP tag. *UAS-FSR-γ* is similar to *UAS- FSR-β*, except that the exon 14 was frame-shifted here to prevent β isoform translation and tagged with tdTOMATO. When transcribed in all neurons, *elav-GAL4* drove FSR- γ expression in most of the cilia while FSR-β can only be produced in anterio-medial part of JO. When expressed in subsets of the Johnston's organ (JO) neurons, the β isoform-producing construct can only be translated in neurons that project to zones C and E of the antennal motor and mechanosensory center (AMMC). In contrast, FSR-γ can be produced by all JO neurons. In the femoral CHO, FSR-β and FSR-γ were expressed in different groups of neurons. In abdominal CHO, most of neurons are FSR-γ positive. In haltere, elav-GAL4 drove

FSR-β expression symmetrically in sensilla of both dorsal posterior and ventral anterior pedicellus. On the other hand, FSR-γ is expressed mainly in complementary parts of pedicellus. At wing hinge campaniform sensilla, FSR-β is expressed in most of cilia while FSR-γ only can be detected at basal part of it. In the wing vein campaniform sensilla, FSR-β was expressed in slow-adapting neurons and FSR-γ was in fast-adapting neurons.

Materials and methods

i. **Two step quantitative real-time PCR (QRT-PCR).** Whole 3rd instar larvae, whole adult, 100 adult antennae, 100 halteres, and 180 legs were harvested separately, homogenized, and the total RNAs were purified using an Insect RNA microprep kit (ZYMO Research). Total mRNA was transcribed into cDNA by Transcriptor reverse transcriptase (Roche Applied Science), with a standard protocol. Quantitative real-time PCR was performed using a LightCycler 480 system with SYBR Green I master mix (Roche Applied Science), following a standard 40 cycle protocol: this included annealing at 58℃ for 7 sec and elongating at 72℃ for 8 sec. Primers were designed using the Primer3 program (http://www.embnet.sk/cgi-bin/primer3_www.cgi) (Steve Rozen, 1998). The *rp49* ribosomal protein gene was amplified as a quality and quantity control. Two to four sets of isoform-specific primers were used to perform QRT-PCR to control for bias due to differences in primer efficiency. The primers are listed in table 4-1. A standard curve for each primer pair was generated by amplifying the serially diluted template plasmid (10^{1}~ 10^{5} -copies) with *nompC* null cDNA from 96~120 APF pupa (Fig 4-1S). Each experiment was repeated three times. The results were normalized to an average *rp49* reading within individual group. Due to the unavoidable overlap of the target region, the value for the alpha isoform was obtained by subtracting the gamma result from the combined alpha+gamma result.

ii. **Fly stocks.** Several GAL4 lines were used to drive transcription of full-length splicing reporters. *elav-GAL4 and nompC-GAL4*(attP154) were obtained from the Bloomington stock center (Bloomington stock center # 8760 and #36369). A fly stock with the transgene *nompC^{28}-GAL4* (Sun et al., 2009) was a gift from Dr. Daniel F. Eberl. The Johnston's organ-specific GAL4 lines, JO15, NP0761, NP1245, NP3259, NP5021, NP5035, NP6250, NP6264,

and NP6303 (Table 4-2) (Kamikouchi et al., 2006), were gifts from Drs. Ryan Kavlie and Joerg T. Albert.

iii. **Full length splicing reporter gene constructs.** *nompC* exons 1~11 were amplified from *UAS-nompCγ* construct by primers FSPex1-11SpeI_S (5'-catga actagt ccggattgtggagcagtaactag) and FSPex1-11XbaI_as (5'-acg tctaga aactccacgtttcgcttatcg). A single-nucleotide "T" insertion was introduced into exon 14 by amplifying two overlapping fragments, exon 11.9~14 and exon 14~18, with primers FSPex11.9-18XbaI_S (5'-gtt tctaga cgttctcattgaaaatgagcagaaggaagtgattgcccacacggtagttcagcgatacttgcaagaactctggcatggctccc)/ SP_ex14_TTC_AS (5'-caaacctgaatgcgctgAataagtatccgacatc) and SP_ex14_TTC_S (5'-gatgtcggatacttatTcagcgcattcaggtttg)/ FSPex16m-18XhoI_as (5'-gatga ctcgag gacctgtgccggtggctgttg) for FSR-14G from a *nompC* BAC clone. For the FSR-15T construct, primers SP_ex15_TTC_S (5'-gatgtcagacacctatTcaacgcattcaggtag) and SP_ex15_TTC_AS (5'-ctacctgaatgcgttgAataggtgtctgacatc) were used. Capital letter in the primers indicates the insertion base. The two fragments were then extended by PCR to form exon 11.9-18. eGFP (for FSRgamma) or tdTOMATO (for FSRbeta) were ligated to the 3' end of exon 18, and the whole construct was subcloned to 5xUAS inserted pTattB vector, pTUAS-attB (Fig 4-2B, Appendix A-4 and 5).

iv. **Wing vein extracellular potential recording.** (referred to in Chapter 5 but described here for convenience) We followed the protocol developed by Dickinson (Dickinson and Palka, 1987). The wing was cut at the tip and hinge, and two electrodes are connected to each end via saline pools. The stimulating probe was controlled by a piezoelectric step driver (Burleigh, Inc), and positioned so as to press 2~6um at the side of a campaniform sensillum. We used SuperScope II (GW Instruments, Inc.) for data acquisition and analysis.

Results

i. QRT-PCR showed the tissue distribution of *nompC* transcript isoforms.

To assay the expression level of *nompC* isoforms in different sense organs and developmental stages we performed two-step, quantitative, real-time PCR (QRT-PCR). Total mRNA of fly body parts, such as adult antenna, leg, and haltere were harvested to roughly represent CHO, ESO, and campaniform sensilla, respectively. The second segment of adult

antenna includes the largest chordotonal organ (CHO). Leg has many external sensory organ (ESO), and also includes a smaller, femoral CHO. Most campaniform sensilla (CS), a specialized ESO, are located on the haltere. RNA preparations were also made from whole adult bodies, and from the body wall of 3rd instar larvae. Total cDNAs were reverse-transcribed using random primers, and *nompC* segments were amplified using isoform-specific primer pairs (Table 4-1, Fig 4-1A). Absolutely quantity is calibrated for each pair of primers (Fig S4-1) by mixing in serial dilutions of the corresponding single isoform plasmid with total cDNA from *nompC* null mutant flies. An *rp49* primer set was used to establish a reference total cDNA level: all data for the same body part is normalized to the *rp49* value. The copy numbers of *nompC* transcript isoforms from different body parts should not be compared directly.

Overall, the γ transcript isoform is the most abundant. It is 7.3-fold more abundant than the β isoform in larvae and about 4- to 6-fold more abundant in whole adult body, leg, and antenna (Fig 4-1 B, C, D, F). The β isoform is produced at relatively higher levels in halteres, where it is about half of γ isoform expression (Fig 4-1E). Expression of the α isoform varied a lot between which may reflect it is an unstable, non-conserved, and truncated transcript. Expression of δ isoform is negligible (data not shown). These results indicate that the γ isoform is the major expression form, and suggest that the β isoform may have a specific function in the haltere.

There is no gender difference in *nompC* isoform expression. Male flies have about double the amount of *nompC* transcripts in whole body group when I tested the same amount of total cDNA for each sample. Female fly has larger body mass than male, therefore, more mRNA were collected from non-neuron tissues (Fig. S4-2). This indicates *nompC* transcript is not abundant in embryo.

ii. Building splicing reporter genes to reveal isoform expression patterns.

Because there is no NOMPC antiserum that can distinguish these two isoforms, splicing reporters were needed to reveal isoform expression patterns at cellular resolution. Splicing reporters need to produce differently labeled products depending on which alternate exon set is used without interfering with the potential splice regulatory sites in introns or exons.

My first failed attempt at constructing a reporter gene fused the genomic region of *nompC* from exon 12 to half of exon 16, with eGFP-tdTOMATO dual fluorescence gene. The grand design ideal was based on that of the Orengo group, who used eGFP and dsRed as the markers for alternative splicing screenings (Orengo et al., 2006). The whole construct was placed downstream of a UAS promoter. A single T nucleotide was inserted at exon 14 to generate a frameshift from the first to the third frame (Fig 4-2A). The eGFP is on first frame and tdTOMATO is on third frame. So in this 14T reporter gene, β isoform-positive cells, which translate exon 14, should express a protein that includes tdTOMATO and γ isoform expressing cells, which use exon 15, should express an eGFP-tagged protein. A second construct was the same, except that the insertion was in exon 15, so the fluorescent tags were reversed. Unfortunately, these reporter genes did not express any protein in my system so I redesigned simpler reporters. Without exon 1-11, they may be mis-folded or not be inserted to membrane.

The second, successful design is based on full-length *nompC* cDNA except for the region of interest, exon 12 to exon 18, which was derived from a genomic fragment (Fig. 4-2B). The UAS-FSR-γ construct has a single "T" nucleotide inserted near the end of exon 14 to generate a frame shift which leads to an early stop codon in exon16. A *eGFP* tag is ligated to the end of *nompC* fragment. Therefore, UAS-FSR-γ can only be translated into a full-length NOMPC-eGFP fusion protein if exon 15, not exon 14, is used. Conversely, UAS-FSR-β has a point "T" insertion in exon 15 and tdTOMATO fused at the C-terminus of NOMPC, and can only be translated into NOMPC-β-tdTOMATO if exon 14, and not exon15, is used. tdTOMATO is two tenden repeats of TOMATO which is a drivative of eGFP. The structure of TOMATO is almost identical to eGFP, and both marker are wildly used in life imaging (Shaner et al., 2004). The only down-side of tdTOMATO is that it is twice the size of eGFP.

The reporter genes were integrated into the ΦC31 integrase-mediated integration site attp at 86Fb locus in third chromosome. The GFP tag for attp site was removed by expressing CRE. Adult issues of interest are dissected and mounted directly for confocal imaging. The parameters of laser strength, signal gain, and offset were optimized to eliminate crosstalk between eGFP channel and tdTOMATO channel.

The splicing reporters are expressed in the cilia tips of mechanosensory neurons where the

endogenous NOMPC expressed, but in some cells, they also expressed throughout cell bodies and axons. Overexpression of FSRs by *nompC-GAL4* or *elav-GAL4* cannot rescue *nompC* null mutant eclosion defect. It probably is due to the tag at C-terminus of reporter genes interrupts NOMPC tetramer formation, but it does not affect the splice reporter protein production. Although *elav-GAL4* is expressed in all neurons including *nompC* expressing ones, the expression patterns of *UAS-FSR* constructs driven by *nompC*^{28}*-GAL4* and *elav-GAL4* are similar. This indicates that the splicing mechanism is neuron type specific and independent of transcriptional driver. Because *elav-GAL4* produces stronger and more reliable expression than *nompC-GAL4* lines, all the data shown here are UAS-FSRs overexpressed by *elav-GAL4*. This also enables us to see if the reporter splicing is also regulated in neurons where *nompC* is not normally expressed.

iii. A correlation with sensory adaptation: splice reporter expression in wing blade sensilla.

The clearest indicator of the functional significance of the different isoforms comes from their expression in the isolated sensilla on the wing blade. There are eight CS on the wing vein, and they belong to two groups (Dickinson and Palka, 1987). The early development group includes GSR, dTSM, ACV, and L3-2, and they are fast-adapting sensilla which only respond to onset and offset of the stimulus. The late development includes L3v, pTSM, L3-1, and L3-3, and they are slow-adapting sensilla which fire continuously during stimulus (Fig. 4-3A).

On wing vein sensilla, FSR-β is produced in L3v, pTSM, L3-1, L3-3, and dHCV. FSR-γ is produced in GSR, dTSM, ACV, and L3-2 sensilla (Fig. 4-3B). The signal of FSR-γ in GSR is weak because of its position. Two isoform expression patterns fit perfectly with two group described by Dickinson. The early and late development stage may switch the alternative splicing mechanism and lead to different isoform expression and different neuron responses.

iv. Splice reporters expressions in external sensory organs

1) Differentiated expression patterns in campaniform sensilla of the haltere and wing base.

There are three arrays of campaniform sensilla (CS) on the haltere, dorsal pedicellar array,

ventral pedicellar array, and dorsal scabellal array. In pedicellar arrays, each row has arched collar between sensilla. The collars make the receptor field of CS directional. Each array contains about 100 of sensilla.

The splice reporters have complex, and partially symmetric patterns of reporter gene expression, with partially overlapping sets of cells expressing each form. FSR-β is expressed strongly in the posterior two rows of sensilla in the dorsal pedicellar array and the anterior two rows on the ventral pedicellar array. FSR-γ is expressed in all pedicellar sensilla but more strongly in dorsal anterior and ventral posterior parts. On the dorsal surface, FSR-β is expressed in the distal two rows while FSR-γ is in every CS (Fig. 4-4). FSR-β positive CSs arranged in symmetrical pattern on haltere rod may reflect that these sensilla sensing the angular force of the same time-course while haltere swinging, and γ isoform is respond for fast-changing type of torsion. This data is consistent with QRTPCR result that β isoform is more abundant in haltere.

Several groups of more sparsely distributed campaniform sensilla are found at the wing base (Cole and Palka, 1982). They have different shapes. FSR-β is expressed in all sensilla, including d.Rad.A-E group where FSR-γ is majorly expressed in d.Rad.A group and barely detectable in part of d.Rad.B, C, and E group (Fig. 4-5).

2) Tactile bristles in notum and leg produce FSR-γ only.

In bristle of notum, only FSR-γ is detected (Fig. 4-6A, B). In previous chapter, TEC recording from notum bristle ESO showed that bristles of flies expressing NOMPCγ only have the same adapting ratio as the bristles of 51D control flies. This result supports the observation on notum. In leg, most of the tactile ES neurons expressed FSR-γ in femur (Fig. 4-6C), tibia (Fig. 4-6D), tarsus (Fig. 4-6E), and few sex comb bristles (Fig. 4-6F). At distal end of first tarsomere, two campaniform sensilla were detected; one expressed FSR-β and another expressed FSR-γ (Fig. 4-6F).

Chemosensory neurons can produce both FSR-β and FSR-γ

Multimodal hairs are slimmer than tactile bristles and innervated with one tactile neuron and four chemosensory neurons (Murphey et al., 1989). According to the morphology of nerve ending, some of multimodal hairs are FSR-β or FSR-γ positive on the leg (Fig. 4-6E), and the

reporter genes were expressed in chemosensory neurons. The FSR-γ signals were observed in other chemosensory neurons as well. There is a line of ES bristles at anterior dorsal wing margin and chemosensory bristles in every fifth position of dorsal and ventral wing margin (Milan et al., 2001). *elav-GAL4* mis-expressed FSR-γ were observed in those chemosensory bristles (Fig. 4-6G and G'). FSR- γ also can be found in chemosensory bristles on third segment of antenna (Fig. 4-6H). These data indicates the splicing mechanism for *nompC* isoforms exist in chemosensory neurons. Unfortunately, I did not observe any signal in ES bristles at anterior wing margin, which may be due to weak signal and thick cuticle.

vi. Splice reporters expressions in chordotonal organs

Chordotonal organs (CHO) use attachment cell to attach to cuticular apodemes or to the hypodermis to sense tension of the joint as a proprioceptor. They also sense sound and gravity by attaching to hinge of 3rd segment antenna.

In Johnston's organ, FSR-γ is expressed in all CHO while FSR-β expression is more limited to anterio-medial side (Fig. 4-7A). In the femoral CHO, FSR-β and FSR-γ are mainly produced in two groups with a little overlap (Fig. 4-7B-C). In abdominal CHO, most of the neurons are FSR-γ positive with 1 to 2 neurons expressing FSR-β (Fig. 4-7D).

vii. FSR- β is specifically expressed in JO neurons that respond to low-frequency stimuli.

Johnston's organ (JO), the auditory organ at second segment of antennae in fly, has 480 scolopidia attached to the hinge of the third segment of antennae. When the arista is deflected or vibrated, it twists the hinge and stretches CHOs, and the NOMPC and other ion channels are activated (Fig. 1-2D). JO axon bundles project into five separated zones in brain antennal motor and mechanosensory center (AMMC) (Kamikouchi et al., 2006). Neurons projected to zone A and B are activated by near field sound, and thos projected to zone C and E are responsive to phasic stimulus, like wind and gravity (Kamikouchi et al., 2009; Sun et al., 2009). In order to identify the group of neurons can express NOMPC isoforms (Fig. 4-7A), I used well-defined GAL4 lines specific for different subsets of these (Table 4-2) to express the splicing reporter genes.

I detected FSR-γ production when this reporter was driven by any of the subset-specific-

GAL4 lines I tested, JO1, JO3, JO4, JO15, JO25, JO27, JO29, JO30, and JO31. , indicating that the gamma isoform is expressible in neurons projecting to all zones. In contrast, FSR-β is produced only when expressed under the control of the JO3, JO4, and JO31 GAL4 lines (Fig. 4-8). Zone C and E are the overlap expression fields in these three GAL4 lines. These data indicate that γ isoform can be expressed in all zones, but β isoform can only be made in zone C and E. I do not have any marker to differentiate these two zones. FSR-β was not detected in JO when expressed by *JO1-GAL4* because *JO1-GAL4* generates weak signals.

Neurons project to zone C and E of AMMC respond to lower frequency stimuli, such as wind and gravity, or probe deflection (Kamikouchi et al., 2009). The specific expression of the β isoform in low frequency-sensitive JO neurons and in slowly-adapting CS on the wing vein strongly suggests that the β isoform is specialized for responding tonically to low-frequency stimuli.. Thus by alternative splicing, NOMPC divides and expands its receiving range for diverse mechanical stimuli.

Table 4-1 Primers for QRTPCR

Primers	Sense	Anti-sense	Product size
RP49	TACAGGCCCAAGATCGTGAA	ATCTCCTTGCGCTTCTTGGA	168 bp
nC10-11	ACTCTCGACAAAGGAAAAAGAGC	CTTATCGGTGGCTTGAAGGA	136 bp
nC11-1	AAGGAAGTGATTGCCCACAC	GATGGGCACCTTGTTGAACT	174 bp
nC11-2	TCCTTCAAGCCACCGATAAG	ACTATGAAGGCCACGAGCAG	172 bp
nC11-3	GATTGCCCACACGGTAGTTC	GGGCACCTTGTTGAACTTGT	163 bp
Alpha 1	ATTTCTCACCGGAGGATCTG	TTGTCAACTTGCGTTTGCTC	151 bp
Alpha 2n	TCCTGGCCATCTTTGTGTTT	ACGGCGAAGAACAACAACTC	175 bp
Alpha 3n	CCAATTTCTCACCGGAGGAT	GGCGTGGCTACATTTTTGAT	175 bp
Beta 1	ACTTCAGTGACGATGACATGC	GAAGACCGCGAAGAAGAGG	171 bp
Beta 21	ATCAATCCCATGCGACACTT	ACAAGCCAAATTTCCACTCG	175 bp
Beta 22	GACCGAGGTGCTCTTCAAAT	ACAAGCCAAATTTCCACTCG	143 bp
Beta 3	CGCCGGTGGAGAATTATGT	AAGTGTCGCATGGGATTGAT	154 bp
Gamma 2n	CCGTATTGGGTTGAGTACCTG	CTTGGACAAGCCAAATTTCC	156 bp
Gamma 31	GCCCACTCAACCGTATTGG	ACAAGCCAAATTTCCACTCG	161 bp
Delta 1	CACCTATCAACGCATTCAGG	GACAGGGCCACTGAGTCTTG	169 bp

Table 4-1 Primers for QRTPCR. RP49 primers are used to detect the ribosomal protein gene *rp49*, which is expected to be similarly expressed in all cells, as a control for total cDNA. nC10-11 and nC11-1~3, which amplify from shared, non-alternate exons, assay total *nompC* transcript levels. There are three alpha isoform detection primer sets, four beta isoform detection primer sets, and two gamma isoform detection primer sets. All the primer sets pass linear amplification quality control (Figure S4-1)

Figure 4-1 QRT-PCR reveals *nompCγ* is predominant isoform

A) Map of the primer set locations for QRTPCR. For α+ isoform, primers were chosen from the end of exon 12 and the beginning of exon 15 (orange arrows). Primers for β isoform were chosen from exon 13, 14, and 16 (dark gray arrows). Primers for γ isoform were chosen from exon 15 to 16 (brown arrows). Primers for δ isoform were chosen from exon 15, 16, and 18 (light gray arrows). Primers for all *nompC* transcripts are chosen from the non-alternate exons 10, 11, and 12 (black arrows).

B-F) Each bar shows the data from one pair of primers. Data were normalized by average *rp49* reading within the same type of sample. γ isoform is the most abundant form. β isoform levels are a quarter or less of γ isoform levels in most samples, except in the haltere where it is about half of γ isoform quantity.

B) Third instar larvae body walls have 7.3 fold γ isoform (322±83) to β isoform (44±7).

C) Whole adult flies have 4.3 fold more γ isoform (645±266) than β isoform (150±76).

D) Fly antenna have 5.9 fold more γ isoform (558±209) than β isoform (94±37).

E) Fly halteres have 2.3 fold more γ isoform (1143±177) than β isoform (496±391).

F) Fly legs have 5.1 fold more γ isoform (2025±522) than β isoform (397±162).

Figure 4-1 QRT-PCR reveals *nompCγ* is predominant isoform

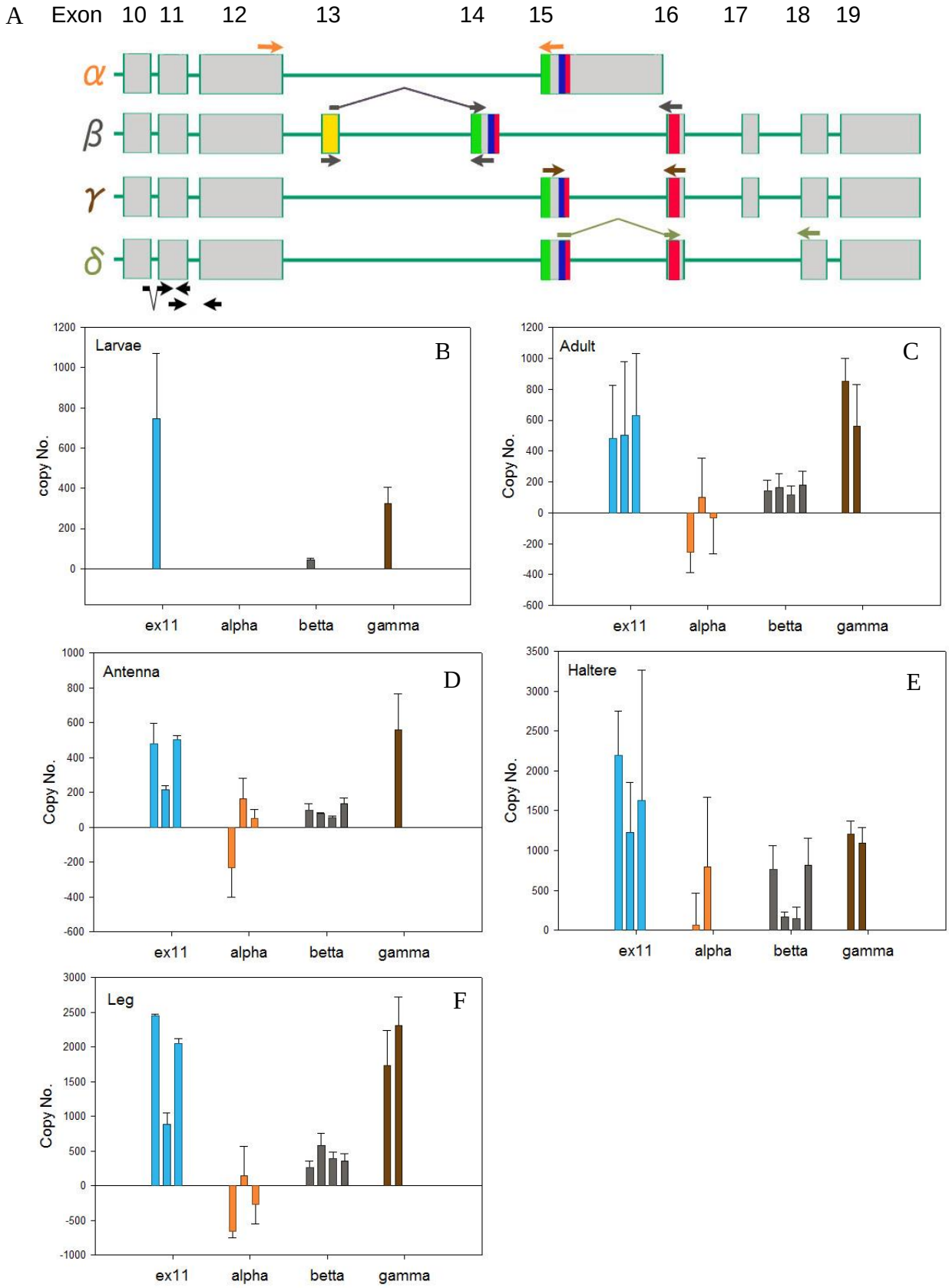

Figure S4-1 Quality control of primer pairs for QRT-PCR

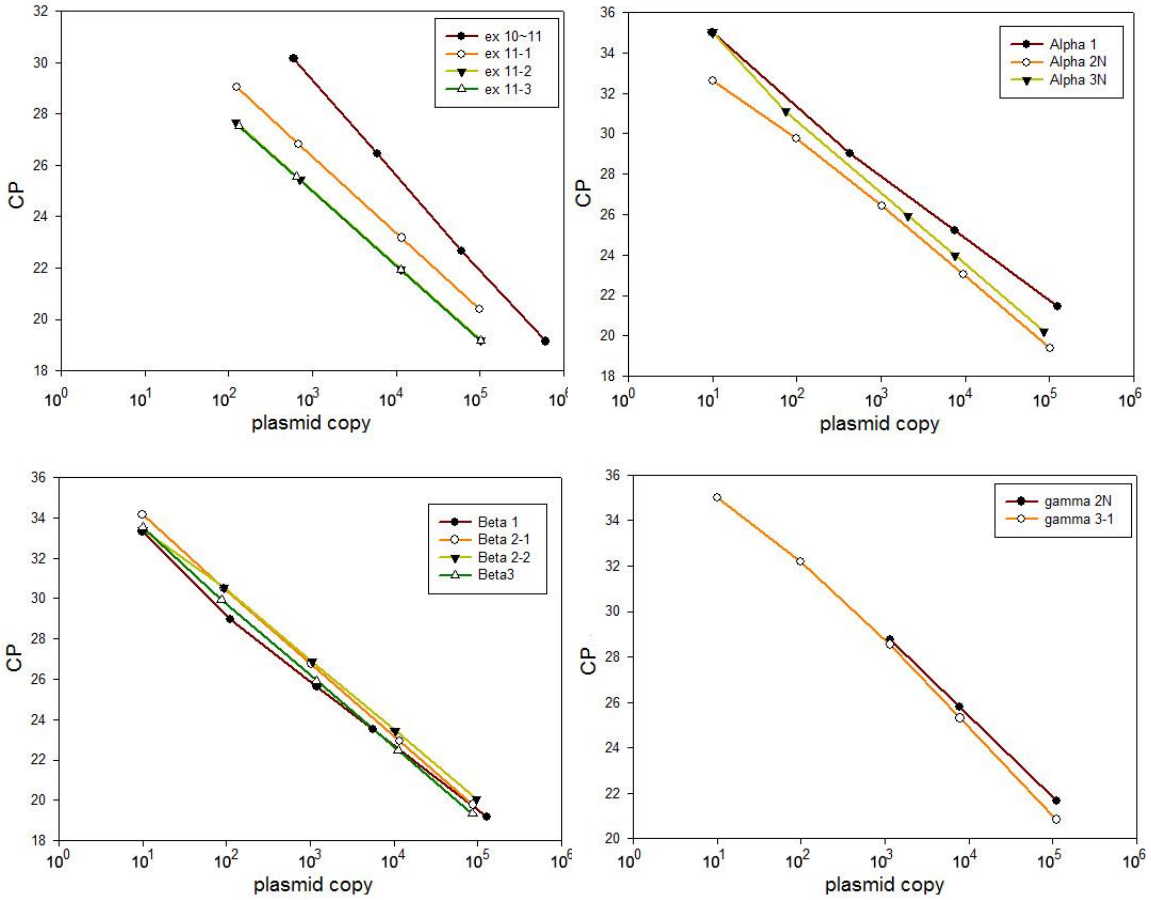

Figure S4-1 Quality control of primer pairs. A standard curve for each primer pair was generated by adding serial dilutions 10^1~ 10^5 of the appropriate isoform plasmid into cDNA prepared from *nompC* null mutant 96~120 hrAPF pupae. These controls show the linear range of each primer pair.. All the experiment readings beyond minimal CP number were discarded.

S4-2 No difference in *nompC* isoforms expressions between male and female flies

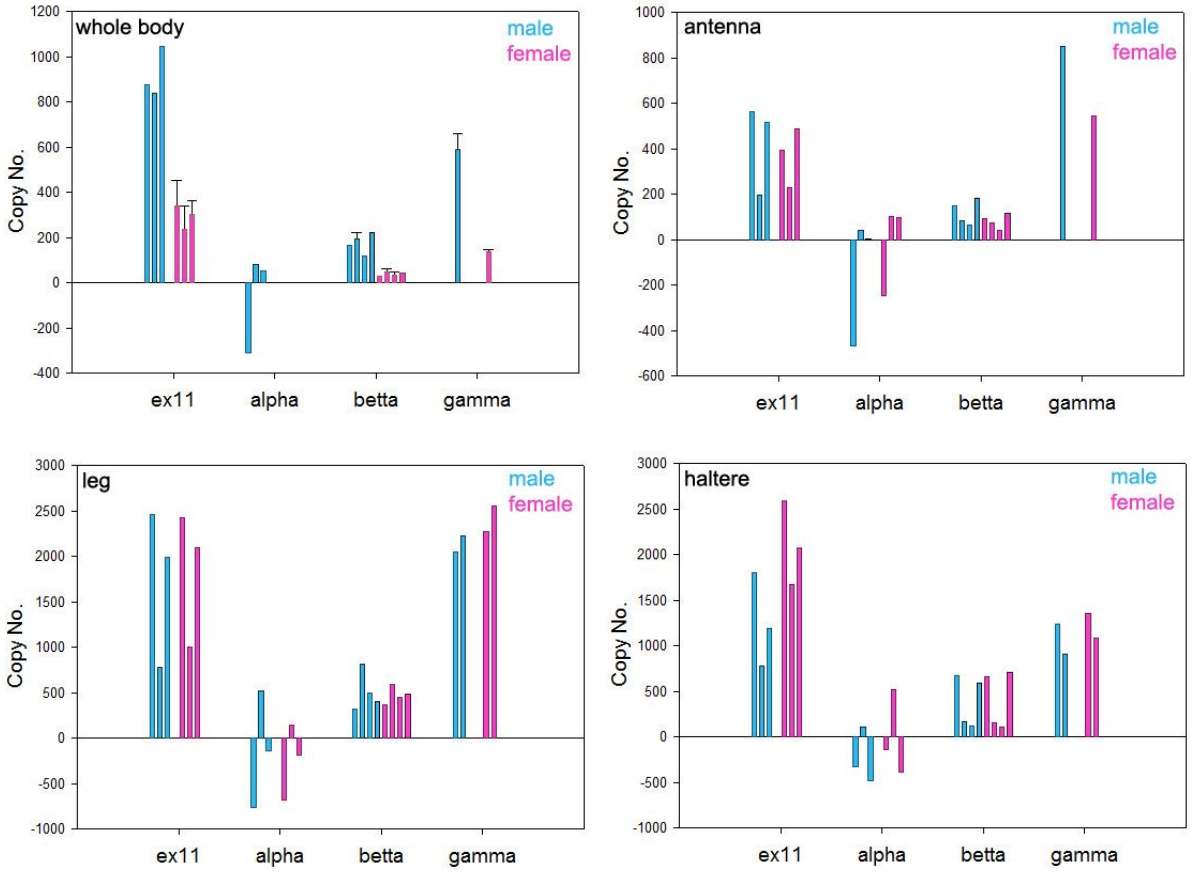

Figure S4-2 There is no difference in *nompC* isoform expression between male and female flies. Male flies have about double amount of *nompC* in whole body, consistent with their body size difference when normalized with *rp49* values, for total cDNA.

Figure 4-2 Assembly splice reporter constructs.

A) First attempt at splicing reporter design. UAS-atg is ligated to *nompC* exons 12~16 genomic region, which encode the transmembrane region of the protein only, and to a tandem eGFP-tdTOMATO tag. In the 14T construct, a single "T" nucleotide insertion was inserted near the end of exon 14. When exon 14 is included in a mRNA, translation past the insertion in 14T causes a downstream shift from frame +1 to +3. This leads to the eGFP sequence being translated out of frame, and the tdTOMATO being translated correctly. The γ isoform is translated with correct eGFP tag, excluding the frameshift in 14T. Therefore β isoform generating mechanism will produce a NOMPC- tdTOMATO fusion protein and γ isoform mechanism will produce a NOMPC-eGFP fusion protein. The 15T construct, with point insertion in exon 15, gives an eGFP-labelled beta from and a tdTOMATO-labelled gamma isoform. This was intended to control for possible differences in fluorescence signal strength between the eGFP and tdTOMATO.

B) Successful splice reporter design. A full length splicing reporter (FSR) is composed of a 5xUAS transcription activator sequence followed by *nompC* exon 1-12 cDNA, genomic region from exon 12 to exon 18, and either an eGFP or a tdTOMATO tag, for FSR-γ or FSR-β respectively. A single-nucleotide insertion near the end of exon 14 in FSR-γ generates a frameshift to an open reading frame that ends with a stop codon in exon 16, so that only γ isoform can be translated with eGFP tag. Conversely, FSR-β has point insertion near the end of exon 15 so only a full-length β isoform fusion can be translated.

Figure 4-2 Assembly splice reporter constructs

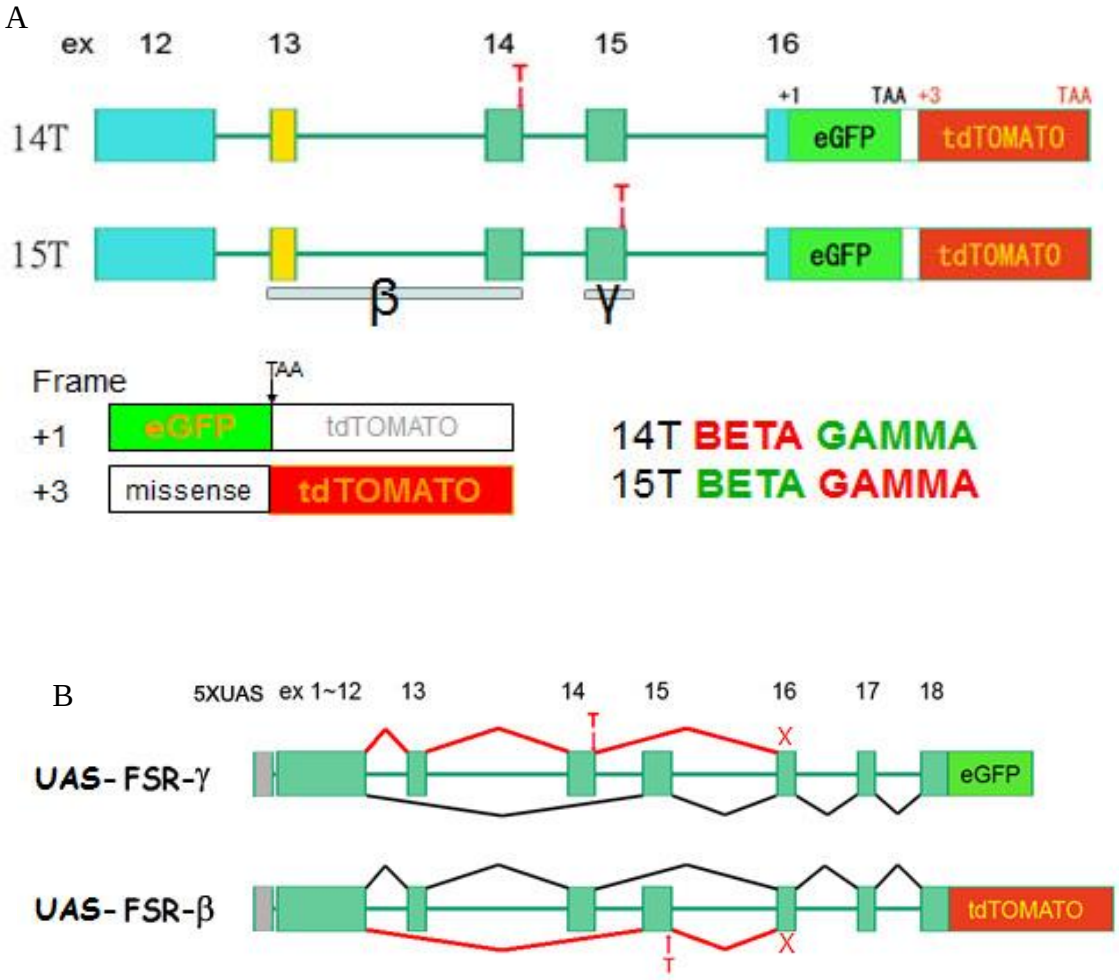

Figure 4-3 Isoform expression patterns on wing vein.

A) Schematic of fly wing. dHCV, dorsal humeral cross-vein sensillum; GSR, giant sensillum of the radius; p-TSM and d-TSM, proximal and distal twin sensilla of the margin; L3-v, ventral sensillum of L3; ACV, sensillum of the anterior cross vein; L3-1, L3-2, L3-3, first, second, and third sensilla of L3.

B) FSR-β and FSR-γ are expressed in different campaniform sensilla on the wing vein. FSR-β (red) is expressed in dHCV, pTSM, L3v, L3-1, and L3-3. FSR-γ (green) is expressed in GSR, dTSM, ACV, and L3-2.

Figure 4-4 Isoform expression patterns on haltere.

A) Schematic of haltere dorsal side,from Figure 2A of (Cole and Palka, 1982).

B) *elav-GAL4* drives *UAS-FSR-β* (red) and *UAS-FSR-γ* (green) in all neurons. FSR-γ was produced mainly in the anterior part of dorsal pedicellus array and in all dorsal scabellum sensilla. FSR-β was produced in the posterior two rows of sensilla on the dorsal pedicellus and in the distal 2~3 rows of sensilla on the dorsal scabellum. The focal plane of DIC image in (B) and (D) are different. The one with clear scabellum sensilla is the dorsal focal plane.

C) Schematic of haltere ventral side, from Figure 2B of (Cole and Palka, 1982).

D) FSR-γ was produced mainly in posterior rows of sensilla in the array on the ventral pedicellus, and FSR- β was expressed in the anterior rows of sensilla in v.Ped.

Figure 4-5 Isoform expression patterns on wing hinge, in flies expressing *UAS-FSR β* and *UAS-FSR γ* under the control of *elav-GAL4*.

A) Schematic of wing hinge is adapted from Cole's paper (Cole and Palka, 1982). d.Rad.A - d.Rad.E = sensilla fields of the dorsal radius.

B-E) FSR-β is produced in all sensilla, including d.Rad.A-E group. In contrast, FSR-γ is primarily expressed in the d.Rad.A group and barely detectable in part of d.Rad.B, C, and E group.

Figure 4-3 Isoform expression patterns on wing vein.

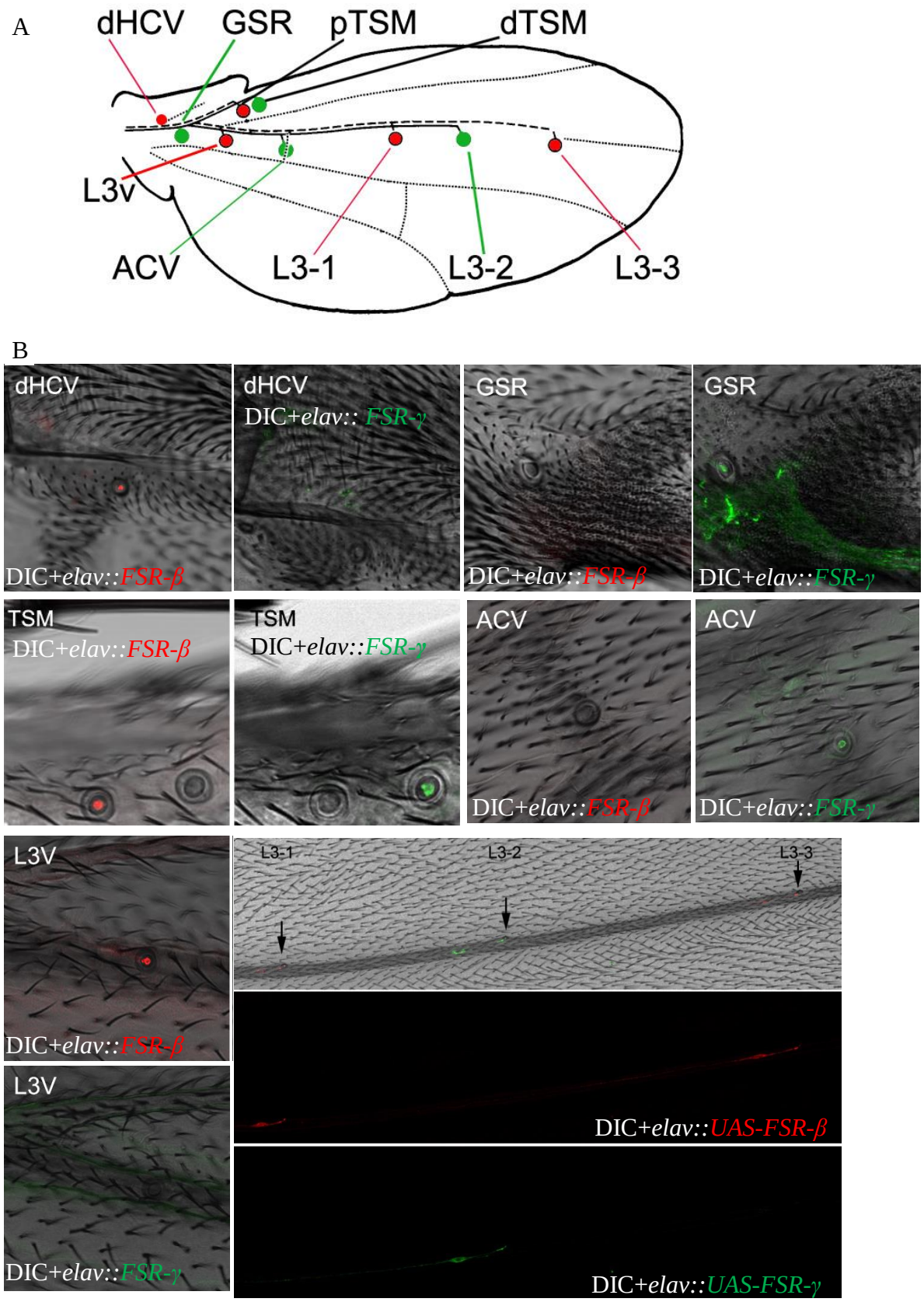

Figure 4-4 Isoform expression patterns on haltere.

A

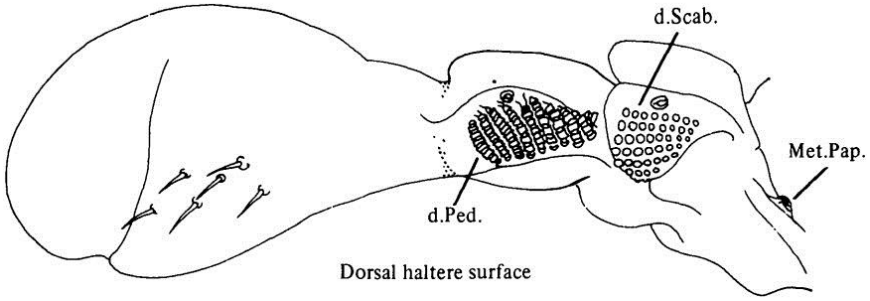

B

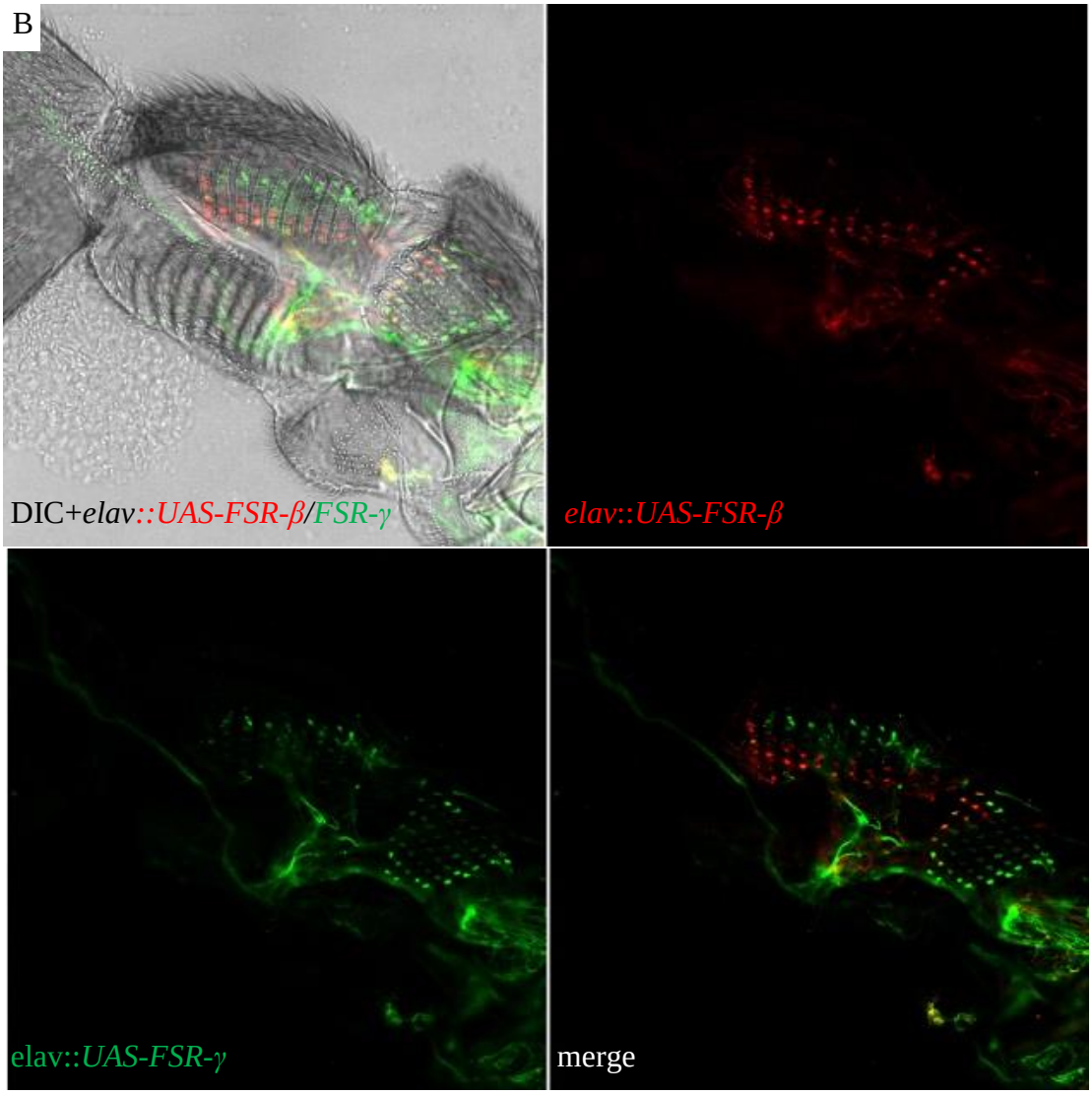

Figure 4-4 continued

C

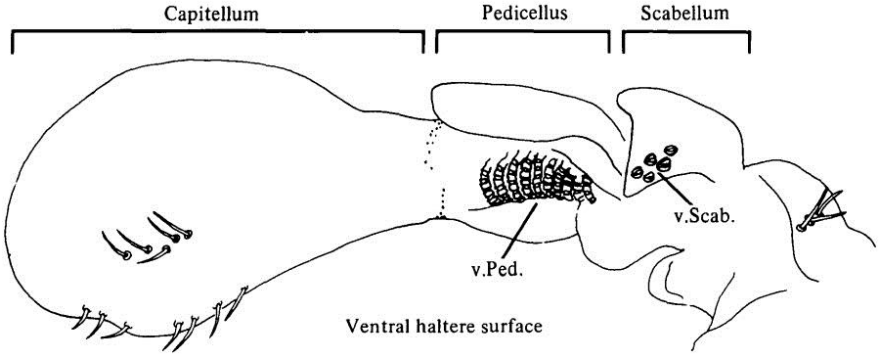

D

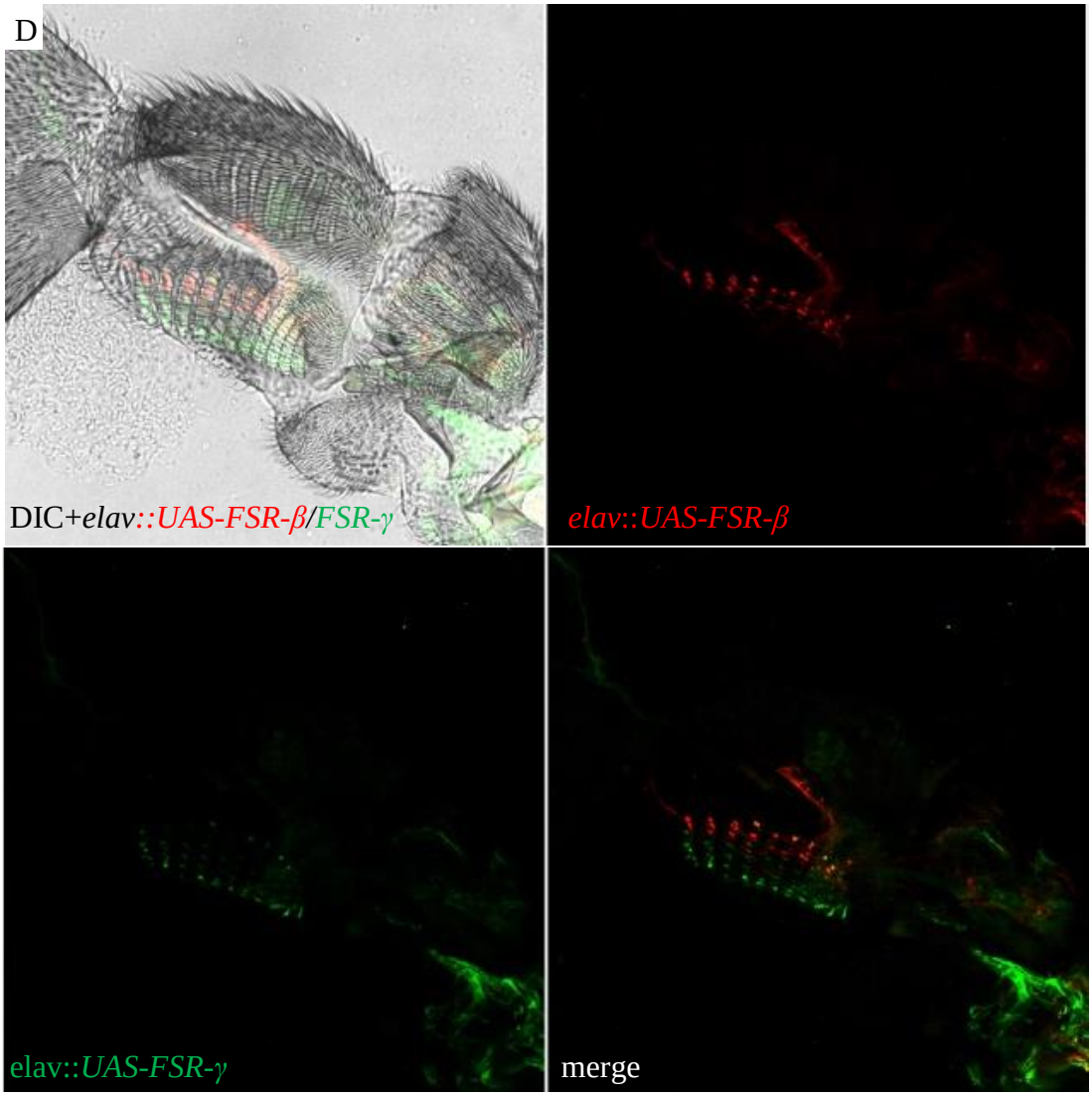

Figure 4-5 Isoform expression patterns on wing hinge.

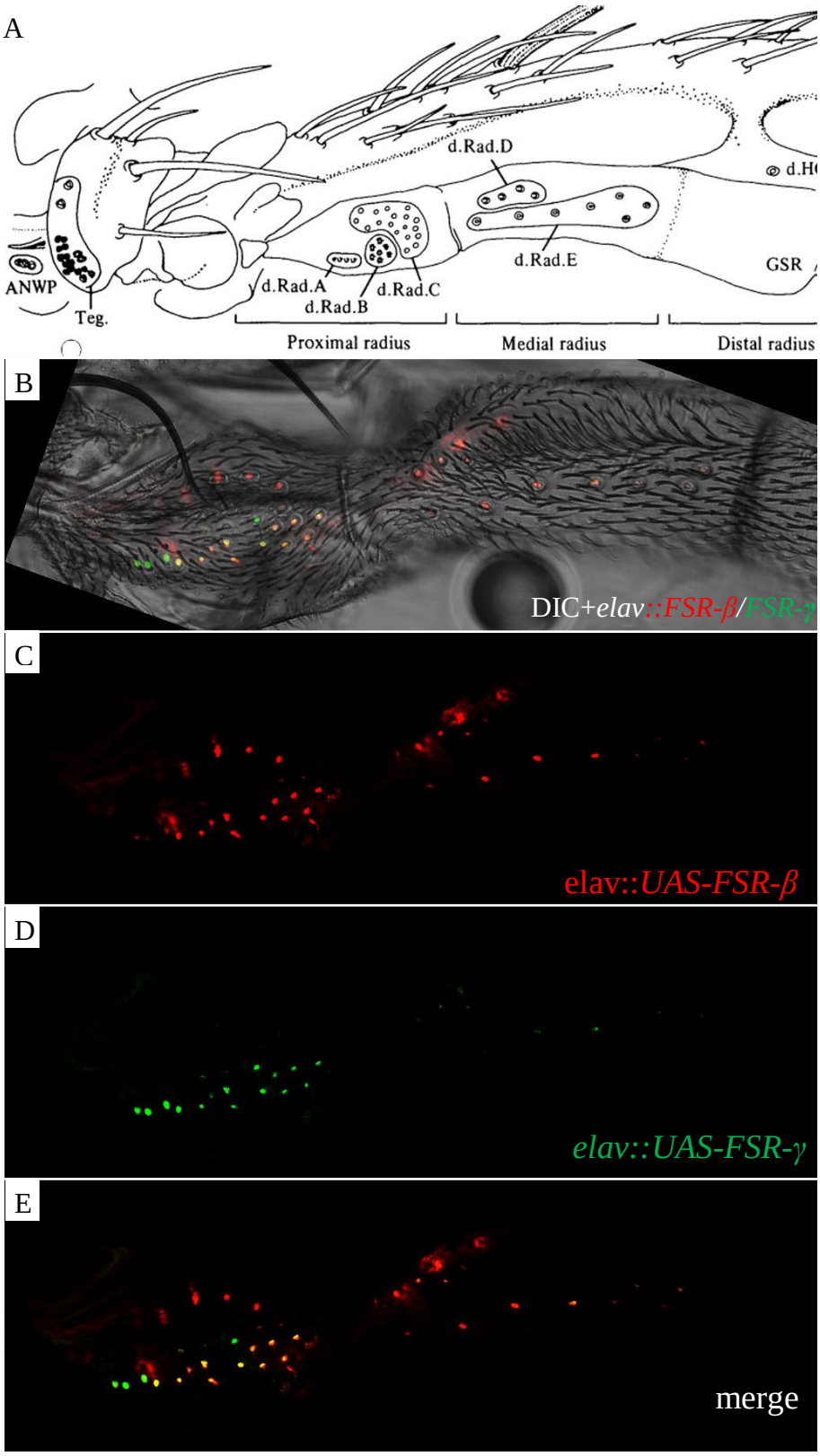

Figure 4-6. Only FSR-γ can be misexpressed in ESO of notum and most of legs.

A) In notum, FSR-γ is expressed in every mechanic ESO. No FSR-β signal is detected.

B) 20X zoom of single ESO. FSR-γ is at the base of the bristle, the ES neuron.

C) FSR-γ is expressed in most of femur bristle ESOs (arrow heads). No FSR-β signal is detected.

D) FSR-γ is expressed in most of tibia bristle ESOs (arrow heads). No FSR-β signal is detected.

E) FSR-γ is expressed in some of tarsus bristle ESOs (arrow heads) and chemosensory bristles. Some of chemosensory bristles express both FSR-γ and FSR- β (red arrow).

F) FSR-γ is expressed in part of sex comb bristle ESOs and sensilla near the joint. FSR-β signal is detected in sensilla near the joint.

G-H) elav-GAL4 drove FSR-γ expression in the chemosensory bristles at anterior wing margin. FSR-γ are labeled with arrow head in H.

I) elav-GAL4 drove FSR-γ expression in the chemosensory bristles at 3ed segment of antenna.

Figure 4-6 Only γ isoform can be produced in ESO of notum and most of legs

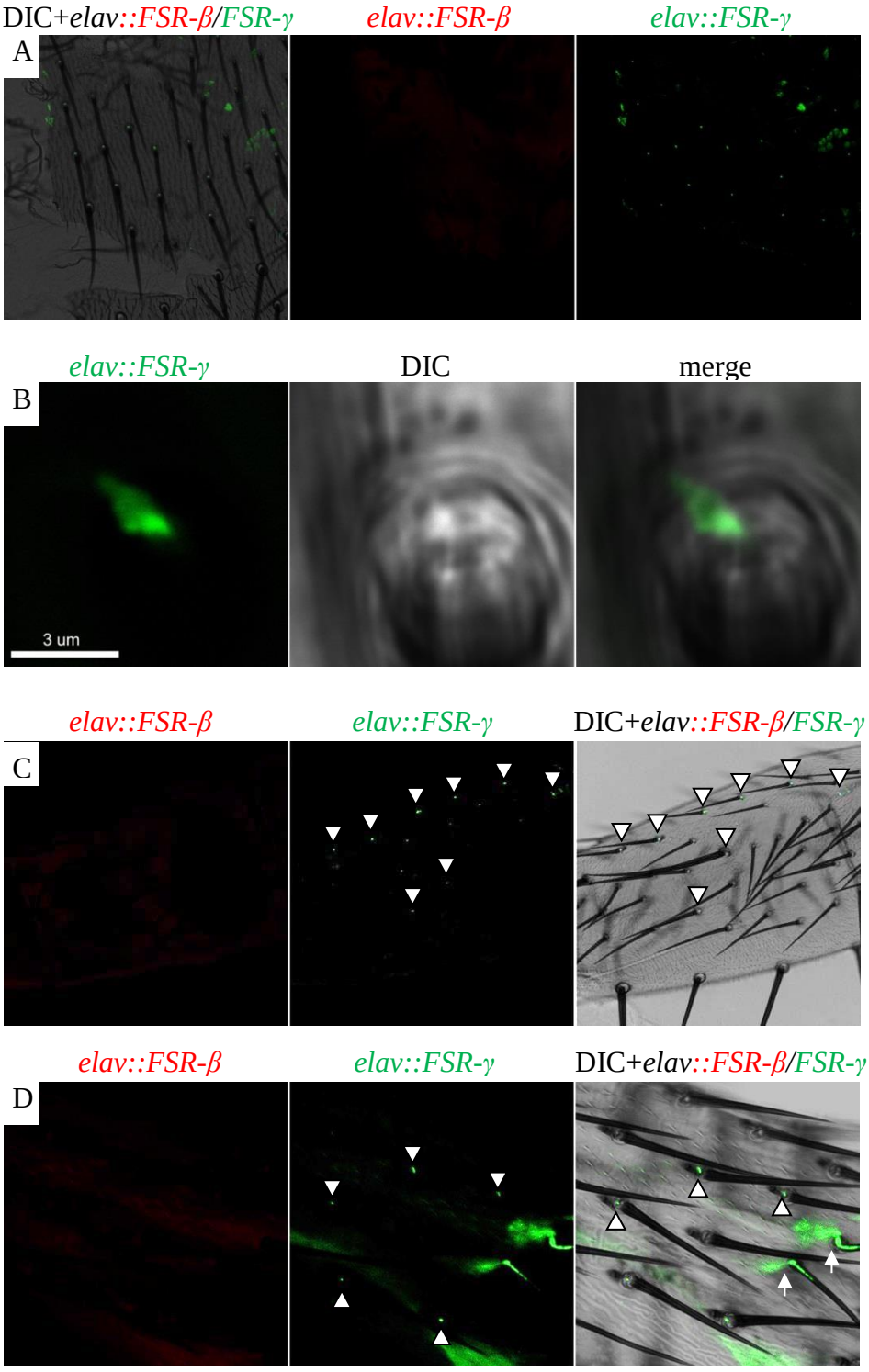

Figure 4-6 continued

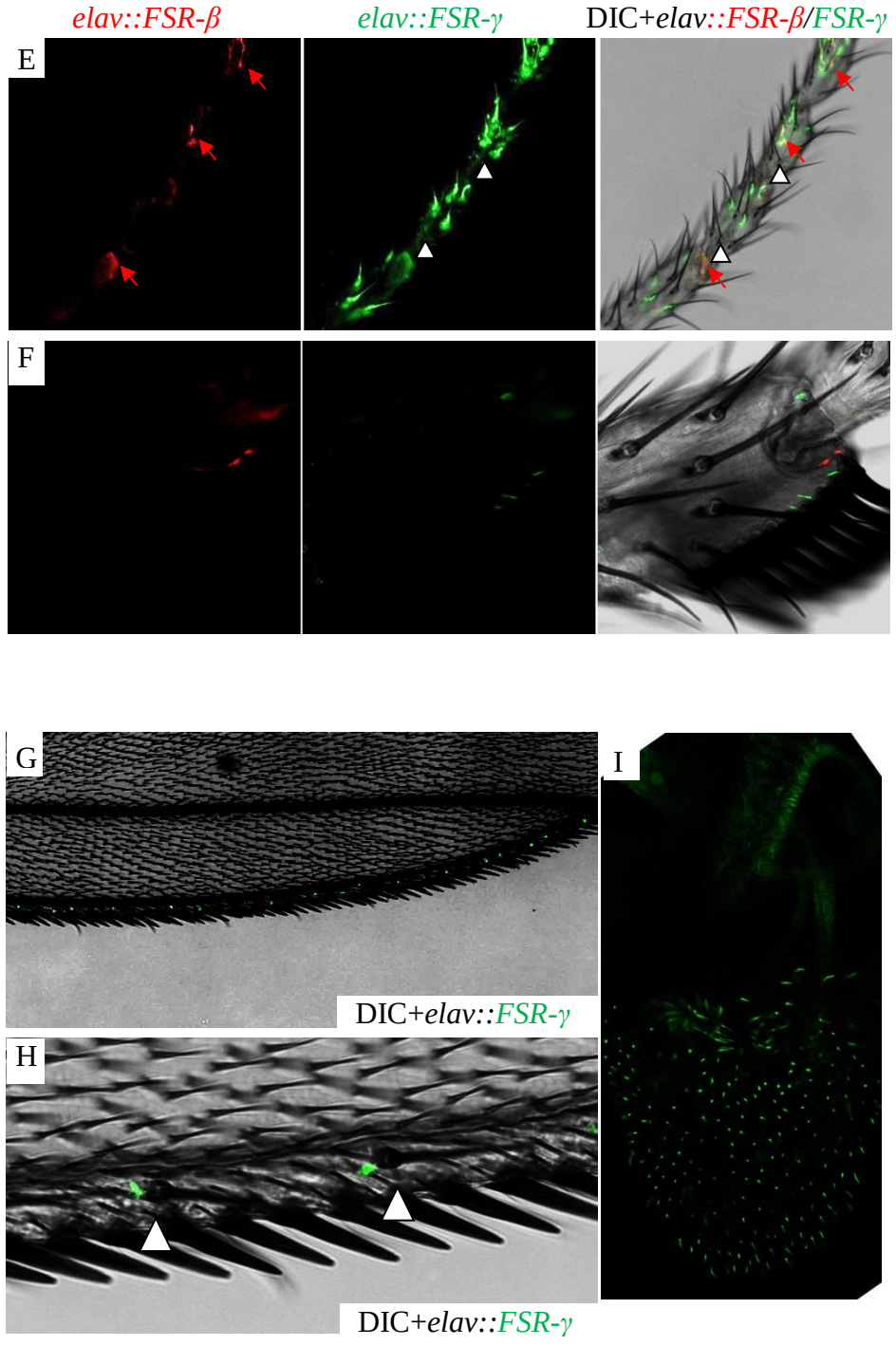

Figure 4-7 Differential isoform expression patterns in chordotonal organs.

All panels show expression, in flies carrying both *UAS-FSR-β* and *UAS-FSR-γ*, both under control of the pan-neuronal *elav-GAL4* driver.

A) In the second segment of antenna, FSR-γ was expressed in most or all of the of the chordotonal neurons. FSR-β expression is limited to a single group of neurons in the medial part of Johnstons organs, plus a few others scattered around.

B-C) Femoral chordotonal organs in the legs show an anatomical separation of neurons into two groups. The proximal group produces mainly FSR-γ, and distal group produces mainly FSR-β with a little mix.

D) In a chordotonal organ in the ventral abdomen, FSR-γ is produced in most of the abdominal CHOs, and FSR-β is produced in few CH neurons. A neuron expressing both isoforms is labeled with arrow.

Figure 4-7 Differential isoform expression patterns in chordotonal organs.

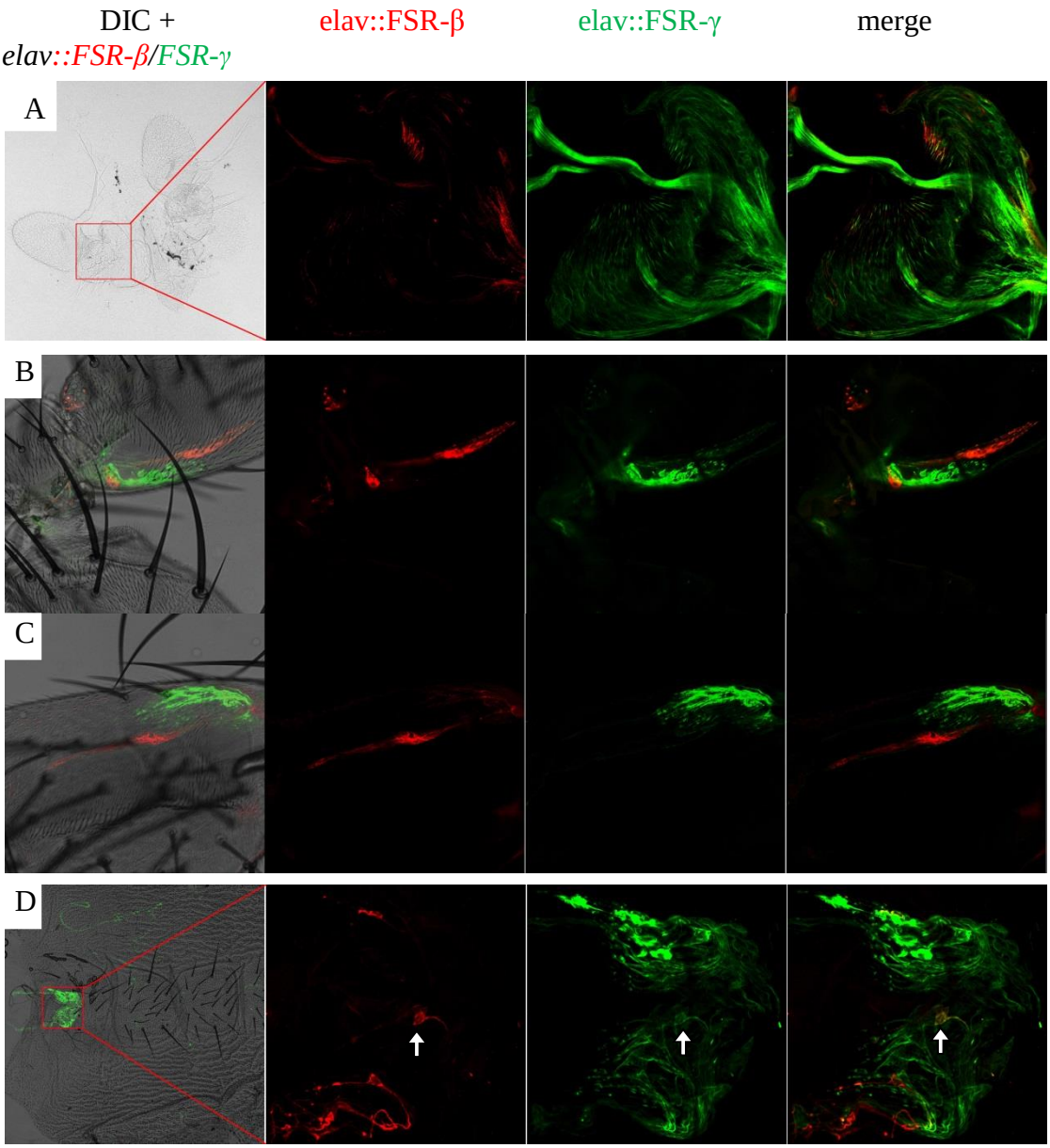

Table 4-2 Johnston's Organ specific GAL4 lines

FSR β	FSR γ	Strains (original name)	Labels in the brain: zones	Labels in the brain: subareas	Labels in other cells: nonneural cells in a2	Labels in other cells: ESN	Labels in other cells: ORN	Labels in other cells: arista	Labels in other cells: forehead	
x	o	JO1 (NP0761)	A B C D E	AA AP AV1 AV2 AD BI BO CL CM DA DP EVM EVP EDM EDP EDC	–	–	–	–	–	3rd
o	o	JO3 (NP1245)	A B C D E	(*AA*) AP AV2 BI BO CL CM DA DP EVM EDP EDM EDC	–	–	–	–	–	2nd
o	o	JO4 (NP6303)	A C E	AA AP AV1 AV2 CL CM EVM EDM EDP EDC	–	–	–	–	–	2nd
x	o	JO15 (JO15)	AB	(*AA*) AP AV1 AV2 AD BO	–	–	–	–	–	3rd
x	o	JO25 (NP5021)	A	(*AA*) AP AV2 AD	–	–	+	+	n.d.	X
x	o	JO27 (NP6264)	(A) B	(*AA* AP AV2) BI	+	–	+	–	n.d.	2nd
x	o	JO29 (NP3259)	A D	A DA DP	+	–	–	–	n.d.	X
x	o	JO30 (NP5035)	A D	A DA DP	+	–	n.d.	n.d.	n.d.	X
o	o	JO31 (NP6250)	C E	CL CM EVM EDM EDP EDC	–	+	–	–	+	2nd

Adapted from Kamikouchi et al., J of COMPARATIVE NEUROLOGY, 2006

Table 4-2 Johnston's Ogran-specific GAL4 lines used in this experiment. The table is taken from Kamikouchi et al., J Comp Neurol, 2006. Expression results (Fig. 4-7) are summarized in the left columns: o = expression; x = no expression.

Figure 4-8 FSR-γ in all zones and FSR-β isoform in zone C & E of JO neurons

FSR-γ can be produced in neurons projecting to all AMMC zones. In contrast, FSR-β can only be produced by JO3, JO4, and JO31 – expressing neurons which project to AMMC zone C and E.

Figure 4-8. FSR-γ in all zones and FSR-β isoform in zone C & E of JO neurons.

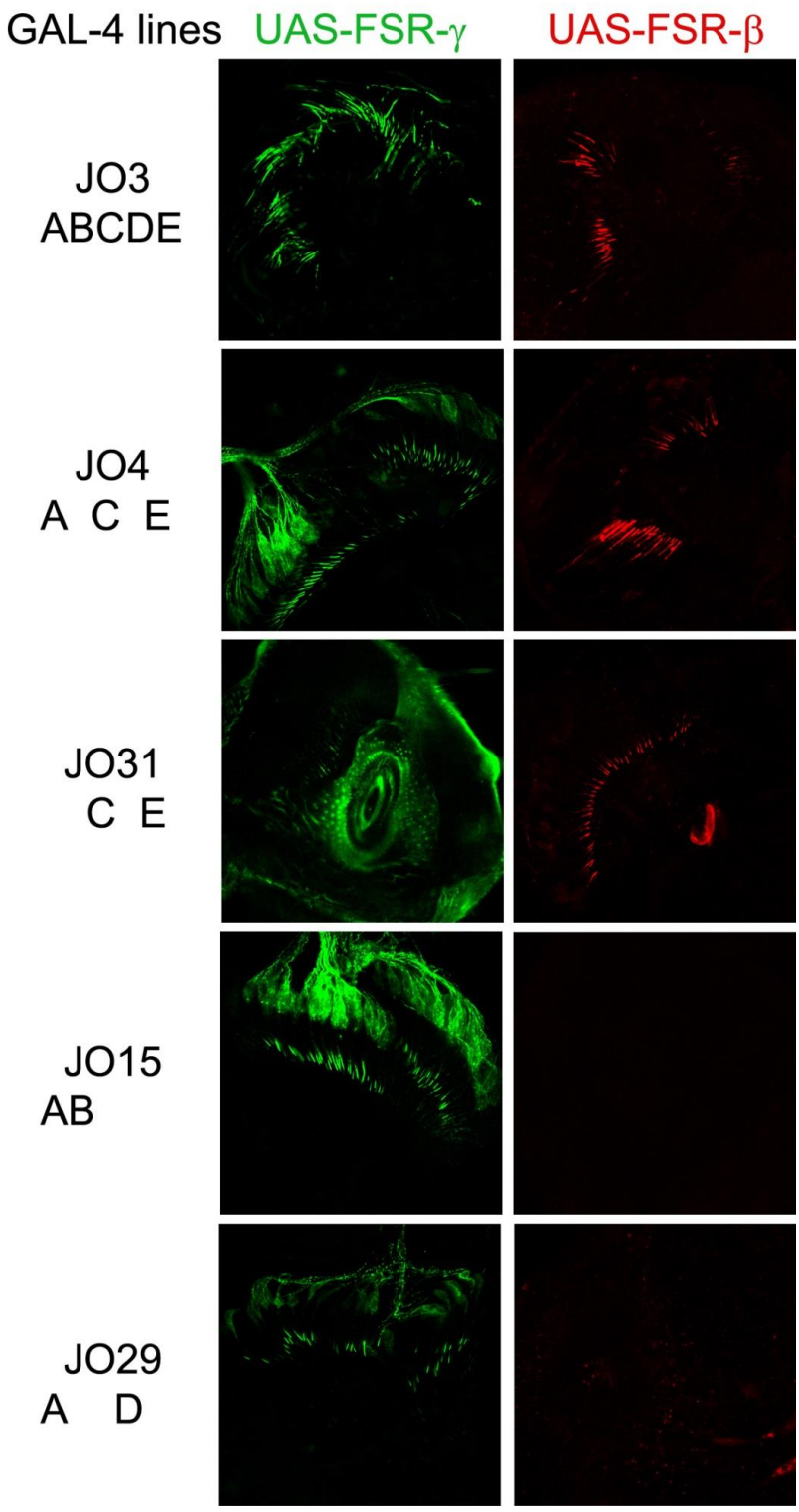

Figure 4-8 continued

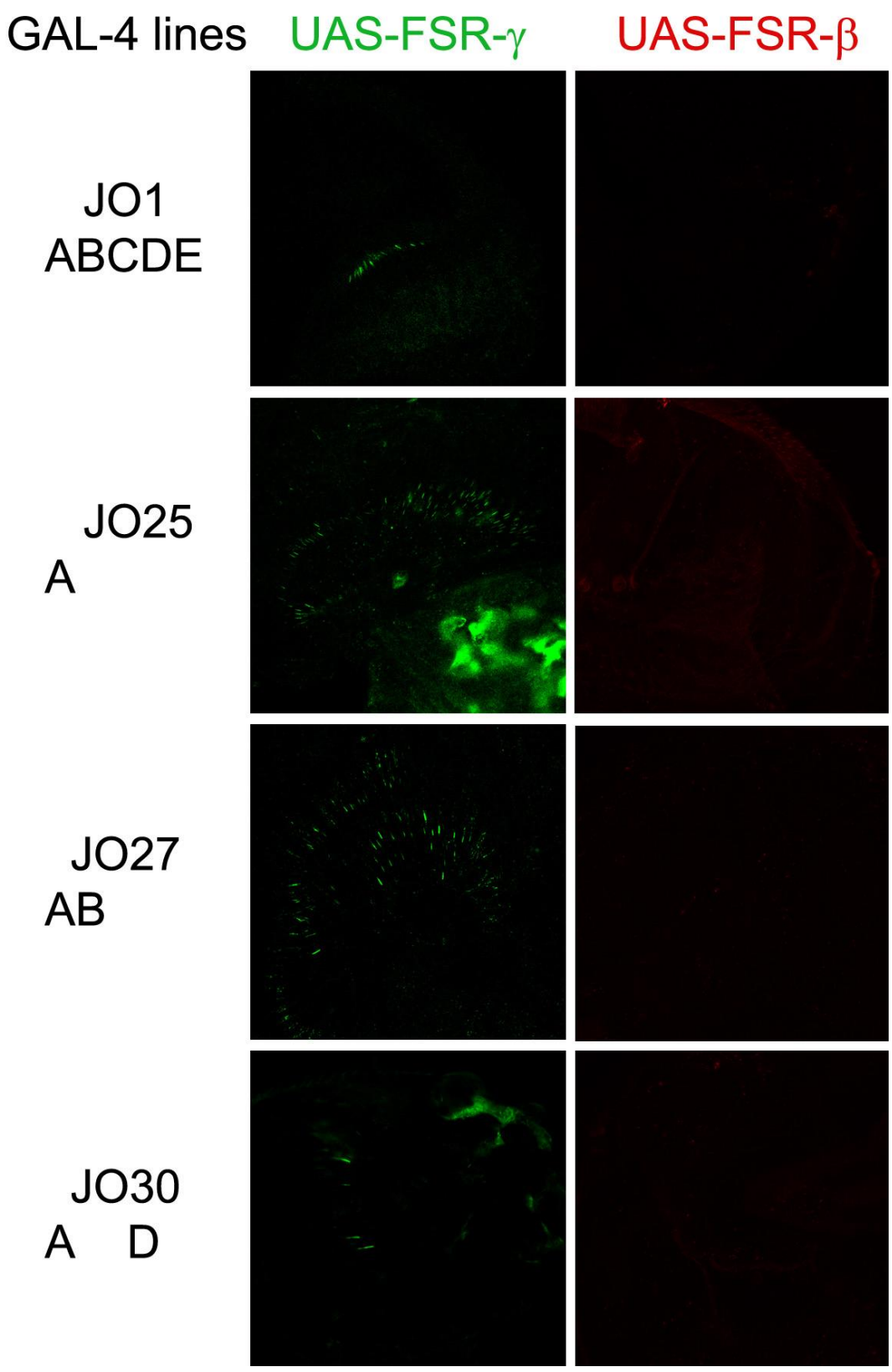

Chapter 5 Conclusions

In this study, we isolated *nompC* transcripts including either of two exons, each of which encodes the pore domain and TM6 of the channel protein. The β and γ isoforms lead to different receptor current adaptation kinetics, which correlate with the distinct functional properties of the sensory organs that express them.

i. NOMPCβ and NOMPCγ have different mechanosensory kinetics

In measurement of NOMPC–dependent receptor currents in mechanosensory bristles, bristles in flies expressing β or γ isoforms both showed adapting bristle mechanoreceptor currents but differed in their current properties, with bristles expressing the γ isoform having a greater peak amplitude, faster adaptation and a proportionally smaller non-adapting current than bristles expressing the β isoform.

The tactile sense can be divided into two categories, phasic and tonic sensory receptors. Phasic sensory receptors, like Meissner's corpuscle and Pacinian corpuscle in human skin, are activated at the onset and offset of the physical stimulus. Tonic receptors, like Merkel cells and Ruffini endings, are firing continuously throughout the stimulus. Phasic and tonic sensors cover the basic need of tactile sense, highly sensitive to the change and knowing the sustained stimulus without desensitization. The current kinetics of β and γ isoform-expressing bristles resemble the properties of phasic and tonic sensory receptor, respectively.

ii. Possible mechanisms for isoforms to have different kinetics

The Ca^{2+} influx may play an important role for adaptation. In turtle hair cells, the adaptation of mechanical transducer is driven by a rise in intracellular [Ca^{2+}] (Ricci and

Fettiplace, 1998). The hair bundle recoils after the peak current by at most 200 micro seconds, and this is considered as a process of fast adaptation (Ricci et al., 2000). The time constant of the mechanical relaxation was increased when extracellular [Ca^{2+}] was reduced. It is possible that NOMPCβ is less permeable to divalent cations; therefore, there is less intracellular Ca^{2+} and slower adaptation. One example is that the TRPM3α1 channel has longer pore region and less divalent current than α2 isoform (Oberwinkler et al., 2005). Adding EGTA into artificial receptor lymph did not affect my MRC recording. One way to test the importance of Ca^{2+} influx is measuring MRC while controlling intracellular [Ca^{2+}] by misexpressing calcium binding proteins such as calbindin or calmodulin in fly. Functional NOMPC can be expressed in S2 cells (Yan et al., 2013). Patch recording and calcium image of NOMPC isoform expressing S2 cell shall reveal more detailed properties involving calcium dependence, chloride dependence, and other factors.

Calcium has many ways to affect channel open probability. The 3rd ankyrin repeat of TRPV1 binds to calmodulin, and this binding is Ca^{2+}-dependent (Rosenbaum et al., 2004). This interaction increases the adaptation of TRPV1 receptor current. Another example is that in fly phototransduction, TRP channel need Ca^{2+} influx to maintain PIP_2 level (Hardie et al., 2001). Calcium influx may directly turn on other channel. During excitation-contraction coupling, ryanodine receptor RYR1 on the sarcoplasmic reticulum membrane are activated by physically contacted $Ca_v1.1$ channel on cell membrane when Ca^{2+} influx via $Ca_v1.1$ (Lamb, 2000).

iii. Two isoforms expressed on wing blade and JO correlate with sensory adaptation

The kinetics of the different isoforms corresponds to the properties of the sensilla producing those isoforms. When isoform-specific splice reporters, were expressed in the wing blade campaniform sensilla, FSR-β was produced in tonic sensilla and FSR-γ was in phasic ones (Fig. 4-3) (Dickinson and Palka, 1987). In JO neurons, FSR-β was produced in those projecting to zones C and E of the antennal motor and mechanosensory center (AMMC), and these neurons respond to slow or static stimuli such as wing and gravity (Kamikouchi et al., 2009; Sun et al., 2009). MRC and these expression patterns of the isoforms suggest that NOMPCβ is involved in tonic response, and NOMPCγ is involved in phasic response in those sensors.

iv. Sensilla properties change in flies with only NOMPCγ isoform.

To test whether NOMPC isoforms determine sensilla adaptation properties, I performed extracellular recording from individual campaniform sensilla on the wing vein, following Dickinson's protocol (Dickinson and Palka, 1987). This method records action potentials evoked by mechanical stimulation of individual, identified sensilla on an excised wing. The fast-adapting sensilla are reported to respond to sustained pressure stimuli with one or two large-amplitude spikes at the stimulus onset. In contrast, slow-adapting sensilla fire throughout the stimulus. We hypothesized that if this difference in adaptation properties is determined by the NOMPC channel isoform expressed in each sensillum, then flies expressing single isoforms in all neurons should show the same properties in all sensilla.

I attempted to record wing nerve potentials when stimulating the ACV or the L3-1 sensilla, representing fast- and slow-adapting neurons respectively. In flies expressing only the NOMPCγ isoform, both sensilla show large-amplitude spikes and fast adaptation (Fig. 5-1). This preliminary result suggests that γ isoform expression makes the slow-adapting L3-1 sensillum become fast-adapting, like γ isoform-positive ACV sensillum. The smaller spikes from slow-adapting sensilla, either in controls or in wings expressing only β isoform NOMPC, were undetectable in my setup, as the signal/noise ratio was too low.

NOMPC is most likely the mechanical transducer in the ESO because no other known channel is reported opening when mechanical stimulus apply. It is debatable in CHO transduction. Two TRPV channels, NANCHUNG and INACTIVE, expressed at proximal cilium of CHO are electrically coupled with NOMPC to amplify the feedback gain (Gopfert et al., 2006). Other evidence suggests TRPV channels are the major components of the transduction complex. The sound-evoked antennal rotation is increased in *inactive* or *nanchung* null mutant flies but reduced in *nompC* mutant flies, and the receptor current is complete abolished in these TRPV mutant flies, but only reduced in *nompC* mutant (Lehnert et al., 2013). Because both NOMPC and TRPV mutants affect antennal rotation, the proper stiffness of cilium seems crucial for the transduction. $nompC^{f00642}$ is a mutant allele only has auditory perception defective but not negative gravitaxis (Sun et al., 2009). Observing the NOMPC protein distribution in this allele may tell us more about its function. Other channels may also help determine the neuron firing

properties. In *eag* mutant flies, which lack a voltage-gated potassium channel, the dTSM was transformed from fast-adapting to a more tonic response (Palka, 1993).

v. The biological functions of tonic and phasic sensory receptors

Sensory feedback for walking behavior includes the tactile sense from bristles and the proprioceptive feedback from the femoral CHO. The climbing assay results indicate that mutant flies expressing both NOMPCβ and NOMPCγ isoforms perform better than those expressing only one isoform, and that mutant flies expressing the γ isoform climb faster than those expressing the β isoform only. Considering that tactile bristles produce only the γ isoform, the proprioceptive feedback of walking is contributed by at least the NOMPCβ in CHO. Two isoforms may have different function in two groups of CHO for walking. Little is known about the functions of different groups within the femoral CHO. The two isoforms may sense different types of stimulus there, as in the wing vein sensilla and JO neurons. There are two campaniform sensilla sensing the joint position at distal end of first tarsomere, one expressing FSR-β and another expressing FSR-γ (Fig. 4-6F). Detecting limb motion and posture needs both phasic and tonic sensor. NOMPC- β may detect the posture, and NOMPCγ may sense the initiation and stop of a movement. Observing splice reporter expressions in sensors near all joints will further support the idea that the two isoforms are needed there. A detailed measurement of leg movement in flies expressing isoform(s) may be needed to decipher isoform functions in walking.

Another function of femoral CHO and abdominal CHO may be detecting the substrate vibration from the courtship (Mazzoni et al., 2013) or other communications.

Campaniform sensilla on the wing blade probably respond to the wing load when they are not beating. In courtship pulse song, detecting the paused wing is crucial for the tempo. The wing is needed to keep straight all the time to avoid damaging flight ability. If the wing is bent by external force, phasic sensilla should trigger a cleaning reflex to restore it, and the tonic sensilla could check the status after the restoration.

Only dipteran insects have halteres, and the halteres swings when the wings beat. The wingbeat frequency in flight is about 200Hz in fly (Chakravorty et al., 2014). Single channels composed of either β or γ isoform subunits do not respond fast enough but arrays of

campaniform sensilla on the haltere may detect the angular force of the beating. In the pedicellar arrays, FSR-β is symmetrically produced in sensilla of the dorsal posterior two rows and the ventral anterior two rows. I did not find literature describing detailed haltere movement, but I suspect that if the halteres swing up and down, the FSR-β - expressing rows of are placed to sense lateral movement. It should not be hard to observe if we acquired a high-speed camera. Bees and wasps do not have halteres so I suspect that they have CS array at their wing hinge.

vi. The selective force for multiplication of *nompC* isoforms in evolution

The evolutionary evidence suggests that the duplication of exon 14, included in the β isoform, and exon 15, included in the γ isoform, are conserved across Diptera, Lepidoptera and Coleoptera, and another independent triplication happened in Hymenoptera. The multiplication of pore region happened only within Holometabola which happens to be the most successful evolved superorder among all animal.

The common trait of holometabolan insects is that they change their body structure dramatically between larvae stage to adult stage. The advantage of this transform is increasing the diversity of appendages to accommodate the environment. If the urgent need for more NOMPC isoforms is because those appendages adapted different functions, we should find trace of these correlations. The haltere evolved only in Diptera, and the CS on it undoubtedly helps flight control as a gyroscope. The femoral CHO and abdominal CHO may detect the substrate vibration from the courtship or other communications which is prevalent among insects (Mazzoni et al., 2013). In Hymenoptera, most of the ants do not have wings but still maintain three NOMPC isoforms. Maybe these isoforms play a role in keeping social structure of bee, wasp, and ants.

Figure 5-1 Sensilla properties change in flies with only NOMPCγ isoform in wing sensilla**.**

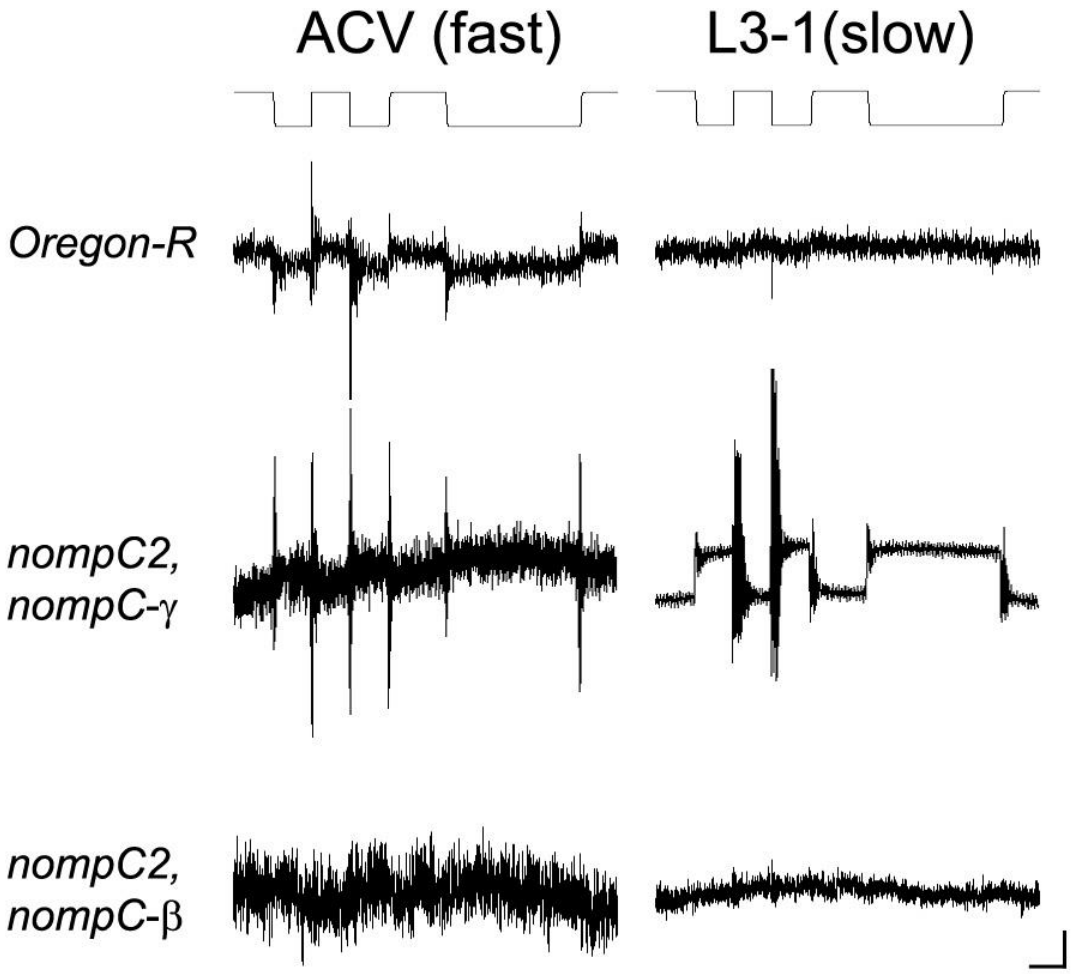

Figure 5-1 Wing vein extracellular recording showing the responses of fast adaptive sensilla ACV and slow adaptive sensilla L3-1 to downward pressure (trace on the top). Fast-adapting responses were recorded in control *Oregon-R* flies, and *nompC*^{2}*, nompCγ* flies but no responses were recorded in *nompC*^{2}*, nompCβ* flies. L3-1 sensilla are switched to fast adaptive sensor in NOMPCγ-expressing flies. Slow adaptive response was not detected. The responses were averaged over 5 trials. Calibration bar, 50uV, 200 msec.

Bibliography

Avidor-Reiss, T., Maer, A.M., Koundakjian, E., Polyanovsky, A., Keil, T., Subramaniam, S., and Zuker, C.S. (2004). Decoding cilia function: defining specialized genes required for compartmentalized cilia biogenesis. Cell *117*, 527-539.

Bischof, J., Maeda, R.K., Hediger, M., Karch, F., and Basler, K. (2007). An optimized transgenesis system for *Drosophila* using germ-line-specific phiC31 integrases. Proceedings of the National Academy of Sciences of the United States of America *104*, 3312-3317.

Branson, K., Robie, A.A., Bender, J., Perona, P., and Dickinson, M.H. (2009). High-throughput ethomics in large groups of *Drosophila*. Nature methods *6*, 451-457.

Cao, E., Liao, M., Cheng, Y., and Julius, D. (2013). TRPV1 structures in distinct conformations reveal activation mechanisms. Nature *504*, 113-118.

Chakravorty, S., Vu, H., Foelber, V., and Vigoreaux, J.O. (2014). Mutations of the *Drosophila* myosin regulatory light chain affect courtship song and reduce reproductive success. PloS one *9*, e90077.

Chan, W.P., Prete, F., and Dickinson, M.H. (1998). Visual input to the efferent control system of a fly's "gyroscope". Science *280*, 289-292.

Cheng, L.E., Song, W., Looger, L.L., Jan, L.Y., and Jan, Y.N. (2010). The role of the TRP channel NompC in *Drosophila* larval and adult locomotion. Neuron *67*, 373-380.

Chung, Y.D., Zhu, J., Han, Y., and Kernan, M.J. (2001). nompA encodes a PNS-specific, ZP domain protein required to connect mechanosensory dendrites to sensory structures. Neuron *29*, 415-428.

Clark, A.G., Eisen, M.B., Smith, D.R., Bergman, C.M., Oliver, B., Markow, T.A., Kaufman, T.C., Kellis, M., Gelbart, W., Iyer, V.N., *et al.* (2007). Evolution of genes and genomes on the *Drosophila* phylogeny. Nature *450*, 203-218.

Cole, E.S., and Palka, J. (1982). The pattern of campaniform sensilla on the wing and haltere of *Drosophila* melanogaster and several of its homeotic mutants. Journal of embryology and experimental morphology *71*, 41-61.

Corey, D.P., Garcia-Anoveros, J., Holt, J.R., Kwan, K.Y., Lin, S.Y., Vollrath, M.A., Amalfitano, A., Cheung, E.L., Derfler, B.H., Duggan, A., *et al.* (2004). TRPA1 is a candidate for the mechanosensitive transduction channel of vertebrate hair cells. Nature *432*, 723-730.

Dickinson, M.H., and Palka, J. (1987). Physiological properties, time of development, and central projection are correlated in the wing mechanoreceptors of *Drosophila*. The Journal of neuroscience : the official journal of the Society for Neuroscience *7*, 4201-4208.

Dubchak, I., Brudno, M., Loots, G.G., Pachter, L., Mayor, C., Rubin, E.M., and Frazer, K.A. (2000). Active conservation of noncoding sequences revealed by three-way species comparisons. Genome research *10*, 1304-1306.

Eberl, D.F., Hardy, R.W., and Kernan, M.J. (2000). Genetically similar transduction mechanisms for touch and hearing in *Drosophila*. The Journal of neuroscience : the official journal of the Society for Neuroscience *20*, 5981-5988.

Effertz, T., Wiek, R., and Gopfert, M.C. (2011). NompC TRP channel is essential for *Drosophila* sound receptor function. Current biology : CB *21*, 592-597.

Fenton, M.B., and Bell, G.P. (1981). RECOGNITION OF SPECIES OF INSECTIVOROUS BATS BY THEIR ECHOLOCATION CALLS. J Mammal *62*, 233-243.

Frazer, K.A., Pachter, L., Poliakov, A., Rubin, E.M., and Dubchak, I. (2004). VISTA: computational tools for comparative genomics. Nucleic acids research *32*, W273-279.

French, L.B., Singh, A., Luik, R., and Harris-Warrick, R.M. (2005). Structural requirements for rapid inactivation and voltage dependence in splice variants of lobster Shaker potassium channels. Journal of receptor and signal transduction research *25*, 73-97.

Gees, M., Owsianik, G., Nilius, B., and Voets, T. (2012). TRP channels. Comprehensive Physiology *2*, 563-608.

Gisselmann, G., Gamerschlag, B., Sonnenfeld, R., Marx, T., Neuhaus, E.M., Wetzel, C.H., and Hatt, H. (2005). Variants of the *Drosophila* melanogaster Ih-channel are generated by different splicing. Insect biochemistry and molecular biology *35*, 505-514.

Goodman, M.B., Lumpkin, E.A., Ricci, A., Tracey, W.D., Kernan, M., and Nicolson, T. (2004). Molecules and mechanisms of mechanotransduction. The Journal of neuroscience : the official journal of the Society for Neuroscience *24*, 9220-9222.

Gopfert, M.C., Albert, J.T., Nadrowski, B., and Kamikouchi, A. (2006). Specification of auditory sensitivity by *Drosophila* TRP channels. Nature neuroscience *9*, 999-1000.

Grueber, W.B., Jan, L.Y., and Jan, Y.N. (2003). Different levels of the homeodomain protein cut regulate distinct dendrite branching patterns of *Drosophila* multidendritic neurons. Cell *112*, 805-818.

Grunert, U., and Gnatzy, W. (1987). Macromolecules in the receptor lymph of campaniform sensilla. Histochemistry *86*, 617-620.

Hardie, R.C., Raghu, P., Moore, S., Juusola, M., Baines, R.A., and Sweeney, S.T. (2001). Calcium influx via TRP channels is required to maintain PIP2 levels in *Drosophila* photoreceptors. Neuron *30*, 149-159.

Hoy, R.R., and Robert, D. (1996). Tympanal hearing in insects. Annual review of entomology *41*, 433-450.

Kamikouchi, A., Inagaki, H.K., Effertz, T., Hendrich, O., Fiala, A., Gopfert, M.C., and Ito, K. (2009). The neural basis of *Drosophila* gravity-sensing and hearing. Nature *458*, 165-171.

Kamikouchi, A., Shimada, T., and Ito, K. (2006). Comprehensive classification of the auditory sensory projections in the brain of the fruit fly *Drosophila* melanogaster. The Journal of comparative neurology *499*, 317-356.

Kang, L., Gao, J., Schafer, W.R., Xie, Z., and Xu, X.Z. (2010). C. elegans TRP family protein

TRP-4 is a pore-forming subunit of a native mechanotransduction channel. Neuron *67*, 381-391.

Keil, T.A. (1997). Functional morphology of insect mechanoreceptors. Microscopy research and technique *39*, 506-531.

Kernan, M.J. (2007). Mechanotransduction and auditory transduction in *Drosophila*. Pflugers Archiv : European journal of physiology *454*, 703-720.

Ketten, D., and Bartol, S. (2005). Functional measures of sea turtle hearing:final report to the Office of Naval Research.

Kwan, K.Y., Allchorne, A.J., Vollrath, M.A., Christensen, A.P., Zhang, D.S., Woolf, C.J., and Corey, D.P. (2006). TRPA1 contributes to cold, mechanical, and chemical nociception but is not essential for hair-cell transduction. Neuron *50*, 277-289.

Lamb, G.D. (2000). Excitation-contraction coupling in skeletal muscle: comparisons with cardiac muscle. Clinical and experimental pharmacology & physiology *27*, 216-224.

Lee, G., Abdi, K., Jiang, Y., Michaely, P., Bennett, V., and Marszalek, P.E. (2006). Nanospring behaviour of ankyrin repeats. Nature *440*, 246-249.

Lee, J., Moon, S., Cha, Y., and Chung, Y.D. (2010). *Drosophila* TRPN(=NOMPC) channel localizes to the distal end of mechanosensory cilia. PloS one *5*, e11012.

Lehnert, B.P., Baker, A.E., Gaudry, Q., Chiang, A.S., and Wilson, R.I. (2013). Distinct roles of TRP channels in auditory transduction and amplification in *Drosophila*. Neuron *77*, 115-128.

Levitt, N., Briggs, D., Gil, A., and Proudfoot, N.J. (1989). Definition of an efficient synthetic poly(A) site. Genes & development *3*, 1019-1025.

Li, W., Feng, Z., Sternberg, P.W., and Xu, X.Z. (2006). A C. elegans stretch receptor neuron revealed by a mechanosensitive TRP channel homologue. Nature *440*, 684-687.

Liao, M., Cao, E., Julius, D., and Cheng, Y. (2013). Structure of the TRPV1 ion channel determined by electron cryo-microscopy. Nature *504*, 107-112.

Lis, A., Wissenbach, U., and Philipp, S.E. (2005). Transcriptional regulation and processing increase the functional variability of TRPM channels. Naunyn-Schmiedeberg's archives of pharmacology *371*, 315-324.

Lishko, P.V., Procko, E., Jin, X., Phelps, C.B., and Gaudet, R. (2007). The ankyrin repeats of TRPV1 bind multiple ligands and modulate channel sensitivity. Neuron *54*, 905-918.

Mazzoni, V., Anfora, G., and Virant-Doberlet, M. (2013). Substrate vibrations during courtship in three *Drosophila* species. PloS one *8*, e80708.

Merritt, D.J., and Murphey, R.K. (1992). Projections of leg proprioceptors within the CNS of the fly Phormia in relation to the generalized insect ganglion. The Journal of comparative neurology *322*, 16-34.

Milan, M., Weihe, U., Tiong, S., Bender, W., and Cohen, S.M. (2001). msh specifies dorsal cell fate in the *Drosophila* wing. Development *128*, 3263-3268.

Misof, B., Liu, S., Meusemann, K., Peters, R.S., Donath, A., Mayer, C., Frandsen, P.B., Ware, J.,

Flouri, T., Beutel, R.G., *et al.* (2014). Phylogenomics resolves the timing and pattern of insect evolution. Science *346*, 763-767.

Montell, C. (2005). *Drosophila* TRP channels. Pflugers Archiv : European journal of physiology *451*, 19-28.

Murphey, R.K., Possidente, D., Pollack, G., and Merritt, D.J. (1989). Modality-specific axonal projections in the CNS of the flies Phormia and *Drosophila*. The Journal of comparative neurology *290*, 185-200.

Oberwinkler, J., Lis, A., Giehl, K.M., Flockerzi, V., and Philipp, S.E. (2005). Alternative splicing switches the divalent cation selectivity of TRPM3 channels. The Journal of biological chemistry *280*, 22540-22548.

Orengo, J.P., Bundman, D., and Cooper, T.A. (2006). A bichromatic fluorescent reporter for cell-based screens of alternative splicing. Nucleic acids research *34*, e148.

Palka, J. (1993). Neuronal specificity and its development in the *Drosophila* wing disc and its derivatives. Journal of neurobiology *24*, 788-802.

Pedersen, S.F., Owsianik, G., and Nilius, B. (2005). TRP channels: an overview. Cell calcium *38*, 233-252.

Rajan, A., Tien, A.C., Haueter, C.M., Schulze, K.L., and Bellen, H.J. (2009). The Arp2/3 complex and WASp are required for apical trafficking of Delta into microvilli during cell fate specification of sensory organ precursors. Nature cell biology *11*, 815-824.

Ricci, A.J., Crawford, A.C., and Fettiplace, R. (2000). Active hair bundle motion linked to fast transducer adaptation in auditory hair cells. The Journal of neuroscience : the official journal of the Society for Neuroscience *20*, 7131-7142.

Ricci, A.J., and Fettiplace, R. (1998). Calcium permeation of the turtle hair cell mechanotransducer channel and its relation to the composition of endolymph. The Journal of physiology *506 (Pt 1)*, 159-173.

Rosenbaum, T., Gordon-Shaag, A., Munari, M., and Gordon, S.E. (2004). Ca2+/calmodulin modulates TRPV1 activation by capsaicin. The Journal of general physiology *123*, 53-62.

Salamov, A.A., and Solovyev, V.V. (2000). Ab initio gene finding in *Drosophila* genomic DNA. Genome research *10*, 516-522.

Shaner, N.C., Campbell, R.E., Steinbach, P.A., Giepmans, B.N., Palmer, A.E., and Tsien, R.Y. (2004). Improved monomeric red, orange and yellow fluorescent proteins derived from Discosoma sp. red fluorescent protein. Nature biotechnology *22*, 1567-1572.

Sharma, Y., Cheung, U., Larsen, E.W., and Eberl, D.F. (2002). PPTGAL, a convenient Gal4 P-element vector for testing expression of enhancer fragments in *Drosophila*. Genesis *34*, 115-118.

Shin, J.B., Adams, D., Paukert, M., Siba, M., Sidi, S., Levin, M., Gillespie, P.G., and Grunder, S. (2005). Xenopus TRPN1 (NOMPC) localizes to microtubule-based cilia in epithelial cells, including inner-ear hair cells. Proceedings of the National Academy of Sciences of the United States of America *102*, 12572-12577.

Sidi, S., Friedrich, R.W., and Nicolson, T. (2003). NompC TRP channel required for vertebrate sensory hair cell mechanotransduction. Science *301*, 96-99.

Steve Rozen, H.J.S. (1998). Primer3. In Primer3, H.J.S. Steve Rozen, ed. (Copyright (c) 1996,1997,1998 Whitehead Institute for Biomedical Research.

).

Sun, Y., Liu, L., Ben-Shahar, Y., Jacobs, J.S., Eberl, D.F., and Welsh, M.J. (2009). TRPA channels distinguish gravity sensing from hearing in Johnston's organ. Proceedings of the National Academy of Sciences of the United States of America *106*, 13606-13611.

Sutton, K.A., Jungnickel, M.K., Ward, C.J., Harris, P.C., and Florman, H.M. (2006). Functional characterization of PKDREJ, a male germ cell-restricted polycystin. Journal of cellular physiology *209*, 493-500.

Tang, Z.Z., Sharma, S., Zheng, S., Chawla, G., Nikolic, J., and Black, D.L. (2011). Regulation of the mutually exclusive exons 8a and 8 in the CaV1.2 calcium channel transcript by polypyrimidine tract-binding protein. The Journal of biological chemistry *286*, 10007-10016.

Thompson, J.D., Gibson, T.J., and Higgins, D.G. (2002). Multiple sequence alignment using ClustalW and ClustalX. Current protocols in bioinformatics / editoral board, Andreas D Baxevanis [et al] *Chapter 2*, Unit 2 3.

Walker, R.G., Willingham, A.T., and Zuker, C.S. (2000). A *Drosophila* mechanosensory transduction channel. Science *287*, 2229-2234.

Welling, A., Ludwig, A., Zimmer, S., Klugbauer, N., Flockerzi, V., and Hofmann, F. (1997). Alternatively spliced IS6 segments of the alpha 1C gene determine the tissue-specific dihydropyridine sensitivity of cardiac and vascular smooth muscle L-type Ca2+ channels. Circulation research *81*, 526-532.

Wittekindt, O.H., Visan, V., Tomita, H., Imtiaz, F., Gargus, J.J., Lehmann-Horn, F., Grissmer, S., and Morris-Rosendahl, D.J. (2004). An apamin- and scyllatoxin-insensitive isoform of the human SK3 channel. Molecular pharmacology *65*, 788-801.

Yack, J.E. (2004). The structure and function of auditory chordotonal organs in insects. Microscopy research and technique *63*, 315-337.

Yan, Z., Zhang, W., He, Y., Gorczyca, D., Xiang, Y., Cheng, L.E., Meltzer, S., Jan, L.Y., and Jan, Y.N. (2013). *Drosophila* NOMPC is a mechanotransduction channel subunit for gentle-touch sensation. Nature *493*, 221-225.

Yorozu, S., Wong, A., Fischer, B.J., Dankert, H., Kernan, M.J., Kamikouchi, A., Ito, K., and Anderson, D.J. (2009). Distinct sensory representations of wind and near-field sound in the *Drosophila* brain. Nature *458*, 201-205.

Zipursky, S.L., Venkatesh, T.R., Teplow, D.B., and Benzer, S. (1984). Neuronal development in the *Drosophila* retina: monoclonal antibodies as molecular probes. Cell *36*, 15-26.

Appendix

Figure A-1 Map of *nompC-α, -β* , and *–γ* rescue constructs in pTattb vector —BglII, BamHI, EcoRI, KpnI, and PstI

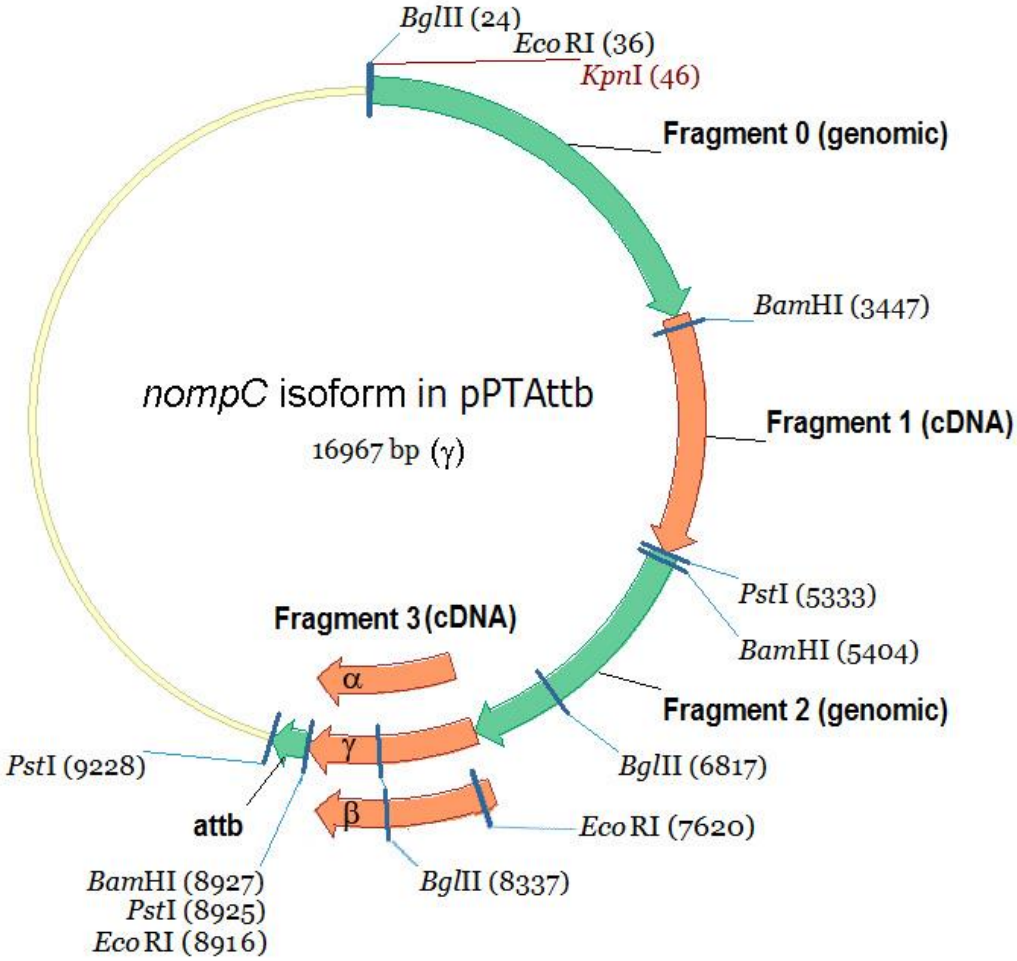

Figure A-2 Map of *UAS-nompC-β* or *-γ* construct in pTattb vector

—*BamHI, BglII, EcoRI, KpnI,* and *XbaI*

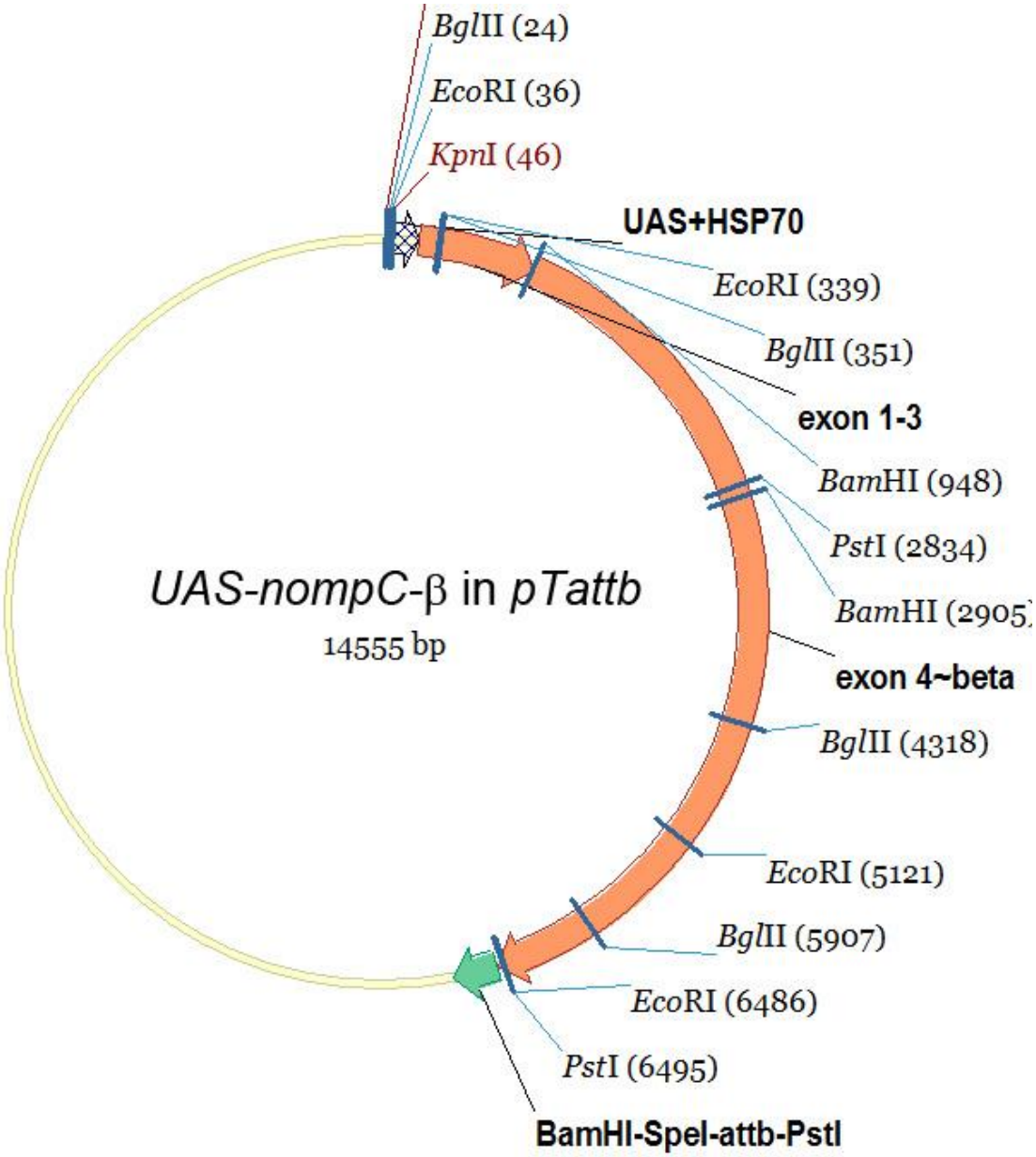

Figure A-3 Map of *UAS-nompC-γ* construct in pTattb vector

—*BamHI, BglII, EcoRI, KpnI,* and *XbaI*

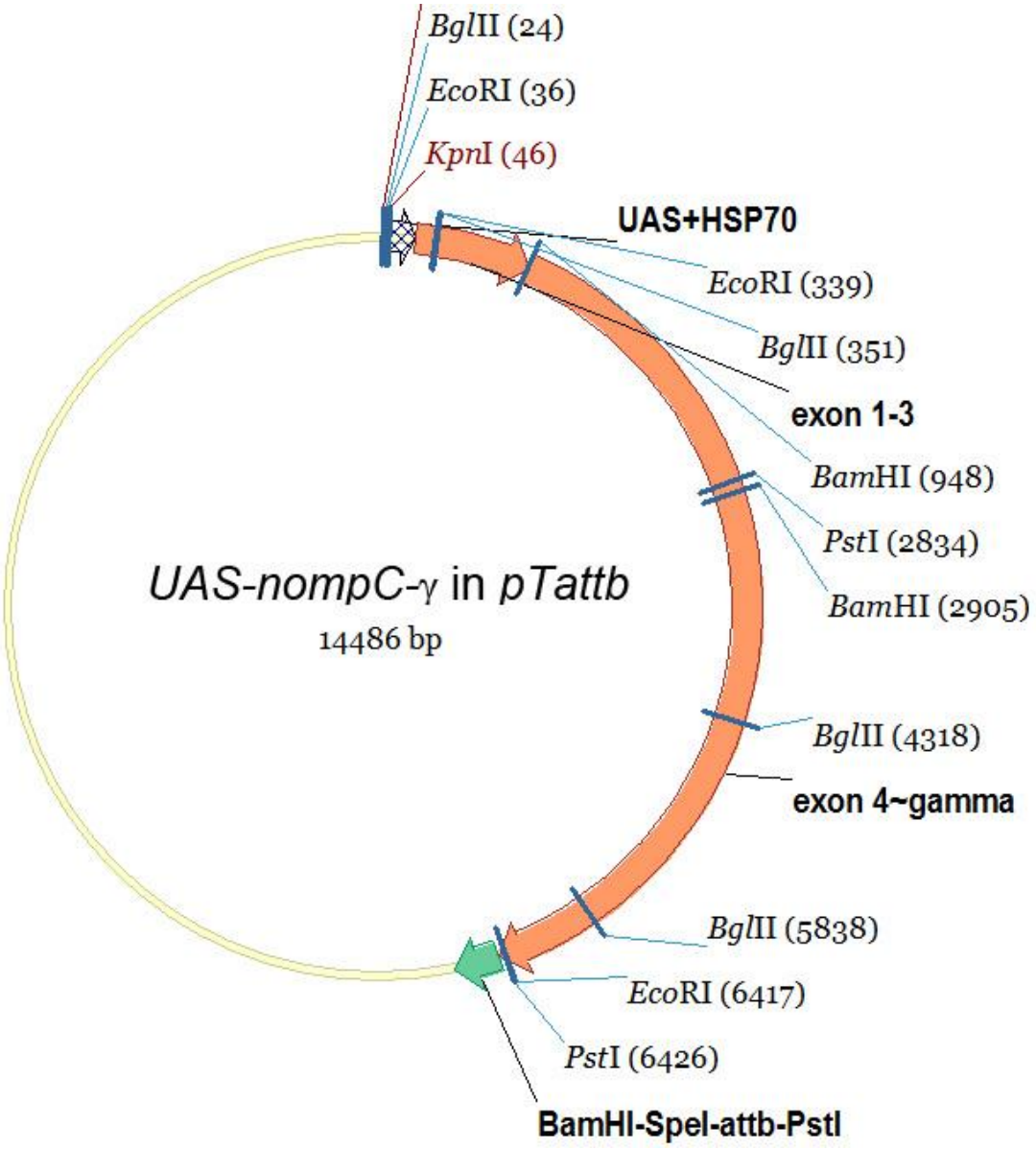

Figure A-4 Map of *UAS-FSR-β* construct in *pTattb* vector

—*EcoRI, PstI, SpeI, XbaI,* and *XhoI*

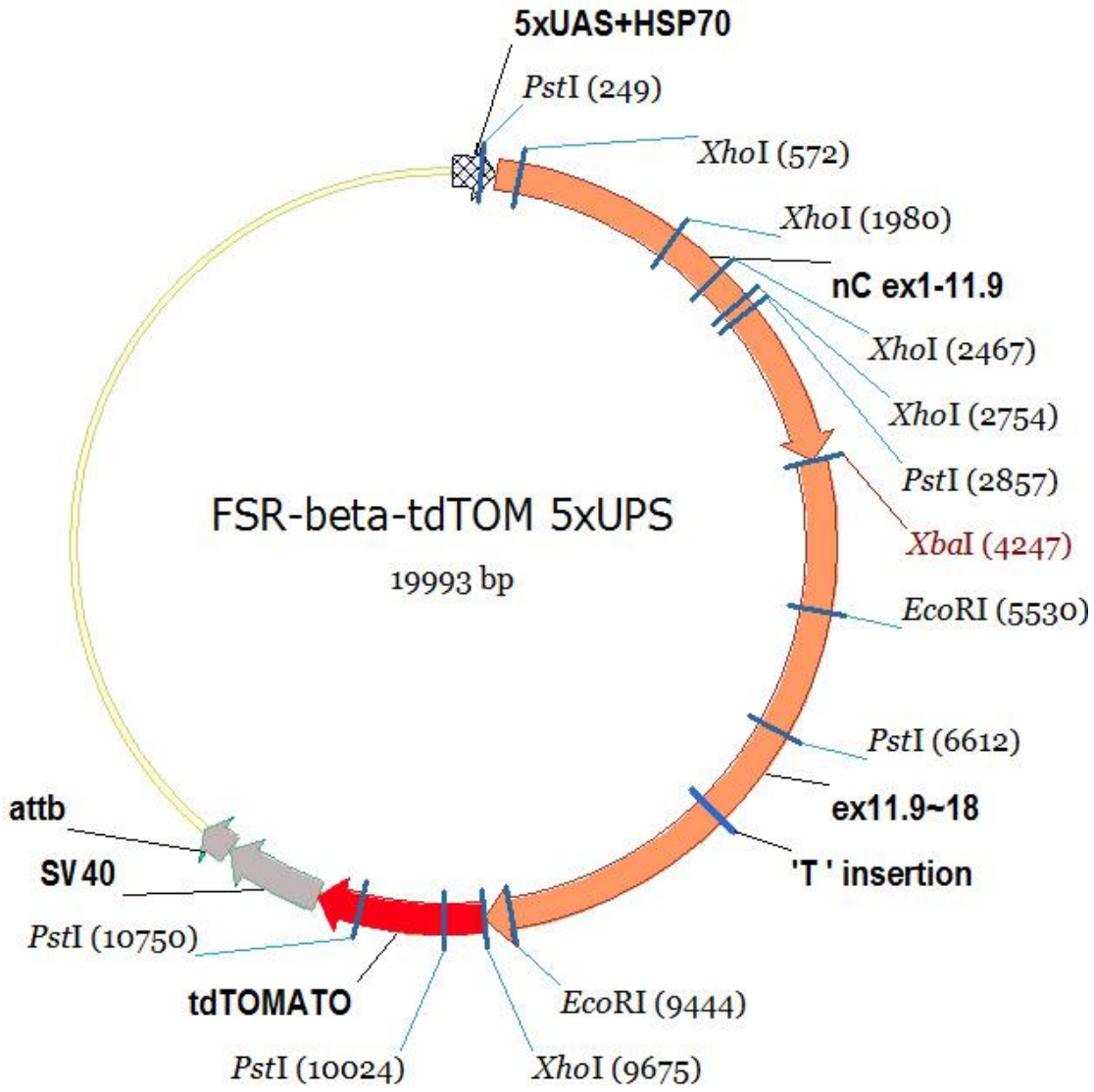

Figure A-5 Map of *UAS-FSR-γ* construct in *pTattb* vector

—*EcoRI, PstI, SpeI, XbaI,* and *XhoI*